To the Graduate Council:

I am submitting herewith a dissertation written by John D. Holder, entitled "Oxide-Metal Eutectic Composite Synthesis." I have examined the final copy of this dissertation for form and content and recommend that it be accepted in partial fulfillment of the requirements for the degree of Doctor of Philosophy, with a major in Metallurgical Engineering.

Ben F. Oliver, Major Professor

We have read this dissertation and recommend its acceptance:

George C. Frazier

Charlie R. Brooks

Lawrence A. Taylor

Peter J. Meschter

Accepted for the Council:

L. Evan Pobl

Vice Chancellor
Graduate Studies and Research

E

OXIDE-METAL EUTECTIC COMPOSITE SYNTHESIS

A Dissertation

Presented for the

Doctor of Philosophy

Degree

The University of Tennessee, Knoxville

John D. Holder

March 1982

3058051

ACKNOWLEDGMENTS

The author would like to express sincere thanks to Drs. G. W. Clark and B. F. Oliver for their hours of invaluable consultation and enthusiasm for the study of the directional solidification of oxide-metal eutectics. A highly esteemed crystal growth scientist, Dr. Clark was the author's group leader at the Oak Ridge National Laboratory and was instrumental in identifying the research problem and helping the author obtain the financial support for the research studies. Dr. Oliver, an outstanding teacher and metallurgist, has guided the author's graduate studies program to provide an excellent and broad education in metallurgical engineering.

This research program was financially supported by the United States Department of Energy and was conducted at the Oak Ridge National Laboratory. The support is deeply appreciated.

The author would like to thank Mrs. S. B. Waters, Mr. L. L. Hall, and Mr. W. H. Farmer for their technical assistance in preparing samples for the experimental investigation and in helping to maintain the crystal growth equipment. Thanks are also extended to Mr. O. B. Cavin for the x-ray studies that he conducted in connection with this investigation.

The author deeply appreciates the personal encouragement that was given him by Drs. R. A. Vandermeer, W. A. Coghlan, P. Meschter, and C. R. Brooks and their aid in obtaining the necessary theoretical insight into the Soret diffusion phenomenon and the thermodynamics of oxide-metal reactions.

Finally, the author would like to thank Mrs. C. L. Dowker, Miss B. L. Ratchett, Miss R. C. Robertson and Mr. J. W. Nave for their many hours of work in preparing illustrations and photographs, and in editing and typing this manuscript.

ABSTRACT

Synthesis of oxide-metal eutectic composites has been investigated with respect to the most basic melt chemistry principles and directional solidification phenomenon. The internal zone growth (IZG) technique has been extensively utilized in this study and in turn significantly developed and better understood. The growth of composite samples 5-cm in diameter has been demonstrated.

The growth of oxide-metal eutectics of both the M_xO_y-M and M_xO_y-M′ (where M′ ≠ M) types have been considered. The Cr_2O_3-Cr and Cr_2O_3-Mo eutectic systems were used as the experimental model systems to test the influence of partial oxygen pressure and solidification parameters on composite composition control and composite microstructure. It was found that partial oxygen pressure of the composite growth environment influences the composition of the melt in a way that can be predicted by regular solution thermodynamics. Also basic thermodynamic principles were utilized to predict the growth of more complex eutectic systems: $(M,M')_xO_y$-M, e.g. $(Cr,Al)_2O_3$-Cr, and M_xMO_z-M′′, e.g. $LaCrO_3$-Mo.

The results of controlled directional solidification experiments indicate that oxide-metal eutectics obey the same coupled growth theories that have been well established for metallic eutectic systems. In the coupled growth studies it was observed that eutectic composite structure could be grown from an extremely metal rich melt at unusually fast growth rates which is indicative of a large thermal gradient at the growth interface. Since solute redistribution can occur in a thermal gradient — called the Soret Effect, the eutectic constitutional supercooling criterion

was rederived to include the Soret diffusion term. The analysis reveals that the constitutional supercooling parameter "[G/R] minimum" is independent of the magnitude of the thermal gradient through the Soret Effect.

TABLE OF CONTENTS

SECTION		PAGE
I.	INTRODUCTION	1
	1.0 Historical Background	1
	2.0 Statement of the Problem	3
II.	THEORETICAL BACKGROUND AND CALCULATIONS	5
	1.0 Selection of Model System	5
	2.0 Thermodynamics of Oxide-Metal Eutectic-Like Systems	9
	2.1 Region of Component Stability	9
	2.2 Uniqueness of T and C	13
	2.3 Composition Control of Oxide-Metal Melts	18
	2.4 Calculation of Cr_2O_3-Mo Melt Composition as a Function of P_{O_2}	26
	3.0 Eutectic Solidification	29
	3.1 Eutectic Growth Theories	29
	3.2 Extremum Growth	36
	3.3 Internal Zone Growth and Skull Melting	37
	4.0 Soret-Modified Eutectic Constitutional Supercooling criterion	43
	4.1 The Soret Effect	44
	4.2 Soret-Modified Solute Redistribution Equation	45
	4.3 Soret-Modified Constitutional Supercooling Criterion	47
	4.4 Comparison to Mollard and Flemings' Calculation	49
III.	EXPERIMENTAL APPARATUS AND PROCEDURE	52

SECTION PAGE

1.0 Verification of Calculated Range of Stability for Cr_2O_3-Cr and $(Cr,Al)_2O_3$-Cr 52

2.0 Determination of Cr-Mo Fiber Composition as a Function of P_{O_2} 54

3.0 Directional Solidification Studies by IZG 57

3.1 Optimization of IZG for Cr_2O_3-Mo Composite Growth 57

3.2 Extremum Growth, Eutectic Morphology abd Growth of Off-Eutectic Composites 63

4.0 Synthesis of Predicted $LaCrO_3$-Mo, W, Cr and $YCrO_3$-Mo, W, Cr Systems 64

IV. RESULTS 65

1.0 Verification of Range of Stability for Cr_2O_3-Cr and $(Cr,Al)_2O_3$-Cr 65

2.0 Cr-Mo Fiber Composition as a Function of P_{O_2} 67

3.0 Optimization of IZG for Cr_2O_3-Mo Composite Growth . . 71

4.0 Investigation of the Growth of Off-Eutectic Composition, Eutectic Morphologies, and Extremum Growth of Cr_2O_3-Mo composites 75

5.0 Synthesis of $LaCrO_3$-Mo, W, Cr and $YCrO_3$-Mo, W, Cr Composites 76

V. CONCLUSIONS 79

VI. DISCUSSION 83

LIST OF REFERENCES 86

APPENDICES 92

VITA 109

LIST OF TABLES

TABLE		PAGE
I.	Known Metal Oxide-Metal Eutectic Systems	2
II.	Table of Symbols for Soret-Modified Constitutional Supercooling Analysis	51
III.	Significant Strip Heater Results	66
IV.	Observed Metal Fiber Composition as a Function of Gas Mixture and Melting Technique	69
A-I.	Calculated Log K_p for Vapor Species in Equilibrium with Cr_2O_3 and Mo at 1500 K, 1800 K and 2200 K	94
C-I.	Calibration Data for Thermox Oxygen Analyzer	101
D-I.	Calculated Values for Mo-Cr Fiber Composition vs $CO-CO_2$ Mixture	106

LIST OF FIGURES

FIGURES		PAGE
1.	Standard Free Energy of Formation vs Temperature for Cr_2O_3, MoO_3 and MoO_2	6
2.	Mo-Cr Equilibrium Phase Diagram	7
3.	$Cr-Cr_2O_3$ Equilibrium Phase Diagram	8
4.	$Al_2O_3-Cr_2O_3$ Equilibrium Phase Diagram	8
5.	Calculated Range of Stability for $Mo + Cr_2O_3$	10
6.	Stability Range of $M' + M_{x/2}O$ vs P_{O_2} and Temperature	11
7.	Calculated Range of Stability for $Cr + Cr_2O_3$	12
8.	Calculated Range of Stability for $Cr + (Cr,Al)_2O_3$	12
9.	Binary Eutectic System (a) Phase Diagram, (b) Free Energy of Mixing Curves Showing Common Tangent at Eutectic Temperature	15
10.	Liquidus Surface with Isotherms of Pseudo-Binary Oxide-Metal Eutectic System	16
11.	Increasing Range of $M + M_xO_y$ Stability Due to Solution Formation at $T > T_E$	20
12.	Approximated $Cr-Mo-Cr_2O_3$ Phase Diagram Depicting Pseudo-Binary $Mo(Cr) + Cr_2O_3$ Eutectic System	28
13.	Typical Binary Eutectic System	29
14.	Region of Coupled Growth Predicted by Metastable Extensions of Liquidus Lines	31
15.	Cline's Predictions Compared with Calculations Using Mollard and Fleming's Constitutional Supercooling Criterion, CSC, and with Holder and Oliver's Experimental Data for Pb-Sn	34

16. (a) Asymmetric Region of Coupled Growth Due to Facetting of β-Phase, (b) Undercooling vs Growth Rate Qualitatively Predicted for Composition Co in (a) 35

17. Heating Instability Calculated by Hartzell and Sekerka for a Rf-Heated Cylinder of Material with an Extremely Temperature Dependent Electrical Conductivity 40

18. Effect of Increased Frequency on the Rf-Heating Instability. . 40

19. Effect of Increased Diameter on the Rf-Heating Instability . . 41

20. Effect of Decreased Temperature Dependence of Electrical Conductivity on the Rf-Heating Instability 41

21. Sketch of Commercially Available Cold Crucible Apparatus . . . 43

22. Comparison of the Soret-Modified Constitutional Supercooling Criterion to Mollard and Flemings' Criterion for the Pb-Sn System 49

23. Calculated Values of Soret Factor, S, for Pb-Sn Alloys 50

24. Diagram of Strip-Heater Furnace 53

25. Waffers of Oxide-Metal Mixtures Used in Strip-Heater Experiments 53

26. Cross Section of Cold Crucible Furnace 56

27. Rf-Heated Hot Press for Large Diameter IZG and Cold Crucible Samples 58

28. Susceptor/Rf Coil/Sample Geometry: (a) Preheat Position, (b) Position for Melt Zone Movement 59

29. Cross Section of 5-cm Diameter IZG Sample showing Internal Susceptor Configuration 60

30. Strip-Heater Melted Waffer of Cr + Cr_2O_3 Mixture 66

31. Strip-Heater Melted Waffer of Cr + $(Cr,Al)_2O_3$ (a) 25×, (b) 125× 67

32. $CO-CO_2$ Gas Mixture vs Chromium Content of Molybdenum Fibers in $Mo(Cr)-Cr_2O_3$ Composites 70

33. Hartzell and Sekerka's Calculations for Rf-Heated $Mo-Cr_2O_3$ Compact (2 cm Diameter, 3 MHz Frequency) 72

34. Melt Splats on Chamber Walls Due to Uncontrollable Melting in Rf-Heating Instability 74

35. Cross Sections of Large Diameter Samples of Mo + Cr_2O_3 Composite Grown by IZG 74

36. Typical Rod Structure of Cr_2O_3-Mo(Cr) Composite Produced by IZG: (a) Transverse, (b) Longitudinal 75

37. Microstructure of Rods in Row or Sheet Array (Transverse Section) 77

38. λ^2R Relationship for Cr_2O_3-40 Mole % Mo Eutectic Composites. . 77

39. Representative Microstructures of Chromite-Metal Melt Zones: (a) $LaCrO_3$-W, (b) $LaCrO_3$-Mo, (c) $LaCrO_3$-Cr, (d) $YCrO_3$-W, (e) $YCrO_3$-Mo, (f) $YCrO_3$-Cr 78

A-1 1500 K Kellogg Diagram for Cr_2O_3-Mo 95

A-2 1800 K Kellogg Diagram for Cr_2O_3-Mo 95

A-3 2200 K Kellogg Diagram for Cr_2O_3-Mo 96

B-1 Approximation of Cr and Cr_2O_3 Activities at 1810°C 99

C-1 Calibration Curve for Thermox Oxygen Analyzer. 103

I. INTRODUCTION

1.0 Historical Background

In 1965, during an investigation of the effects of W on the stoichiometry of UO_2 single crystals, 10% W was added to the UO_2 melt which was then directionally solidified by a new technique, later called internalcentrifugal zone growth. At high magnification, a transverse polished section revealed a uniform array of metal fibers in an otherwise normal UO_2 crystal. It was subsequently determined that the sample was a directionally solidified eutectic composite of UO_2 and W [1]. This was indeed exciting, since at that time the only known oxide-metal eutectic systems were of the type where the oxide component was an oxide of the metal component; e.g., Cr_2O_3-Cr, FeO-Fe, Cu_2O-Cu, ZrO_2-Zr, NiO-Ni, CoO-Co, etc. [2]. Also, eutectic composites research claimed a great excitement because of the growing interest in metal-metal and metal-metal carbide eutectic composites for the gas turbine industry [3,4,5]. A search was begun to discuss other very refractory metal oxide-metal eutectic composites. A list of the systems which have since been synthesized is given in Table I.

After 10 years of oxide-metal eutectic research little still was known about the heterogeneous equilibrium governing the "eutectic-like" composites that were being produced. The approach to discovering a new composite combination was to attempt synthesis under conditions similar to those used for UO_2-W [7]. The effects of composition, oxide stoichiometry, oxygen partial pressure, and impurities were not known. However, references to the importance of these factors appeared in the literature.

Table I. Known Metal Oxide-Metal Eutectic Systems

Oxide Matrix	Metal	Oxide Matrix	Metal
	Binary		
Cr_2O_3	Cr, Mo, W, Re [9,10]	$Nd_2O_3(CeO)$	Nb [9]
$(Cr, Al)_2O_3$	Cr, Mo, W [8,6]	TiO_2	Cr, Nb, Ta, Mo [13,14]
Gd_2O_3	Mo, W [10]	UO_2	Mo, Ta, W [7,12]
$Gd_2O_3(CeO_2)$	Mo [10]	$UO_2(ThO_2)$	W [7]
$HfO_2(CaO)$	Mo, W [7,11]	$Y_2O_3(CeO_2)$	Mo, W [16]
$HfO_2(Y_2O_3)$	W [11]	ZrO_2	Ta, W [13,14]
La_2O_3	Mo, W [7]	$ZrO_2(CaO)$	W [15]
Nd_2O_3	Mo, W [7]	$ZrO_2(Y_2O_3)$	W [15]
$LaCrO_3$	Cr, Mo, W*		
$YCrO_3$	Cr, Mo, W*		
	Ternary		
UO_2-MgO	W [17]	$CaO-CaCr_2O_4$	W [17]
$MgO-ZrO_2$	W [17]	$Cr_2O_3-ZrO_2$	W, Mo [17]
$MgO(Cr_2O_3)$-ZrO	Mo [17]	$Cr_2O_3-HfO_2$	Mo [17]
$Cr_2O_3-LaCrO_3$	W*		
$La_2O_3-LaCrO_3$	W*		

*This work.

For example, some workers reported that Cr_2O_3-W composites could be grown in a sealed W crucible although their best material was porous, poorly aligned, and severely cracked while the crucible suffered appreciable attack from the melt [18]. On the other hand, other researchers grew the Cr_2O_3-Cr eutectic in sealed W crucibles with little or no crucible attack [19] giving rise to questions concerning the solubilities of refractory metals in oxide melts. Liquid-liquid immiscibilities began to be observed [20]. Three oxide-metal mixtures (Cr_2O_3-Ta, Cr_2O_3-Nb and Cr_2O_3-V) were reported [13] to produce binary eutectic composites which seemed to defy the simple rules of thermodynamics, i.e. oxides of Ta, Nb, and V are more stable than Cr_2O_3. Clearly, by 1975 there was a need for a fundamental study of the high-temperature melt chemistry of oxide-metal eutectic-like systems.

2.0 Statement of the Problem

Synthesis of oxide-metal eutectic-like composites will be investigated with respect to basic eutectic directional solidification phenomenon and melt chemistry. Arguments will be considered that will help to promote the development of two phase oxide-metal composite growth understanding in terms of either pure binary eutectic reactions or pseudo-binary eutectic reactions. A model will be sought to aid in predicting the influence of the crystal growth environment, particularly the partial oxygen pressure, on the resulting composite composition and the control of the oxide melt composition. Other related problems such as component stability in the oxide melt and oxidation volatilization will be discussed in light of the experience gained in the growth of oxide-metal composite materials.

The internal zone growth (IZG) technique will be utilized to grow oxide-metal eutectic-like composites for this study. IZG has proven to be the best suited direction solidification method for the oxide-metal composites of interest [7]. Also, IZG has recently been numerically simulated to study the relationships of most parameters critical to the directional solidification of oxide-metal composites [21,22]. A comparison of actual IZG conditions required for composite growth with those simulated numerically will be made where possible. However, it must be realized that at best the comparison of actual with theoretical will be qualitative due to the difficulties in making measurements at very high temperatures in the presence of a strong Rf field.

The Cr_2O_3-Mo eutectic-like composite has been chosen as the model composite for this investigation. Selection was made on the basis of the

abundance of phase diagram information, available thermodynamic properties, and composite growth experience.

The characteristics of the Cr_2O_3-Mo morphology as a function of directional solidification parameters will be investigated. Also the relationship of the Cr_2O_3-Mo composite composition to the composite growth environment will be determined and compared to that predicted by the thermodynamic model developed to describe the composite producing oxide melt. As a further test of the predicted nature of oxide-metal eutectic-like composites, a closely related ternary system will be investigated for the predictability of composite growth.

Finally, the contribution of Soret induced diffusion at the solidifying interface will be considered. The Soret effect has been predicted to be of little or no consequence in metallic systems where the thermal gradient at the solidification surface is small [23–25]. The Soret effect is reviewed since the thermal gradient at the solidifying interface in oxide-metal composite growth is most likely two orders of magnitude higher than in metallic systems.

II. THEORETICAL BACKGROUND AND CALCULATIONS

1.0 Selection of Model System

The simultaneous solidification of both a metallic phase and an oxide phase from an oxide liquid requires that the environment be reducing to all oxides of the metallic phase and yet oxidizing enough to yield the desired cation valence in the oxide phase [71]. This requirement is depicted in the plot of standard free energy of formation of oxides as a function of temperature given in Fig. 1. Using the nomogram in Fig. 1 the partial pressure of oxygen or appropriate mixture of either hydrogen and water or carbon monoxide and carbon dioxide can be determined which satisfy the oxidizing/reducing requirement. With this type of information, the model system chosen for this study must be one which has no higher cation valence oxides of the oxide phase in the region between the free energy of formation curve of the most stable oxide of the metallic phase and the curve of the desired oxide phase. Fortunately, the free energy of formation for most oxides which can be used to construct plots similar to Fig. 1 [26,27,69] is abundantly available in this graphical form and in tabulated form.

Another consideration in choosing a model system was oxidation volatilization; i.e., the temperature gradient induced transport of material away from a solid or liquid surface in the form of vapors of metastable hypo- or hyperstoichiometric oxide species [71]. Such information is difficult to obtain. The most detailed work has been done on oxides of chromium, molybdenum and tungsten [28–33]. The partial pressures of known

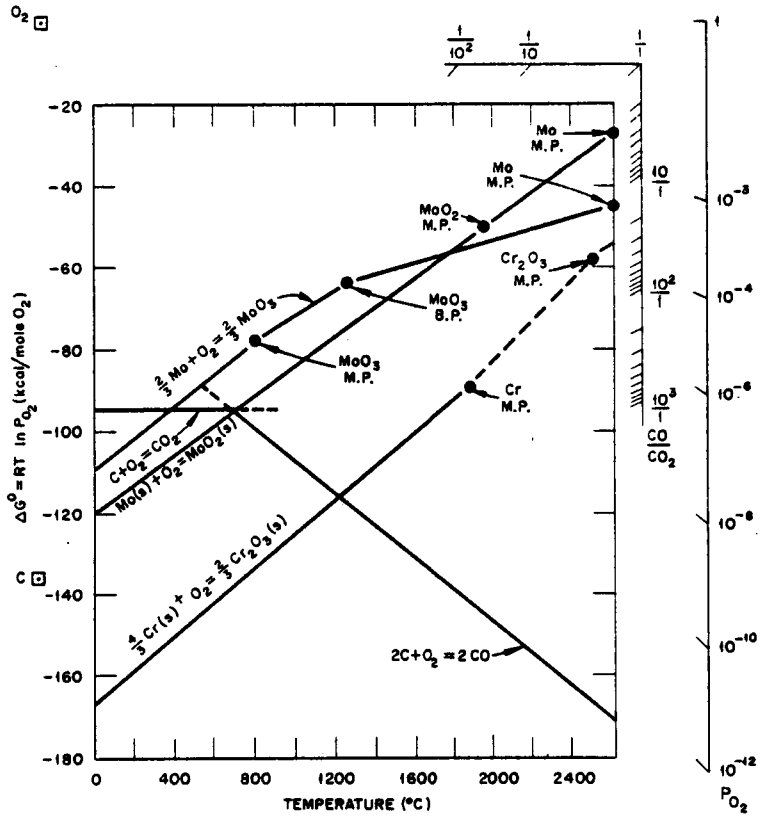


Fig. 1. Standard Free Energy of Formation vs Temperature for Cr_2O_3, MoO_3 and MoO_2.

vapor species over Mo and Cr_2O_3 were calculated for the oxygen pressures of interest and are given in Appendix A. Though somewhat high, they are not prohibitive.

A third consideration was the availability of phase diagram information and the freedom of alloying suggested by this information for candidate systems. The sesqui (III) oxide of chromium, Cr_2O_3, with molybdenum was chosen as the model oxide-metal eutectic system since it satisfies all the initial consideration much better than any other oxide-metal mixture known to give a eutectic composite. There is an adequate range of oxygen pressures over which the components in the mixture should be stable. Oxidation volatilization should not be a problem, and the available phase diagrams suggest the sought after simplicity; e.g., Mo

and Cr are completely miscible in both the solid and liquid states (see Fig. 2) [34] which greatly simplify the regular solution description of that side of the proposed Cr_2O_3-Mo-Cr ternary as will be discussed. In addition to the Mo-Cr simplification, an immiscibility exist in the Cr-Cr_2O_3 [9] binary system (see Fig. 3) which gives an immediate value for the regular solution parameter α' that will be of great importance in relating liquid composition and the resulting composite composition to the crystal growth gaseous environment.

As a bonus it is found that Cr_2O_3-Al_2O_3 [35] is completely miscible in both the solid and liquid states, an ideal system (see Fig. 4), suggesting a simple quaternary for oxide alloying studies; e.g., $(Cr,Al)_2O_3$-Mo(Cr). Also, Cr_2O_3 forms eutectics with Cr and Re in addition to Mo (see Table I) and Mo forms a eutectic with σ-phase Re-Mo [36,37] suggesting the possibility of oxide-metal-metal ternary eutectic, a type of system not yet reported synthesized.

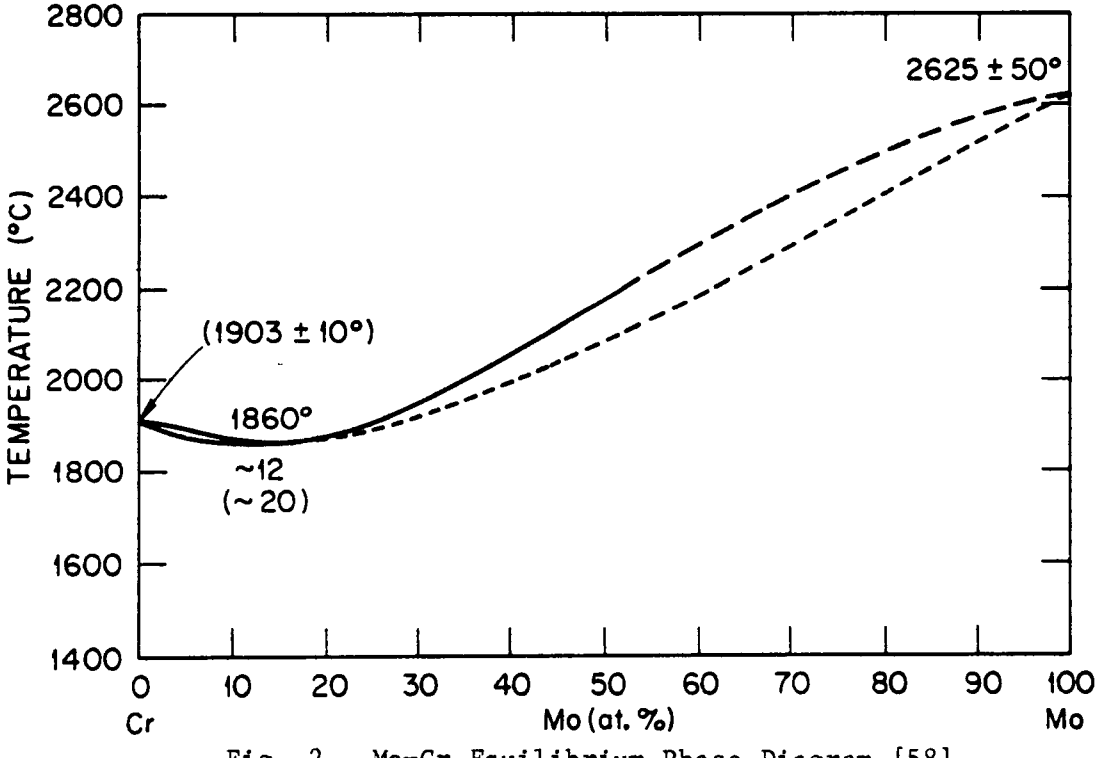


Fig. 2. Mo-Cr Equilibrium Phase Diagram [58].

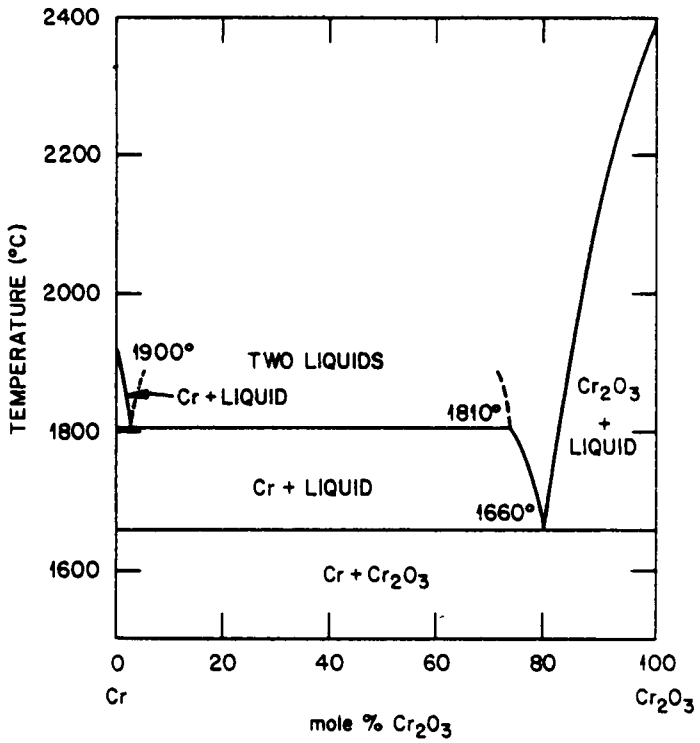


Fig. 3. Cr-Cr_2O_3 Equilibrium Phase Diagram [9].

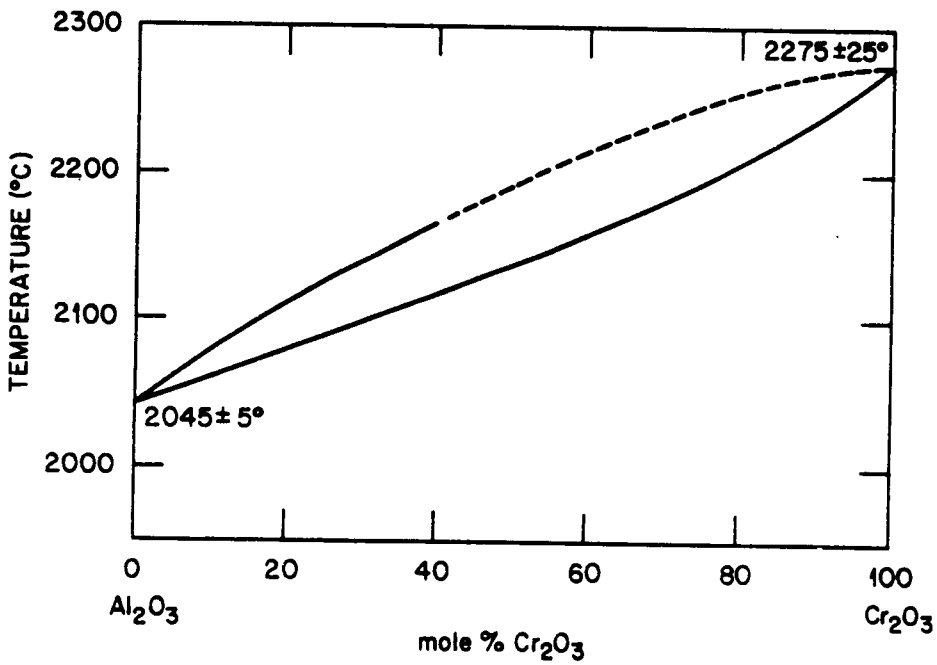


Fig. 4. Al_2O_3-Cr_2O_3 Equilibrium Phase Diagram [55].

2.0 Thermodynamics of Oxide-Metal Eutectic-Like Systems

2.1 Region of Component Stability

As already mentioned in the selection of a model system for this study, the partial pressure oxygen environment of the melt must be such as not to oxidize the metallic phase nor reduce the oxide phase when considering the eutectic reaction

$$\text{Liquid} \rightarrow M_xO_y + M'$$

where either $M = M'$ or $M \neq M'$. At a temperature just slightly below the eutectic temperature where only the solid phases exist, the situation of oxidation or reduction of the phases is well defined. If there is very little solubility of either component in the other, the free energy of formation of the oxides of each should very closely specify the limits within which the oxygen pressure must be maintained. A slight increase in temperature to the eutectic temperature allows a liquid of eutectic composition to be in equilibrium with the two solid phases. Thus, the oxygen pressure suitable for the solid phases must also be suitable for the liquid phase in equilibrium with them.

A very large range of oxygen pressures or equivalent hydrogen-water or carbon monoxide-carbon dioxide mixtures should be usable for the environment of the melt from which both Cr_2O_3 and Mo phases can be simultaneously grown. This range is given in Fig. 5 plotted as partial oxygen pressure versus temperature instead of free energy of formation versus temperature. The calculation is made using the standard free energy of formation for $\frac{4}{3}Cr + O_2 \rightarrow \frac{2}{3}Cr_2O_3$ and $Mo + O_2 \rightarrow MoO_2$, and by taking the activities of solid Cr, Cr_2O_3, Mo and MoO_2 as unity (the standard states are pure, solid species).

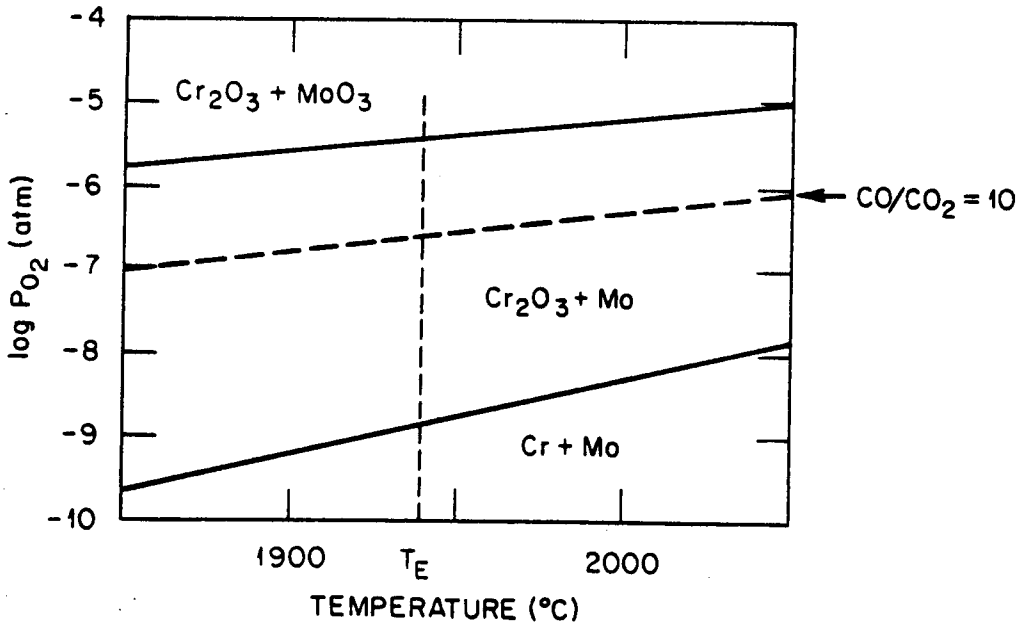


Fig. 5. Calculated Range of Stability for Mo + Cr_2O_3.

A large range of partial oxygen pressures which will allow the oxide-metal eutectic reaction to occur is necessary for the synthesis of the eutectic composite by directional solidification [40,71]. For in the technique of directional solidification, a superheating of the liquid above the eutectic temperature is necessary in order to create a positive thermal gradient (dT/dx) into the liquid at the solid-liquid interface. If the liquid should be heated above the critical temperature indicated for gas mixture A in Fig. 6, the oxide melt would begin to be reduced. And similarly during cooling, if the very hot solid composite is exposed to the environment of gas mixture B in Fig. 6, the metal phase would begin to oxidize. Or, if the gas mixture represented by curve C is used, the metal component would begin to oxidize in the melt and only oxide phases would be present upon solidification.

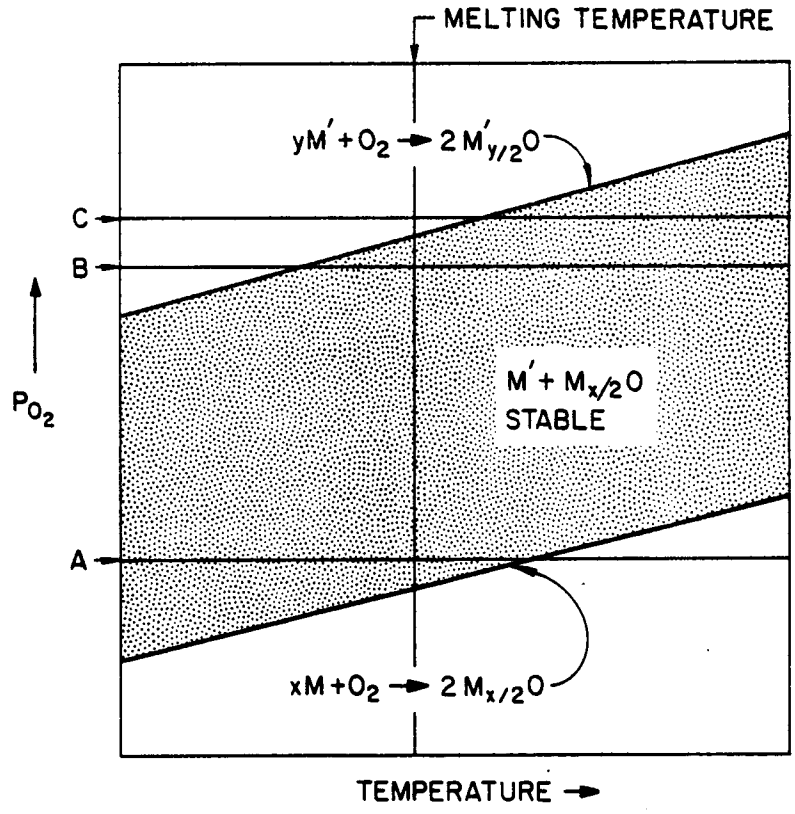


Fig. 6. Stability Range of M' + $Mx/_2O$ versus P_{O_2} and Temperature.

Referring back to Fig. 5 with particular attention to the Cr, Cr_2O_3 curve, an immediate difficulty is recognized if a directionally solidified eutectic composite of Cr_2O_3-Cr is proposed. Even though a range in partial oxygen pressure exists above the melting point as shown in Fig. 7, the few degrees of superheating calculated would be insufficient to allow directional solidification by conventional techniques. More freedom to superheat the Cr_2O_3-Cr oxide melt can be obtained by adding, for example, Al_2O_3 to lower the activity of the chromium oxide in the melt resulting in a larger range of stability as shown in Fig. 8. (The calculations made in constructing Figs. 7 and 8 are given in Appendix B). This argument will be presented again in more formal thermodynamic terms when the regular solution model is considered in order to relate composite composition to the partial oxygen pressure of the crystal growth environment.

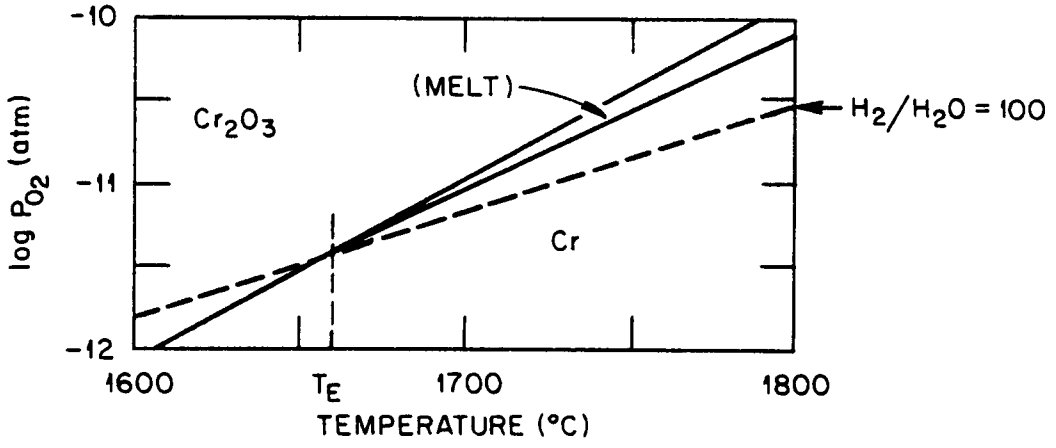


Fig. 7. Calculated Range of Stability for Cr + Cr_2O_3.

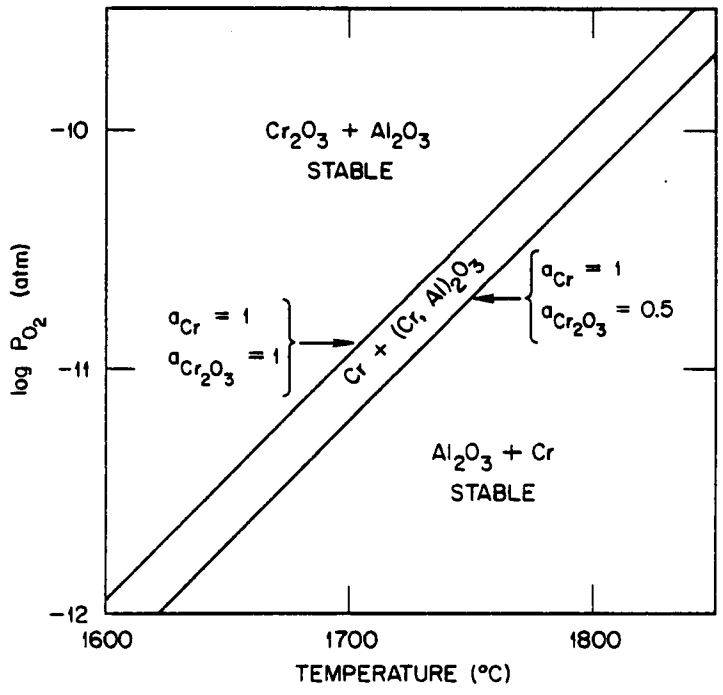


Fig. 8. Calculated Range of Stability for Cr + $(Cr,Al)_2O_3$.

2.2 Uniqueness of T and C

Since the discovery of the eutectic-like microstructure of UO_2 and W grown from the melt [1], many very similar oxide-metal eutectic-like composites have been synthesized [14]. Because of the reactiveness and the very high melting temperatures of the components forming the systems, there have not been any differential thermal analysis experiments to determine whether or not a pure eutectic reaction is occurring reported. In fact, melting temperatures apparently have not been accurately measured for any oxide-metal eutectic system. Thus, there remains some question as to whether or not UO_2-W, ZrO_2-W, Cr_2O_3-Mo, etc. are binary eutectic systems. A consideration of the fundamental aspects of the uniqueness of temperature and composition of the binary eutectic reaction should help to resolve this question for oxide-metal eutectic-like composite systems.

A eutectic reaction will occur upon slowly heating a mixture of crystalline phases if the following conditions are met: (1) the crystalline phases are dissimilar enough to be immiscible in one another, (2) other crystalline phases of intermediate composition are not formed when the mixture is equilibrated, and (3) the liquid phase of each component is not so dissimilar from the others as to be immiscible. The eutectic reaction occurs at a unique temperature, below the melting points of the crystalline phases. This unique temperature is called the eutectic temperature. Also, a single unique combination of all the crystalline phases in a eutectic system will totally melt at the eutectic temperature. This unique combination of crystalline phases is called the eutectic composition.

The uniqueness of both the eutectic temperature and eutectic composition can be understood from the standpoint of competing free energies of mixing. At T_E shown for the binary eutectic system given in Fig. 9(a), the free energy of mixing curves in Fig. 9(b) for the α-solid solution (curve I) the β-solid solution (curve II), and the liquid (curve III) share a common tangent line abc, denoting that the three phases are in equilibrium. Clearly a common tangent can only occur at one temperature (below the melting point of either component) and at one unique composition.

When three-phase equilibrium occurs in a condensed two-component system, the three phase equilibrium has zero degrees of freedom according to the Gibbs phase rule. The phase rule gives the number of degrees of freedom, F, that a system containing C components can have, when P phases are in equilibrium. For a condensed system where pressure can be neglected the phase rule is given as:

$$F = C - P + 1 .$$

This is just the case at the eutectic point in a binary eutectic system; i.e., for the eutectic reaction $L \rightleftharpoons \alpha + \beta$ there are zero degrees of freedom. The meaning of zero degrees of freedom is that there can be only one temperature and one composition for which the three phase equilibrium $L \rightleftharpoons \alpha + \beta$ exist.

For the purposes of later discussion it will be necessary to view the phase rule for what sometimes is called the pseudo-binary eutectic reaction. Reactions which seem to behave like simple, two component eutectic reactions but actually consist of three or more components in solution in the melt are often referred to as pseudo binary. Such reactions for example occur on or very near monovariant (one degree of

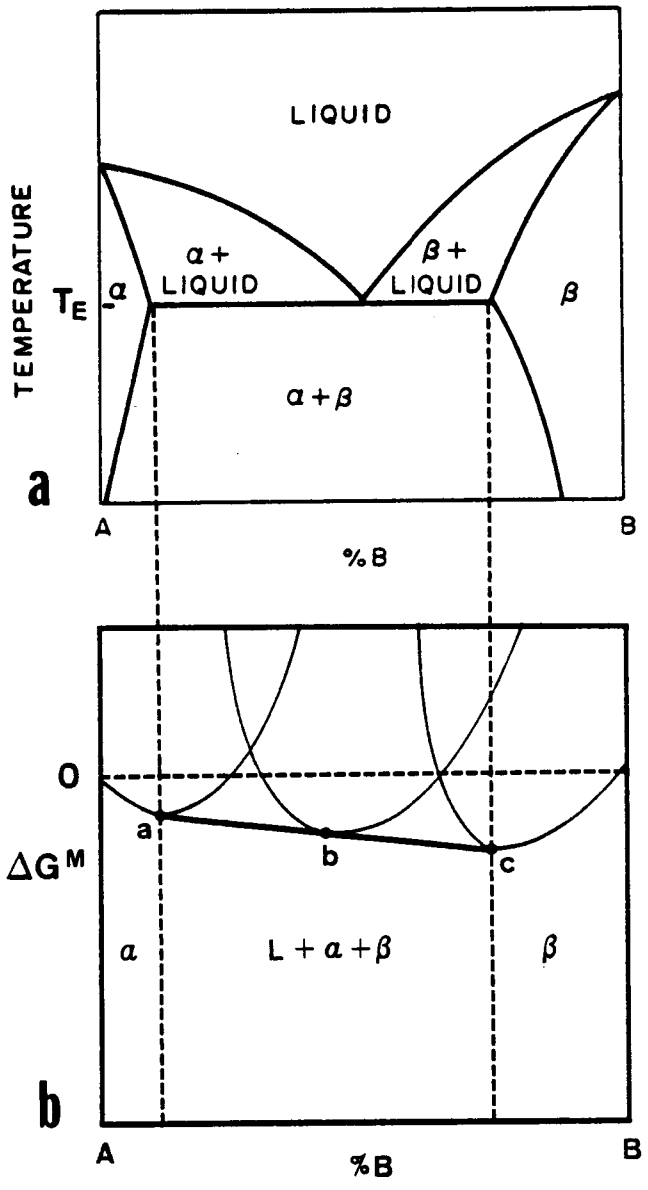


Fig. 9. Binary Eutectic System (a) Phase Diagram, (b) Free Energy of Mixing Curves Showing Common Tangent at Eutectic Temperature.

freedom) compositions in ternary systems. The equilibrium reaction on the monovariant trough as depicted in Fig. 10 would be, first, $L \rightarrow L + \alpha + \beta$; then further cooling would result in $L + \alpha + \beta \rightarrow \alpha + \beta$. During directional solidification when constitutional supercooling is avoided, the liquid freezes as $L \rightarrow \alpha + \beta$ for monovariant and near monovariant compositions. The reaction is in likeness to the simple binary eutectic reaction and thus is termed pseudo-binary.

The joint between two liquidus surfaces as in Fig. 10 is monovariant, therefore, either temperature or composition must be specified to describe any point on the monovariant trough.

In other words, the two step reaction $L \rightarrow L + \alpha + \beta \rightarrow \alpha + \beta$ occurs at all compositions along the monovariant trough. When the composition

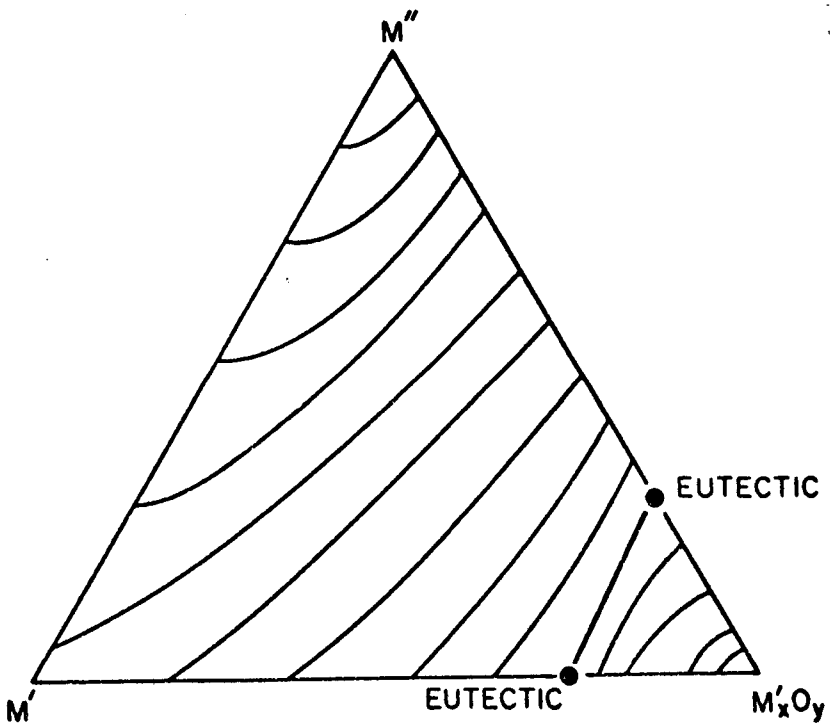


Fig. 10. Liquidus Surface with Isotherms of Pseudo-Binary Oxide-Metal Eutectic System.

is specified, the reaction is completely specified and each specific reaction (different only in composition) occurs at a unique temperature. Thus, if the temperature is specified, then the composition is also set.

Next, the phase rule will be applied to a typical oxide-metal mixture which is known to yield a eutectic-like microstructure. If uniqueness of both eutectic temperature and eutectic composition can be argued, then the phase rule will be satisfied and such systems shall be considered as simple binary eutectic systems. Otherwise, the eutectic-like oxide-metal systems will be shown to be a pseudo-binary eutectic type. The Cr-Cr_2O_3 and Mo-Cr_2O_3 mixtures will be used in this argument to help establish familiarity with these particular phase equilibria even though the argument will remain general in nature and applicable to all such binary systems.

The simplest case to consider is the reaction that would yield a metal and its oxide upon cooling a liquid solution of the two; i.e., L → Cr + Cr_2O_3. The thermodynamic components would be Cr and Cr_2O_3. There are only three phases involved at equilibrium; thus, as the reaction is described, there would be zero degrees of freedom. The oxygen that is dissolved in the Cr can be considered as dissolved oxide just as a hypo-stoichiometric Cr_2O_3 (i.e., Cr_2O_3) can be viewed as Cr dissolved in Cr_2O_3. Therefore, the Cr-Cr_2O_3 system is a simple binary eutectic system. More generally, eutectic-like reactions between a metal and its oxide are purely binary eutectic.

For the oxide-metal combinations of most interest in this study, the oxide is not an oxide of the metal; e.g., L → Cr_2O_3 + Mo. Again, two thermodynamic components are first considered, Mo and Cr_2O_3, and there are three phases just as with the Cr-Cr_2O_3 equilibrium. Likewise, there is no difficulty in assuming that Mo can be dissolved in the oxide to

some small extent by some substitution or interstitial mechanism without disturbing charge neutrality. Also, it is clearly possible to have oxygen and chromium dissolved in Mo at the ratio of Cr/O = 2/3. But it is just as possible to have more or less Cr or O dissolved in the Mo such that the ratio would not be Cr/O = 2/3. This means that it is certainly possible for there to be a $L \rightarrow Cr_2O_3 + Mo$ binary eutectic equilibrium with zero degrees of freedom. However, it is more likely that there is either excess Cr or O dissolved in the Mo-phase such that a new component must be named making the system ternary and the reaction a pseudo-binary eutectic type.

2.3 Composition Control of Oxide-Metal Melts

In directional solidification the control of the composition of the eutectic composite structure is very dependent upon how well the composition of the liquid can be controlled. For the oxide-metal eutectic and pseudo-binary eutectic systems considered in this investigation, the liquid is basically an oxide melt (with excess dissolved metal) which is exposed to a gaseous crystal growth environment. Therefore, the partial oxygen pressure of the gases surrounding the oxide melt will greatly influence the oxygen activity of the melt. The extent to which the oxide melt composition can be controlled or maintained by the gaseous crystal growth environment will now be probed.

The gases in the crystal growth environment must provide a partial oxygen pressure which must be reducing to all oxides of the metallic phase and all higher oxides of the oxide phase. The gases must also be of a sufficient partial oxygen pressure not to reduce the desired oxide phase.

For temperatures below the eutectic temperature, the problem of calculating partial oxygen pressures that can be tolerated in a binary system is made simple when solid solubilities of B in α and A in β are extremely low. The condition of extremely low solubilities makes it a good approximation to treat α like pure A and β like pure B. When this approximation can be made, tables or graphs of standard free energies of formation can be used to calculate equilibrium oxygen pressures for the pure oxide and the stablest oxide of the metal phase.

In other words, when the activities of the condensed phases are approximately unity, the partial oxygen pressure is a simple function of temperature and the standard free energy of formation of the oxide at the temperature considered. Thus, for the reaction $\frac{2x}{y} M + O_2 \rightarrow \frac{2}{y} M_xO_y$

$$P_{O_2} = e - \frac{\Delta G_f^\circ}{RT}$$

where R is the ideal gas constant, T is the temperature, and ΔG_f° is the standard free energy of formation of $\frac{2}{y}$ moles of the oxide M_xO_y at temperature T.

In order to accurately extend these calculations above the eutectic temperature two additional considerations must be met. The first consideration is that for temperatures above the eutectic temperature and below each pure melting point, the standard free energies of formation provided in tables and graphs do not reflect the change of state from crystalline to liquid. Secondly, the activities of components considered to be in the melt are no longer unity. Each of these conditions should cause a divergence in the range of oxygen partial pressures necessary to assure stability of the desired oxide and metal components. That is to say, for the mixture M' and M_xO_y, $M'(s) \rightarrow M'_{(\ell)}$ increases the ΔG_f° for the

reaction $\frac{2x}{y} M'_{(\ell)} + O_2 \rightarrow \frac{2}{y} M'_x O_{y(s)}$, and $M_x O_{y(s)} \rightarrow M_x O_{y(\ell)}$ decreases the ΔG_f° for the reaction $\frac{2x}{y} M_{(s)} + O_2 \rightarrow \frac{2}{y} M_x O_{y(\ell)}$. Also, for the reaction $\frac{2x}{y} M'_{(\ell)} + O_2 \rightarrow \frac{2}{y} M'_x O_{y(s)}$

$$P_{O_2} = \frac{1}{(a_{M'})^{2x/y}} \exp \frac{-\Delta G_f^\circ}{RT}$$

where $a_{M'(\ell)} < 1$, thus increasing P_{O_2}; and, for the reaction $\frac{2x}{y} M_{(s)} + O_2 \rightarrow \frac{2}{y} M_x O_{y(\ell)}$

$$P_{O_2} = [a_{M_x O_{y(\ell)}}]^{2/y} \exp \frac{-\Delta G_f^\circ}{RT},$$

where $a_{M_x O_{y(\ell)}} < 1$, thus decreasing P_{O_2}. Figure 11 shows the approximate total effect. For all practical purposes an extrapolation of the calculations for the condensed phases should be sufficient for determining the range of useful oxygen partial pressures for the $M' + M_x O_y$ eutectic system.

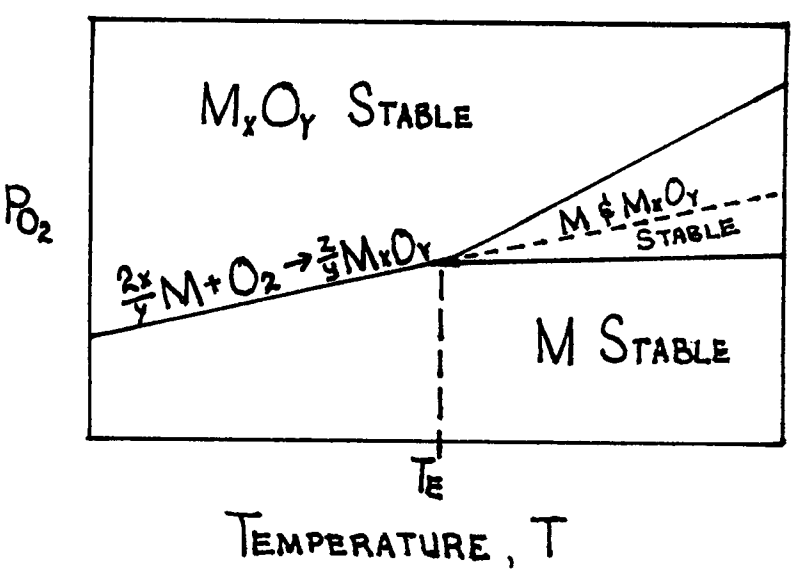


Fig. 11. Increasing Range of $M + M_x O_y$ Stability Due to Solution Formation at $T > T_E$.

In order to calculate the oxygen partial pressures that would be required for fixing the activity oxygen in the oxide liquid to correspond to the pseudo-binary eutectic or monovariant compositions of $L \rightarrow Cr_2O_3 +$ Mo(Cr), a thermodynamic model for the oxide liquid is required.

The simplest, sometimes called the zeroth order, approach for describing a nonideal solution is obtained by treating it as a "regular solution" [38,39]. A binary AB solution which obeys the equations

$$RT\ell n\gamma_B = \alpha' X_A^2 \text{ and}$$

$$RT\ell n\gamma_A = \alpha' X_B^2 \qquad (1)$$

where α' is a constant is termed regular. Equation (1) stems from a generalized power series of the activity coefficients of A and B.

$$\ell n\gamma_A = \alpha_1 X_B + \frac{1}{2}\alpha_2 X_B + \frac{1}{3}\alpha_3 X_B^2 + \ldots \text{ and}$$

$$\ell n\gamma_B = \beta_1 X_A + \frac{1}{2}\beta_2 X_A + \frac{1}{3}\beta_3 X_A^2 + \ldots$$

Substitution of these equations into the Gibbs-Duhem equation, $X_A d\ell n_{\gamma A} = -X_B d\ell n_{\gamma B}$, yields $\alpha_1 = \beta_1 = 0$. If all terms beyond the quadratic term are neglected, then $\frac{1}{2}\alpha 2 = \frac{1}{2}\beta 2 = \frac{\alpha'}{RT}$. The basic nature of the solution thermodynamics at this point is that ℓn_{γ_i} is a quadratic function of X_j and that there is a compositional independence of α'. A more physical interpretation of the regular is given next which will prove useful to help provide values for α'.

Hildebrand defines a regular solution as one which has a non-zero heat of mixing and an ideal entropy of mixing.

Thus, $\Delta G^M = \Delta G^M$, ideal + ΔH^M

$$= RT\ (X_A \ell n a_A + X_B \ell n a_B)$$

$$= RT\ (X_A \ell n X_A + X_B \ell n X_B) + RT\ (X_A \ell n \gamma_A + X_B \ell n \gamma_B)$$

where

$$\Delta H^M = RT\ (X_A \ell n \gamma_A + X_B \ell n \gamma_B) \quad .$$

Recalling that $RT\ell n\gamma_B = \alpha' X_A$ and

$$RT\ell n\gamma_A = \alpha' X_B^2, \text{ then}$$

$$\Delta H^M = \alpha' X_A X_B$$

which is noticeably independent of temperature. Since the "nearest neighbor" model of a binary solution gives a very physical interpretation of the term ΔH^M, it will provide a simple model to help in understanding and selecting α' values.

In the "nearest neighbor" or quasi-chemical model a term called excess heat of mixing, defined as $\Delta H^M - \Delta H^{ideal}$, is thought of as the energy of the sum of the A-A, B-B, and A-B nearest neighbors in a binary solution. The characteristic nearest neighbor interaction energy, E, is written

$$E = E_{AB} - \frac{1}{2}(E_{AA} + E_{BB})$$

where E_{AA}, E_{BB}, and E_{AB} are the potential energies of the interactions. The probability treatment of a 50 atom % solution gives for the enthalpy of solution formation

$$\Delta H^M = ZN_o E X_A X_B$$

where Z is the coordination number of the atoms in the solution and N_o is Avogadro's number. So that

$$\alpha' = Z N_o E .$$

In the quasi-chemical model, $E = 0$ if the solution is ideal, $E < 0$ if ordering is the general tendency of the solution, and $E > 0$ if clustering is the tendency. Thus, $\alpha' = 0$ if the solution is ideal, α' is negative if ordering or compound formation tends to occur, and α' is positive if phase clustering or liquid-liquid immiscibility tends to occur.

An exact value for α' can also be obtained for regular binary systems if an immiscibility exist. From the criterion of phase stability, a critical value of α' exist at the temperature below which a homogeneous solution becomes unstable and phase separation occurs. The critical value of α' is that which makes $\partial^2 \Delta G^M / \partial X_B^2$ and $\partial^3 \Delta G^M / \partial X_B^3$ simultaneously equal to zero at the composition of the miscibility gap temperature maxima. When the miscibility is symmetric with respect to composition ($X_A = X_B = 0.5$), $\alpha' = 2RT_c$ where T_c is the miscibility gap temperature maxima (phase separation occurs for values of $\alpha' > 2RT_c$). Thus, the critical value of α' for phase separation and $\alpha' = 0$ for ideal systems are two exact values of α' which can be used to estimate ΔH^M.

From the phase rule discussion it was concluded that for two phase systems of the type M'-M_xO_y where $M' \neq M$, ternary treatment of components would be necessary in defining compositions. For a regular solution the excess enthalpy, ΔH^M, can be written as

$$\Delta H^M = X_B X_B \alpha'_{AB} + X_A X_C \alpha'_{AC} + X_B X_C \alpha'_{BC} . \qquad (2)$$

Thus, if the α' values of the three binary systems which join to bound the ternary ABC system are known or can be estimated, a value of ΔH^M can be calculated for any ternary composition.

Activities can be determined as a result of the following relationships and conditions:

$$\left(\frac{\partial \Delta G^{xs}}{\partial X_A}\right) = RT\ell n\gamma_A$$

for ideal configurational entropy

$$\left(\frac{\partial \Delta G^{xs}}{\partial X_A}\right) = \left(\frac{\partial \Delta H^M}{\partial X_A}\right)$$

giving

$$\left(\frac{\partial \Delta H^M}{\partial X_A}\right) = RT\ell n\gamma_A \; . \qquad (3)$$

From Eq. (2) and Eq. (3)

$$RT\ell n\gamma_A = \alpha'_{AB}X_B(X_B + X_C) + \alpha'_{AC}X_C(X_B + X_C) - \alpha'_{BC}X_BX_C \; .$$

Thus,

$$a_A = \frac{X_A}{RT} \exp\left[\alpha'_{AB}X_B(X_B + X_C) + \alpha'_{AC}X_C(X_B + X_C) - \alpha'_{BC}X_BX_C\right] \; .$$

The discussion of the regular solution model was begun in order to obtain relationships which will make it possible to calculate an equilibrium partial oxygen pressure for a three component oxide melt which upon freezing will yield the desired two phase oxide-metal pseudo-binary eutectic. This is now possible for a system such as is given in Fig. 10. The following approach should result in the P_{O_2}-composition relationships desired:

First, α' values are estimated for each binary system forming the boundaries of the M'-M-M_xO_y ternary system. Next, the ΔG_f° is calculated for the reaction $\frac{2x}{y} M + O_2 \rightleftharpoons \frac{2}{y} M_xO_y$ at the approximate temperature for the $L \rightarrow M'(M) + M_xO_y$ pseudo-binary eutectic reaction at the approximate temperature of the solidifying interface. Using calculated or estimated values for ΔG_f°, $\gamma_{M_xO_y}$, γ_M and $X_{M_xO_y}$ in the equation

$$\Delta G_f^\circ = -RT\ell n \frac{(a_{M_xO_y})^{2/y}}{P_{O_2}(a_M)^{2x/y}}, \qquad (4)$$

a relationship between P_{O_2} and X_M is established.

In summary, if M_xO_y, M and M' are specified as the components of a pseudo-binary eutectic (monovariant) reaction or a ternary eutectic reaction, Eq. (4) can be used to calculate the equilibrium partial oxygen pressure for the liquid phase at a temperature near the freezing temperature. The same equation can be used to determine the equilibrium melt composition that would be obtained by melting a specific amount of M_xO_y and M' at a fixed partial oxygen pressure. Thus, by using the regular solution model the relationship between the partial oxygen pressure for composite growth from a particular liquid composition can be calculated. However, it must be remembered that the regular solution model is very approximate for most real systems even though most of the assumptions required in its development seem to be well suited to the oxide-metal eutectic systems being considered.

2.4 Calculation of Cr_2O_3-Mo Melt Composition as a Function of P_{O_2}

Assuming that the solubility of Cr_2O_3 in solid Mo and the solubility of Mo in solid Cr_2O_3 is practically negligible, the chemical activity of the solid Mo phase and the solid Cr_2O_3 phase will be taken as unity when only the binary Cr_2O_3-Mo system is considered (the standard state for each component is defined as the pure, solid substance). The parallel assumption will be made for the Cr_2O_3-Cr binary system. And, Raoult's law will be assumed for the activities in the Cr-Mo binary system. Thus, the free energies of the condensed components in the Cr_2O_3-Mo-Cr ternary can be well defined using the regular solution model since the model requires that only the three binary relationships be known to predict ternary relationships.

In order to use the regular solution model to describe the free energy of mixing of the oxide melt, the α' parameters of Eq. (2) must be obtained for each binary system. For the Cr-Mo and Cr_2O_3-Cr systems this is straightforward. Since the Cr-Mo phase diagram indicates the near ideality (i.e., Raoultian behavior) of the mixture, the α' parameter is zero and the free energy of mixing is ideal. Critical temperature of the immiscibility in the Cr_2O_3-Cr system is estimated by extrapolation to be near 2100°C. Since $\alpha' = 2RT_c$, the α' parameter is calculated to be approximately 9600 calories per mole for the Cr_2O_3-Cr binary system.

Obtaining an α' parameter for the Cr_2O_3-Mo eutectic system is much more speculative than either the Cr_2O_3-Cr or Cr-Mo binaries since a phase diagram has not been determined. The eutectic temperature is believed to be approximately 1940°C and melts of compositions as rich in Mo as 40 mole % have shown no immiscibility of the components in the liquid [40].

Thus, α' parameter for Cr_2O_3-Mo is less than or equal to approximately 8900 calories per mole, the value obtained by using the eutectic temperature for T_c in the equation $\alpha' = 2RT_c$. Since it is reasonable to expect that the tendency for the Mo and Cr_2O_3 components to cluster and form immiscible liquid phases similar to the Cr-Cr_2O_3 system, the value of α' for the Cr_2O_3-Mo binary will be taken as the phase relationships between Cr-Mo and Cr_2O_3-Cr.

Since it is reasonable to expect that the tendency for the Mo and Cr_2O_3 components to cluster and form immiscible liquid phases would be similar to the Cr_2O_3-Cr system, an approximate value of 10 Kcal/mole will be used for the α' for both binary systems.

The phase relationships between Cr-Mo, Cr_2O_3-Cr and Cr_2O_3-Mo clearly suggest the character of the ternary system, particularly between the Cr_2O_3-Cr and Cr_2O_3-Mo eutectics. Because of the Raoultian behavior of the Cr-Mo binary, the immiscibility in the Cr_2O_3-Cr binary system is not expected to protrude very deeply into the ternary field, thus allowing a monovariant trough to exist between the Cr_2O_3-Cr and Cr_2O_3-Mo eutectics. A view of the liquids surface of this proposed phase diagram is given in Fig. 12. The eutectic composite formed from a melt of composition near the monovariant trough would be expected to be Cr_2O_3 with fibers or possibly plates of a Mo-Cr solid solution alloy. Thus, the problem will be how to control the melt composition in order to synthesize a proposed Cr_2O_3-Mo(Cr) pseudo-binary eutectic composite. That is, what partial oxygen pressure is required to be in equilibrium with the melt so as not to have the activity oxygen too high thus reducing the activity of chromium in the melt or too low causing an increase in the activity chromium

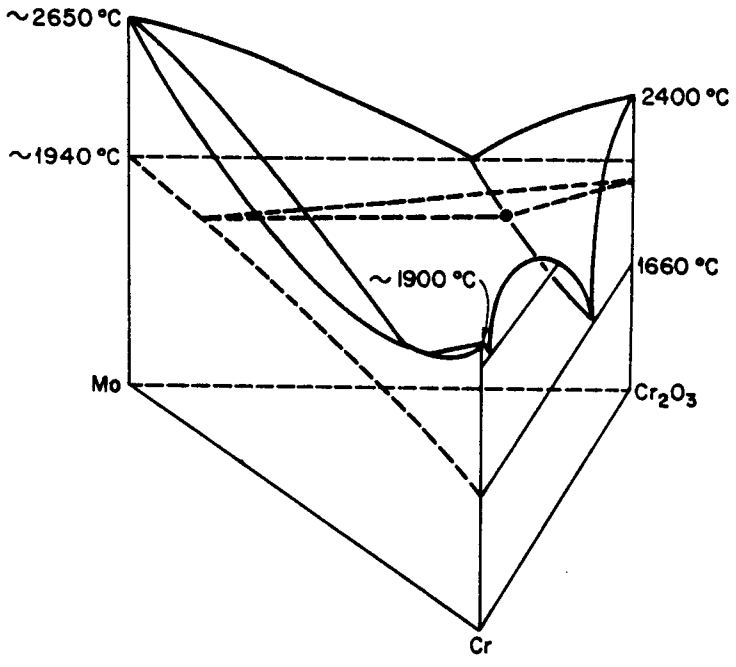


Fig. 12. Approximated Cr-Mo-Cr_2O_3 Phase Diagram Depicting Pseudo-Binary Mo(Cr) + Cr_2O_3 Eutectic System.

in the melt. A solution is obtainable using the regular solution model to calculate the activity coefficients needed in Eq. (4), which is rewritten for the Cr_2O_3-Cr equilibrium as:

$$\Delta G_f^\circ = -RT\ell n \frac{(a_{Cr_2O_3})^{2/3}}{P_{O_2}\ (a_{Cr})^{4/3}} \ . \qquad (5)$$

Example P_{O_2} calculations for Cr_2O_3-25 mole % Mo initial mixture resulting in metallic fibers of Mo-3, 5, 10 and 20 mole % Cr are given in Appendix D.

The relationships given by the regular solution treatment to obtain activity coefficients from Eq. (5) and the predicted Cr_2O_3-Mo-Cr phase diagram (Fig. 12) imply that a reduction in partial oxygen pressure should increase the chromium content of the melt. Even if the inital

mixture were of pure Cr_2O_3 and pure Mo, Cr would be won from the oxide component to be present in solid solution in the metallic phase. Calculations similar to that given in Appendix D could be made for any gas mixture giving partial oxygen pressures within the limits of component stability (recalling Fig. 6) with the result being the predicted Cr content of the resulting metal fiber.

3.0 Eutectic Solidification

3.1 Eutectic Growth Theories

Figure 13 shows schematically a simple binary eutectic phase diagram. The singularity on the liquidus is the so-called eutectic point (eutectic being derived from the Greek word eutektos, meaning easily melted). When a liquid of eutectic composition is solidified, both the α- and β-phases

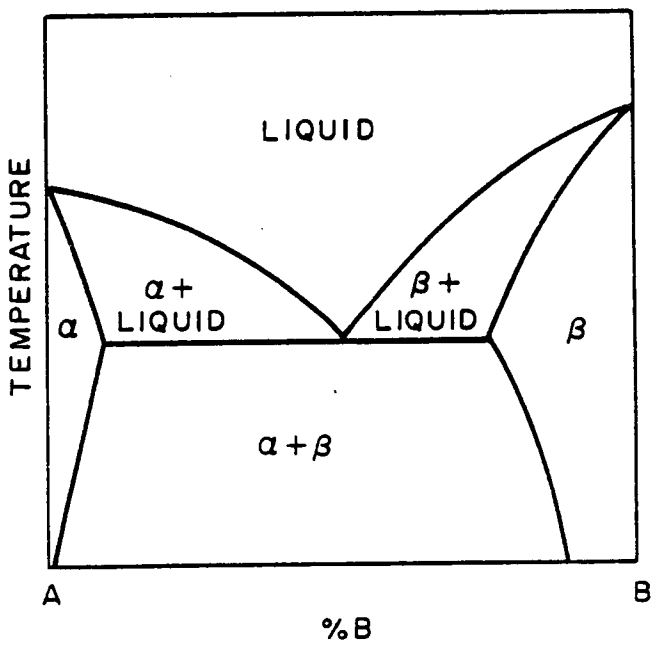


Fig. 13. Typical Binary Eutectic System.

grow simultaneously. Similar to the freezing of a pure element or stoichiometric compound, the eutectic reaction occurs without a change in the liquid composition except for the lateral segregation of A and B atoms at the freezing interface. The near equilibrium freezing of compositions off eutectic, but not rich enough in A or B to produce only the single-phase α or β solid solutions, results in α or β primary structures surrounded by a eutectic structure. In general, off-eutectic compositions form most alloys of commercial importance. Also, in the non-equilibrium but steady-state sense of directional solidification, the localized compositions in both the liquid and solid do not change with time; and under certain conditions, controlled solidification of off-eutectic alloys produces eutectic-like microstructures without equilibrium primary phases.

In 1922, Brady [41] reported that eutectic-like structures could be solidified from compositions on either side of an equilibrium eutectic point. Koffer [42], investigating organic eutectic systems, designated the terms "coupled region" or "coupled zone" to mean the range of compositions near the eutectic composition from which eutectic structures could be grown at sufficient undercoolings. Using binary metal alloys, Scheil [43] demonstrated the growth of eutectic structures from off-eutectic compositions at undercoolings below the metastable extensions of the liquidus lines on the phase diagram (see Fig. 14). The "coupled zone," i.e., region of coupled growth, was hypothesized to extend on both sides of the eutectic point for very low undercoolings in absence of constitutional supercooling. Mollard and Flemings [44], using Jackson

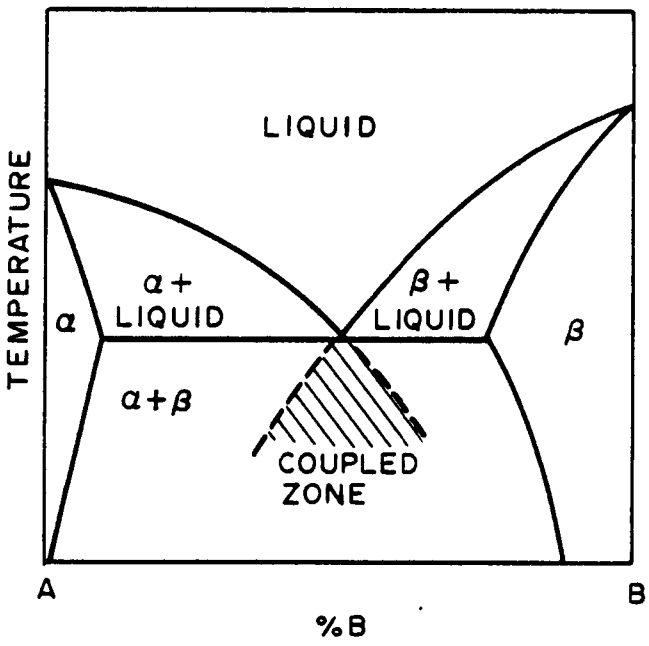


Fig. 14. Region of Coupled Growth Predicted by Metastable Extensions of Liquidus Lines.

and Hunt's [45] expression for the concentration profile preceding a planar eutectic solid-liquid interface in the absence of convection in the liquid, i.e.,

$$\frac{C - C_o}{C_E - C_o} = e - R_x/D \ , \tag{6}$$

derived the important constitutional supercooling criterion:

$$G/R \geqslant \frac{m(C_E - C_o)}{D} \tag{7}$$

where

x = distance into the liquid from the solidification interface,

C = liquid composition at x,

C_O = bulk composition,

C_E = eutectic composition,

R = growth rate,

D = chemical diffusion coefficient,

G = thermal gradient into the liquid at the interface, and

m = liquidus slope for C_0 measured at the eutectic point.

The chief assumptions necessary in considering the solute distribution in the liquid described by Eq. (6) are: (a) the liquid composition at the freezing interface is approximately of the eutectic composition, (b) the distance of lateral redistribution of solute atoms at the interface is much less than the distance of solute redistribution normal to the interface, and (c) that $C_E - C_0 \simeq 0$. Mollard and Fleming's planar interface stability criterion is basically the same as that for single-crystal growth [46] i.e.:

$$G \geqslant m \left(\frac{dC}{dx}\right)_{x=0} \tag{8}$$

The value of m in Eq. (8) corresponds to that at the eutectic point, regardless of the liquidus shape. Thus, the thermal gradient in the liquid at the freezing interface must equal or exceed the constitutional gradient (defined by the slope of the redistribution profile) in order to avoid being constitutionally supercooled which results in the consequential breakdown of a planar solidification interface. Mollard and Flemings' constitutional supercooling criterion affords remarkably good first-order predictions for binary metallic eutectic systems. Their treatment has been extended to ternary [47,48] and quaternary [49] eutectic systems and produced good first-order predictions for coupled growth. The combination of the high undercooling achieved at high growth rates and avoidance of constitutional supercooling at low growth rates greatly

extends the conditions under which eutectic-like microstructures can be achieved in off-eutectic compositions in eutectic systems.

A more involved analysis which treats the freezing interface as a perturbed sinusoidal wave is given by Mullins and Sekerka [50] where time dependent perturbation analysis is used to derive steady-state solutions for dilute binary single crystal growth. Cline [51] has used the technique of Mullins and Sekerka to predict the region of coupled growth at low undercoolings for eutectic systems. The theoretical sophistication introduced by Cline was, first, to take the steady-state equations of Jackson and Hunt [45] and use a sinusoidal perturbation in the shape of the interface to test for stability. This method allows a consideration of both mass and thermal diffusion and does not require that the melting point of the bulk alloy describe the melting point of the solidifying phases as in the simple constitutional supercooling criterion. Cline's analysis predicted a stable eutectic structure along with a range of compositions that may be called a range of "absolute stability." This was also predicted by Sekerka's analysis, i.e., the eutectic structure is the most stable structure of these off-eutectic compositions. Figure 15 compares Cline's predictions with those produced by the constitutional supercooling treatment and the experimental results of several investigators for Pb-Sn alloys [44,47].

A theory of eutectic growth (i.e. coupled growth of α- and β-phases) usually called the competitive growth theory has been suggested by Hunt and Jackson [52]. The basic premise of the competitive growth theory is that dendritic growth which requires longer diffusion distances of rejected components of the melt needs a greater undercooling than does eutectic growth where there are only short lateral diffusion distances.

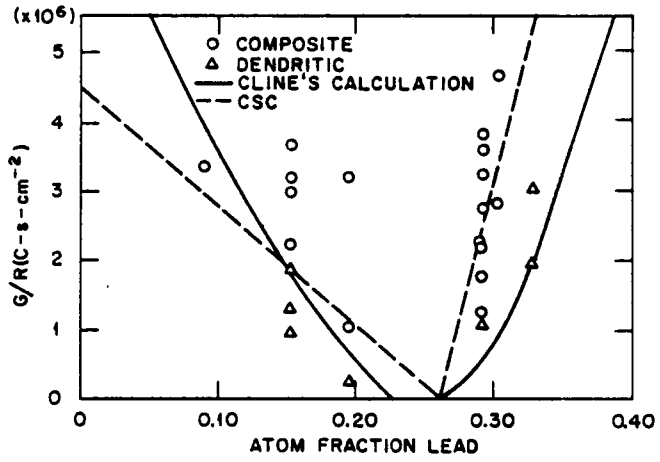


Fig. 15. Cline's Predictions Compared with Calculations Using Mollard and Fleming's Constitutional Supercooling Criterion, CSC, and with Holder and Oliver's Experimental Data for Pb-Sn.

It is therefore possible to hypothesize that sufficiently high growth rates would favor eutectic growth at practically any composition in the eutectic range [67,68].

If some mechanism should be present which would cause the temperature dependence of the growth rate of one phase to be markedly different from the other, asymmetry of the coupled zone could result. For instance, if the β-phase is faceted, a larger undercooling for eutectic growth and still larger undercooling for β-dendrite growth would be required. If the α-phase is non-faceted, a marked asymmetry would occur as described in Fig. 16(a).

Until an acceptable (meaning both usuable and general) description of dendritic growth is available, the competitive growth theory is at

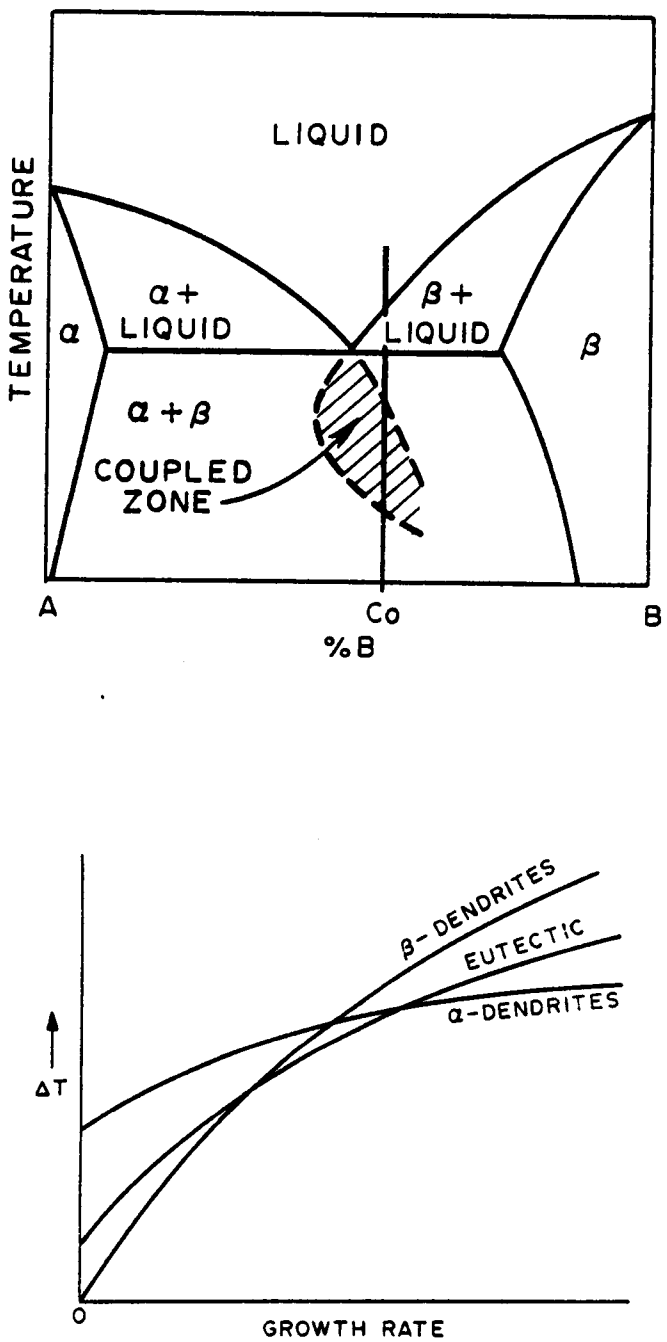


Fig. 16. (a) Asymmetric Region of Coupled Growth Due to Facetting of β-Phase (b) Undercooling vs Growth Rate Qualitatively Predicted for Composition Co in (a).

best only qualitative; i.e., curves such as Fig. (16) cannot be calculated a prior i as yet. Even though qualitative, the ideas of competitive growth should prove useful in discerning the nature of the coupled growth observed in non-metal-metal eutectic solidification; i.e., carbide-metal, boride-metal, nitride-metal, and of particular interest in this study, oxide-metal eutectic solidification.

3.2 Extremum Growth

It should be pointed out that the basis of the constitutional supercooling theories of Mollard and Flemings and Cline, as well as of competitive growth theory, is Jackson and Hunt's solution to the diffusion equations describing the isothermal interface conditions during coupled growth. This work of over a decade ago still undoubtedly offers the best description of the phenomenon of eutectic growth. In addition to the diffusion equations, their analysis yielded extremum eutectic growth conditions similar to what Zener [53] had predicted for the growth of pearlite from austenite in the Fe-C eutectic system.

Using solutions of these diffusion equations and the free-energy parameters for the α-phase-liquid, β-phase-liquid and α-β-interfacial reaction, the average interface undercooling, ΔT, can be calculated. An approximate solution was found to be:

$$\frac{\Delta T}{m} = R\lambda Q^L + \frac{aL}{\lambda} \qquad (9)$$

where R is the growth rate, λ the interlamellar spacing across an α and β lamellar pair, and m, Q^L, and a^L are constants. Of particular importance is the parameter Q^L, which reflects the liquidus slope for each phase and

is a function of α-β spacing, volume fraction, and average chemical diffusion coefficient. The parameter a^L is determined by the volume fraction, liquidus gradients, and interfacial energies of the system.

The values of λ and ΔT in Eq. (9) are not unique for a given value of R. Thus, a logical approach to evaluate its physical significance is to optimize a chosen variable in the equation; e.g., solve Eq. (9) for the condition of growth at a minimum ΔT. This embodies the assumption of a maximum growth rate for a given λ at a constant ΔT. One thus finds the extremum growth conditions to be:

$$\lambda^2 R = \text{constant, or}$$

$$\Delta T \lambda = \text{constant, or}$$

$$(\Delta T)^2 R = \text{constant;}$$

i.e., $(1/\lambda)^2$ and $(\Delta T)^2$ are proportional to R and ΔT is inversely proportional to λ. The merit of assuming a condition defined by a minimum of undercooling has been often confirmed during consideration of unidirectional solidification of binary, ternary, and quaternary metallic eutectic systems [47–49,54–56]. There is no reason to suspect that the same behavior will not also be valid for non-metal-metal eutectic systems such as those having oxide and metal components.

3.3 Internal Zone Growth and Skull Melting

Faced with the need to produce single crystals of UO_2 for testing for reactor fuel cells, A. T. Chapman and G. W. Clark developed a modified, radio frequency, vertical zone growth process which they called

internal centrifugal zone growth (ICZG) [57]. As the name implies, the molten zone is internal and contained by an unmelted outer surface of the sample.

The basic idea of Chapman and Clark drew on the two properties of UO_2 (and most other refractory oxides) which usually make crystal growth difficult, if not impossible; i.e., extremely high melting point and a large dependency of electrical conductivity on temperature. They chose a radio frequency which would result in efficient Rf-heating in a 1-cm rod of UO_2 at its melting point, then relied on the extreme temperature of the outer surface of the sample to have sufficient radiant heat losses to maintain a solid surface. The low thermal conductivity of the oxide was expected to allow a substantial temperature difference to exist between the oxide melt and the outer surface of the cylindrical sample. As a complementary part of the mechanism of maintaining an internal molten zone, it was hypothesized that due to the lower surface temperature of the unmelted wall, its electrical conductivity would be too low to efficiently couple to the Rf-field and there not be significantly heated.

Chapman and Clark's insight was accompanied by a great amount of good fortune. The size of the sintered, cylindrical compact of UO_2 was practically from the beginning perfectly matched to the range of radio frequencies available to them. And the addition of W to the UO_2 compacts from which the UO_2-W eutectic composites were grown did not alter the electrical and thermal properties sufficiently to require any change in the crystal growth process developed for UO_2. However, it was not until the mathematical modeling of ICZG by R. A. Hartzell and R. F. Sekerka [21,22] that the complicated interplay of melting point, electrical

conductivity dependence on temperature, thermal conductivity, radio frequency, Rf-coil design, and sample size was realized.

Hartzell and Sekerka's work was concurrent with the early attempts to grow the Cr_2O_3-Mo eutectic composites [40]. In fact, much of the success in producing directionally solidified Cr_2O_3-Mo composites is due to their description of an Rf-heating instability inherent in materials which have a strong temperature-dependent electrical conductivity. Hartzell and Sekerka calculations predicted that given certain conditions ICZG might be practically impossible due to Rf-heating instabilities.

The heating instability is produced when the Rf-heating efficiency balanced against heat flow in the sample and radiation heat losses at the sample surface changes dramatically with a relatively small change in sample temperature. This is depicted in Fig. 17 by the curve from point 1 to point 2. A second Rf-heating instability can occur when the sample begins to internally melt causing another rapid increase in electrical conductivity. Points 2 and 3 bound the portion of the curve in Fig. 17 which is calculated for this condition. Figures 18, 19, and 20 give the results of Hartzell and Sekerka's calculations for conditions similar to those supposed for Fig. 17 and compares them to calculations for improved conditions of heating stability brought on by increasing radio frequency, increasing sample diameter, or decreasing the temperature dependence of the electrical conductivity of the material.

Two simple rules for matching radio frequency, electrical conductivity and sample diameter resulted:

$$f_{max} = \frac{16h^2 D}{\pi\sigma\mu k_s} \text{ , and} \tag{10}$$

$$f_{min} = \frac{16 D}{\pi\sigma\mu k_s^2} \text{ .} \tag{11}$$

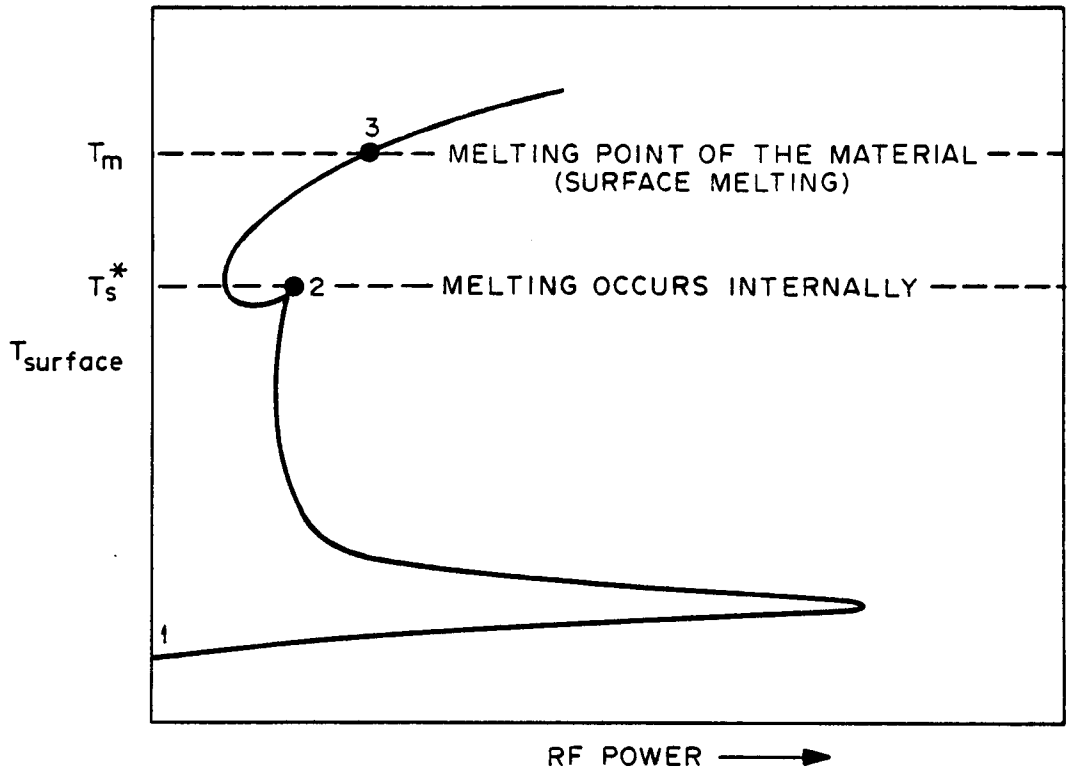


Fig. 17. Heating Instability Calculated by Hartzell and Sekerka for a Rf-Heated Cylinder of Material with an Extremely Temperature Dependent Electrical Conductivity.

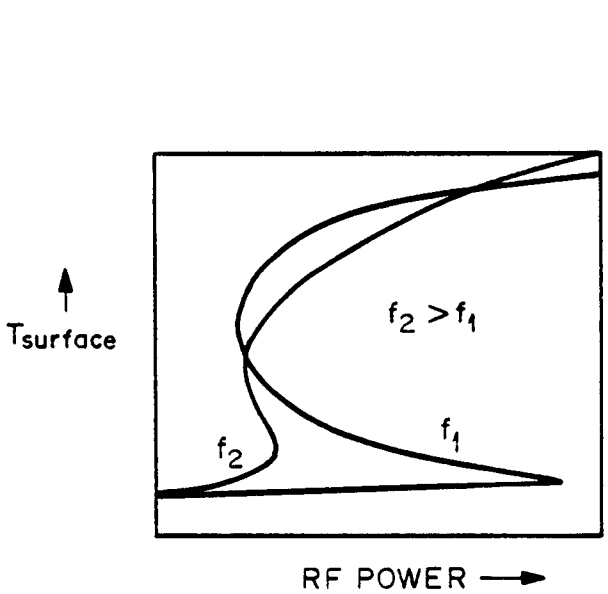


Fig. 18. Effect of Increased Frequency on the Rf-Heating Instability.

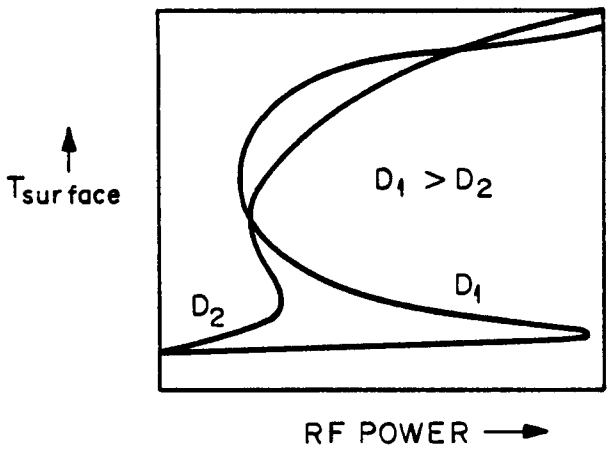


Fig. 19. Effect of Increased Diameter on the Rf-Heating Instability.

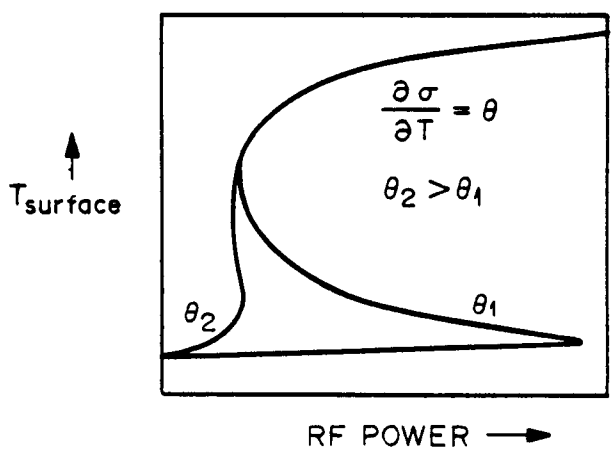


Fig. 20. Effect of Decreased Temperature Dependence of Electrical Conductivity on the Rf-Heating Instability.

D is the diameter of the cylindrical sample, h is a surface cooling coefficient which is proportional to the melting temperature cubed, σ and k_s are the electrical conductivity and thermal conductivity, respectively, of the solid near the melting temperature, and μ is the magnetic permeability. A stable, internal molten zone should be achieved at frequencies within the f_{max} and f_{min} calculated using Eqs. (10) and (11). The usefulness of Hartzell and Sekerka's simple rules is found in helping the experimentalist grasp the first order relationships of sample character and radio frequency. For example, if the frequencies available are restricted, then by increasing the diameter the minimum frequency restriction is reduced as indicated by Eq. (11). Unlike Eq. (11), the parameters in Eq. (10) are for the most part not varable if using the IZG technique. Equation (10) gives the restrictions for avoiding melt loss due to surface melting and Eq. (11) gives the conditions for avoiding melt loss due to the Rf-heating instabilities.

The technique of skull melting or cold crucible melting is also employed in this investigation. Skull melting was first introduced by the Soviets in 1973 for the production of large single crystals of refractory oxides [58]. Internal zone growth is in many ways similar to this technique. The material is melted by Rf-heating and, during slow cooling — usually achieved due to the large mass of the material being processed, large grains are produced which are separated and used in single crystal studies and for gem stones. In skull melting the unmelted wall (the skull) is maintained by conductive heat removal through watercooled fingers surrounding the charge. The bottom of the crucible, also watercooled, and the fingers are arranged so as to suscept as little of the Rf-field as possible. Figure 21 illustrates the design of the

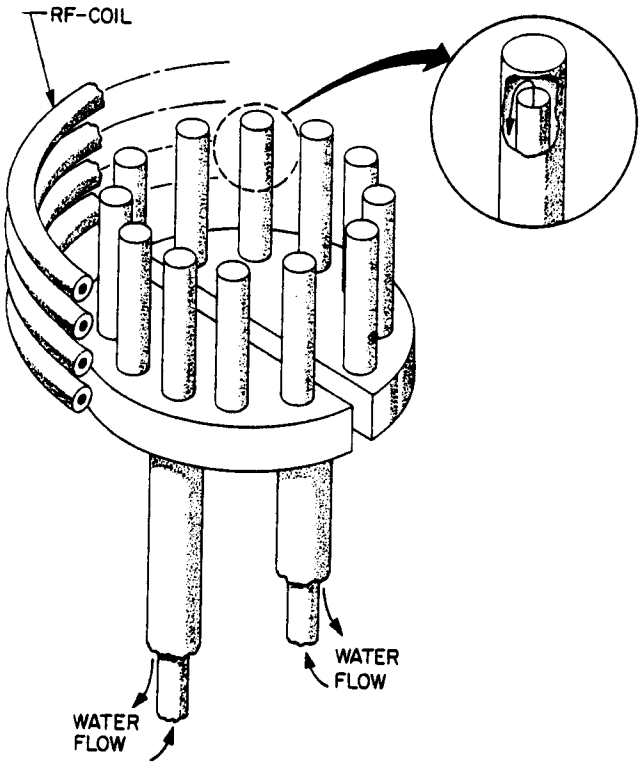


Fig. 21. Sketch of Commercially Available Cold Crucible Apparatus.

conventional cold crucible commercially available for skull melting today [59]. Most of the problems inherent with ICZG are also encountered in skull melting with the major exception of surface melting. The problems of surface melting have been eliminated by using the cold crucible apparatus thus allowing a working frequency in excess of the f_{max} of Eq. (10). This is indeed beneficial when due to a small sample diameter the calculated f_{min} is greater than the calculated f_{max} — conditions which would make internal zone growth impossible.

4.0 Soret-Modified Eutectic Constitutional Supercooling Criterion

Since oxide liquids have much lower thermal conductivities than metal liquids, a much higher thermal gradient at the growth interface is

expected to occur for oxide-metal eutectic composite growth. In fact, gradients 10 to 100 times larger than in typical metal-metal eutectic growth by directional solidification are expected to exist in oxide-metal composite growth. The influence of large thermal gradients upon component unmixing and thus upon eutectic-like composite growth must be considered if the eutectic growth theories commonly applied to metal systems are to be extended to the oxide-metal family of eutectic-like composites.

4.1 The Soret Effect

The phenomenon of the partial unmixing of chemical components in a homogeneous liquid phase due to heat flow is commonly called the Soret or the Ludwig-Soret effect [60–62]. For a two-component, one dimensional system in which a concentration gradient and a thermal gradient exist together (without convective mixing), the flow of solvent and solute can be written as [63]:

$$J_A = - DC \left(\frac{dN_A}{dx} + \sigma_A N_A N_B \frac{dT}{dx} \right)$$

$$J_B = - DC \left(\frac{dN_B}{dx} + \sigma_B N_A N_B \frac{dt}{dx} \right) . \qquad (12)$$

The fluxes are expressed in moles per unit area per unit time with respect to a plane across which no net transfer of molecules occur. N_A and N_B are the mole fractions of components A and B, respectively. C is the average molar density in moles per unit volume of the two-component system, σ_A and σ_B are the Soret coefficients and D is the chemical diffusion coefficient. It should be noted from Eq. (12) that conservation of mass requires $\sigma_A = - \sigma_B$. By convention σ_i is taken as positive when component i migrates in the direction of heat flow.

Attempts have been made to include the Soret effect in solute redistribution equations for the directional solidification of dilute binary alloys [23,24] and binary eutectic alloys [25]. In each earlier analysis the flux equation for component i, when written in the form of Eq. (12), is:

$$J_i = - DC \left(\frac{dN_i}{dx} + \sigma_i N_i \frac{dT}{dx} \right) . \tag{13}$$

Equation (13) is appropriate only for the special case of very dilute alloys where $(1 - N_i) \simeq 1$ [63]. Since this is not the case for most of the eutectic systems of interest, a more general derivation of the constitutional supercooling criterion using the Soret flux term as it appears in Eq. (12) is considered.

4.2 Soret-Modified Solute Redistribution Equation

Fick's second law for one-dimensional diffusion in a two-component liquid can be written as:

$$\frac{dC_B}{dt} = - \frac{dJ_B}{dx} . \tag{14}$$

Equation (14) can be written to include mass flow due to chemical diffusion and the Soret effect as given in Eq. (14) and crystal growth $(J_{B,Growth}) = - RCN_B$, where R is the growth rate in cm/s). This generalization gives:

$$\frac{dC_B}{dt} = DC \left(\frac{d^2 N_B}{dx^2} + \frac{R}{D} \frac{dN_B}{dx} + \sigma_B (1 - 2N_B) \frac{dN_B}{dx} \frac{dT}{dx} \right) . \tag{15}$$

At steady state, $dC_B/dt = 0$, and for a constant thermal gradient, G, Eq. (14) reduces to:

$$\frac{d^2 N_B}{dx^2} + \left(\frac{R}{D} + \sigma_B G - 2\sigma_B G N_B\right) \frac{dN_B}{dx} = 0 \ . \tag{16}$$

If we define $Z = R/D + \sigma_B G - 2\sigma_B G N_B$, Eq. (16) becomes:

$$\frac{d^2 Z}{dx^2} + Z \frac{dZ}{dx} = 0 \ . \tag{17}$$

Equation (17) is solved using the boundary conditions suggested by Mollard and Flemings [44]; i.e., the liquid is approximately eutectic composition at the solid-liquid interface and is bulk composition far out into the melt. These boundary conditions can be written $Z = Z_E$ at $x = 0$ and $Z = Z_o$ at $x = \infty$

where

$$Z_E = R/D + \sigma_B G - 2\sigma_B G\, N_E \text{ and}$$

$$Z_D = R/D + \sigma_B G - 2\sigma_B G\, N_O \ .$$

In this treatment $x = 0$ is fixed at the moving solid-liquid interface. The solution to Eq. (17) using these boundary conditions gives a Soret-modified expression for the solute redistribution ahead of the solidifying interface:

$$N_B = \frac{1}{2} + \frac{R}{2\sigma_B G_D} - \frac{Z_0}{2\sigma_B G} \frac{1 - \dfrac{(Z_0 - Z_E)\exp(-Z_{0x})}{Z_0 + Z_E}}{1 + \dfrac{(Z_0 - Z_E)\exp(-Z_{0x})}{Z_0 + Z_E}} \ . \tag{18}$$

It should be noted that diffusion in the direction parallel to the solid-liquid interface has not been considered. A discussion of the conditions under which lateral diffusion at the solidification front can be neglected is given by Mollard and Flemings [44].

4.3 Soret-Modified Constitutional Supercooling Criterion

From Eq. (18) the concentration gradient at the solidifying interface $x = 0$, can be written in terms of Z_E and Z_0 as:

$$\left.\frac{dN_B}{dx}\right|_{x=0} = \frac{1}{4\sigma_B G}\left(Z_E^2 - Z_0^2\right) . \tag{19}$$

The interface stability criterion [44] requires that the minimum thermal gradient in the liquid at the solid-liquid interface be equal to the liquidus slope at the eutectic point multiplied by the concentration gradient at $x = 0$; i.e.,

$$G_{minimum} = m \left.\frac{dN_B}{dx}\right|_{x=0} , \tag{20}$$

where m is the liquidus slope with respect to component B in K/mole fraction B. For the hypoeutectic case where $N_0 < N_E$, m will be written as m_α; for the hypereutectic case where $N_0 > N_E$, m will be written as m_β. Therefore, using the constitutional supercooling criterion given by Eq. (20), Eq. (19) is solved for the minimum G/R required to achieve a stable, flat solidifying interface for hypoeutectic and hypereutectic compositions:

$$\left(\frac{G}{R}\right)_{minimum} = \begin{cases} \dfrac{-m_\alpha(N_E - N_0)}{D[1 + \sigma_B m_\alpha(N_E - N_0) - \sigma_B m_\alpha(N_E^2 - N_0^2)]} , & N_0 < N_E \\ \dfrac{-m_\beta(N_E - N_0)}{D[1 + \sigma_B m_\beta(N_E - N_0) - \sigma_B m_\beta(N_E^2 - N_0^2)]} , & N_0 > N_E . \end{cases} \tag{21}$$

It is of prime importance to note that within the validity of the assumptions made in this analysis, the thermal gradient, G, does not appear on

the right-hand side of Eq. (21); i.e., the minimum G/R required to avoid consititution supercooling is not a function of G due to the Soret effect.

By inspection, the minimum G/R calculated from Eq. (21) increases to infinity when:

$$\frac{-\sigma_B m_\alpha (N_E - N_0) + \sigma_B m_\alpha (N_E^2 - N_0^2)}{-\sigma_B m_\beta (N_E - N_0) + \sigma_B m_\beta (N_E^2 - N_0^2)} = 1 \tag{22}$$

The significance of Eq. (22) is revealed when we inquire as to how the solute concentration gradient, Eq. (19), varies with changes in G. To do this Eq. (19) is multiplied by the liquidus slope, m_α or m_β, and then differentiated with respect to G to give:

$$\frac{d\left(m \left.\frac{dN_B}{dx}\right|_{x=0}\right)}{dG} = \frac{-\sigma_B m_\alpha (N_E - N_0) + \sigma_B m_a (N_E^2 - N_0^2)}{-\sigma_B m_\beta (N_E - N_0) + \sigma_B m_\beta (N_E^2 - N_0^2)} . \tag{23}$$

When the right-hand side of Eq. (23) — which is the left-hand side of Eq. (22) — is equal to or greater than one, a change in the thermal gradient produces an equal or greater change in the liquidus temperature gradient at the interface. Hence, Eq. (22) defines the conditions under which the onset of interface instability due to constitutional supercooling cannot be overcome by increasing the thermal gradient to growth rate ratio. Therefore, for the conditions

$$\frac{-\sigma_B m_\alpha (N_E - N_0) + \sigma_B m_\alpha (N_E^2 - N_0^2)}{-\sigma_B m_\beta (N_E - N_0) + \sigma_B m_\beta (N_E^2 - N_0^2)} \geq 1 . \tag{24}$$

Constitutional supercooling cannot be avoided, regardless of the value of G/R. Since the usual magnitude of the Soret coefficients for liquid metals is 10^{-3} to 10^{-2} K^{-1} [63], the conditions of Eq. (24) are very extreme and not likely to occur.

4.4 Comparison to Mollard and Flemings' Calculations

Calculations for the Pb-Sn system using Eq. (21) and Mollard and Flemings' Eq. (14) are compared in Fig. 22. For these calculations $D = 6.7(10)^{-6}$ cm^2/s [44], $\sigma_{Pb} = 3.35(10)^{-3}$ K^{-1} [64], $m_\alpha = -120$ K/mole fraction Pb [44], $m_\beta = 350$ K/mole fraction Pb [65], and $N_E = 0.261$ mole fraction Pb [65].

If we rewrite Eq. (21) as

$$\frac{G}{R} = -\frac{mS(N_E - N_0)}{D} \tag{25}$$

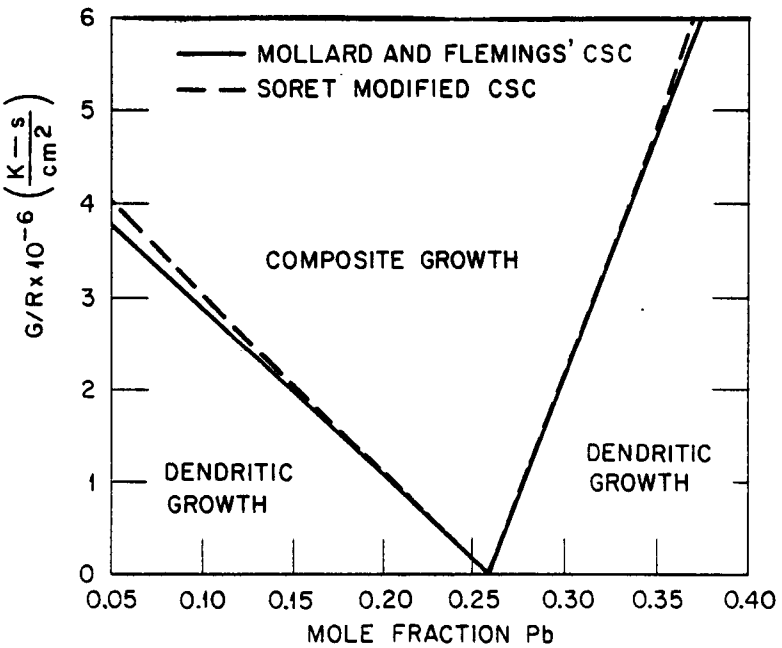


Fig. 22. Comparison of the Soret-Modified Constitutional Supercooling Criterion to Mollard and Fleming's Criterion for the Pb-Sn System.

where $S = [1 + \sigma_B m(N_E - N_O) - \sigma_B m(N_E^2 - N_O^2)]$, the Soret effect can be viewed in terms of a multiplication factor, S. The values of this Soret multiplication factor for the Pb-Sn system are given as a function of N_O, mole fraction Pb, in Fig. 23. When S = 1 there is no Soret effect. When S > 1 the Soret effect increases the minimum G/R required to avoid constitutional supercooling and when S < 1, the minimum G/R is reduced. Conceivably, the Soret effect as given in Eq. (21) could produce the conditions where the minimum G/R would be very small or zero. However, these conditions are extreme and would possibly strain the simple assumptions leading to the derivation of Eq. (21). The symbols used in this discussion are tabulated in Table II.

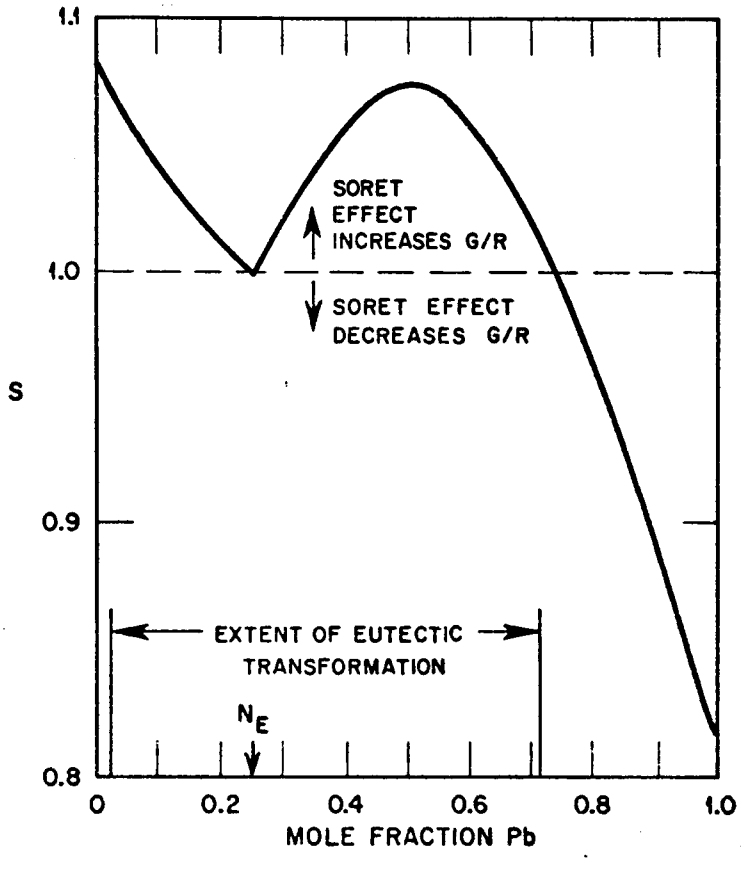


Fig. 23. Calculated Values of Soret Factor, S, for Pb-Sn Alloys.

Table II. Table of Symbols for Soret-Modified Constitutional Supercooling Analysis

t = time, s

x = distance from solidification interface into melt, cm

C = average molar density (moles A + moles B) of melt, moles/cm^3

C_B = liquid composition at x, moles of B/cm^3

N_A = liquid composition at x, mole fraction A

N_B = liquid composition at x, mole fraction B

N_E = eutectic composition, mole fraction B

N_0 = bulk composition, mole fraction B

T = liquid temperature at x, K

G = thermal gradient, dT/dx, in the liquid at x, K/cm

R = solidification rate, cm/s

D = chemical diffusion coefficient, cm^2/s

σ_A = Soret coefficient for component A in A-B liquid, K^{-1}

σ_B = Soret coefficient for component B in A-B liquid, K^{-1}

J_i = flux of i atoms, moles of i/cm^2-s

$J_{B,Growth}$ = flux of B atoms due to crystal growth, moles of B/cm^2-s

m, m_α, and m_β = liquidus slope at the eutectic point where $m = m_\alpha$ for $N_0 < N_E$ and $m = m_\beta$ for $N_0 > N_E$, K/mole fraction B

$Z = R/D + \sigma_B G - 2\sigma_B G N_B$, cm^{-1}

$Z_E = R/D + \sigma_B G - 2\sigma_B G N_E$, cm^{-1}

$Z_0 = R/D + \sigma_B G - 2\sigma_B G N_0$, cm^{-1}

$S = [1 + \sigma_B m(N_E - N_0) - \sigma_B m(N_E^2 - N_0^2)]^{-1}$, dimensionless.

III. EXPERIMENTAL APPARATUS AND PROCEDURE

1.0 Verification of Calculated Range of Stability for Cr_2O_3-Cr and $(Cr,Al)_2O_3$-Cr

A strip-heater furnace was used to heat waffers of compacted Cr_2O_3-Cr and Al_2O_3-Cr_2O_3-Cr powder mixtures in an atmosphere of selected gas mixtures. A schematic diagram of the strip heater furnace is given in Fig. 24. A low voltage, high current dc power supply was used to resistively heat two W or Mo strips which held the oxide-metal waffer. Two spring loaded, Al_2O_3 insulated, W-W(Re) thermocouples were placed against the bottom heater strip to monitor the temperature of the strips which heated the waffer.

An optical pryometer was sited through the observation port to confirm the thermocouple readings. The optical pryometer readings were corrected to compensate for the observation port fused silica window by compacting the temperature of a hot W-lamp element with and without the window in place. The W-lamp element temperature was adjusted to 1600°C by using an Variac variable rheostat to reduce the voltage across the element.

Waffers were prepared by slurry mixing 99.8% pure Cr_2O_3, Cr and Al_2O_3 powders obtained from the Fisher Chemical Company. Cr_2O_3-20 mole % Cr and Cr_2O_3-45 mole % Al_2O_3-10 mole % Cr mixtures were slurry mixed in water for 1-h, vacuum filtered, and dried at 140°C overnight. The mixtures were packed into a Mo-lined graphite die and hot pressed for 30 min at 3.45 MPa (500 psi). Using a high speed, diamond impregnated cut-off saw the hot pressed pieces were cut into waffers measuring approximately 12 × 8 × 1 mm (see Fig. 25).

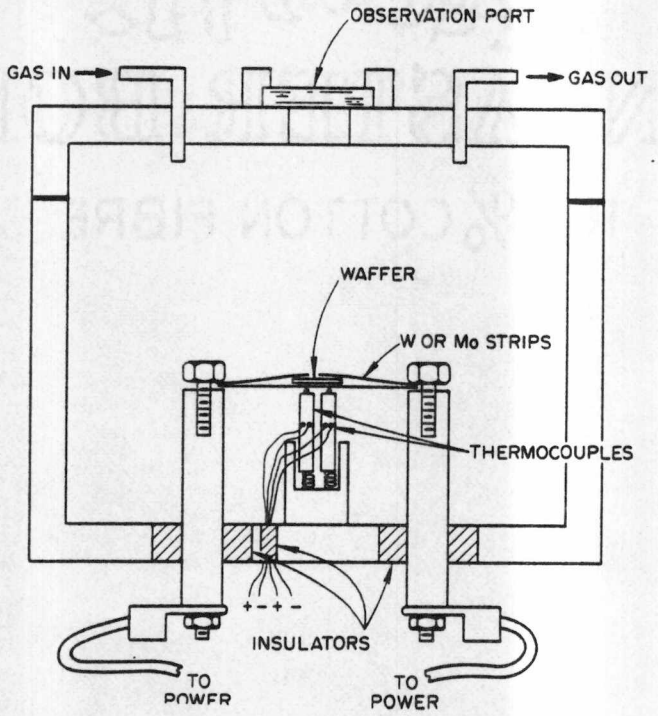


Fig. 24. Diagram of Strip-Heater Furnace.

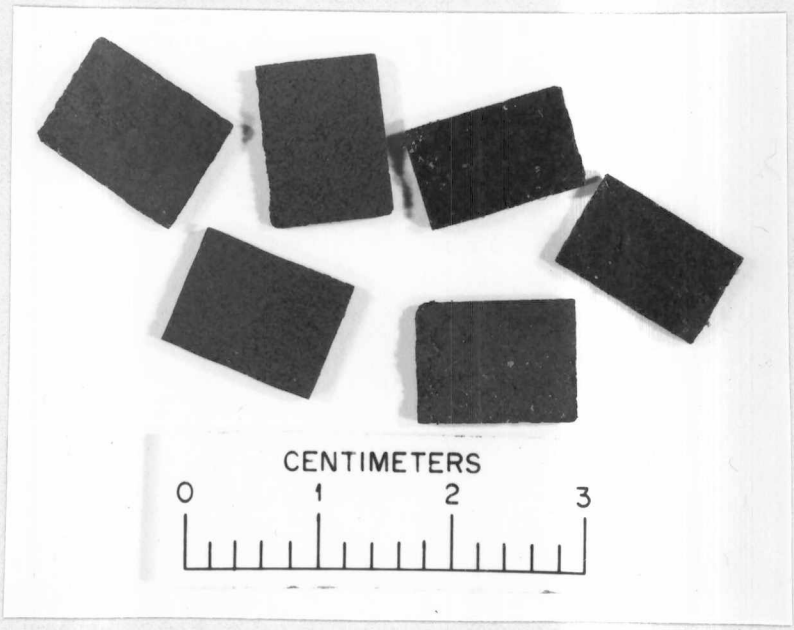


Fig. 25. Waffers of Oxide-Metal Mixtures Used in Strip-Heater Experiments.

The partial oxygen pressure in the strip-heater furnace was set using H_2-H_2O mixtures. Since some water vapor was always present in the as-received gases and since the gases obtained water vapor from the furnace surfaces, a Thermox oxygen analyzer was used to measure the partial oxygen pressure of each gas mixture. The Thermox brand oxygen analyzer is not calibrated in the range of oxygen pressure required for the range of stability of Cr_2O_3-Cr and $(Cr,Al)_2O_3$-Cr. Thus, a calibration for the oxygen analyzer was required; the technique of calibration, gas mixing, and emf measurements for H_2/H_2O mixtures are given in Appendix C.

The heater strips were heated to approximately 1700°C at the hottest part of the strip with 1600°C near the edge of the waffer. The strips were held at temperature for 10 minutes. Rapid heating and cooling was obtained by quickly turning the power supply control rheostat to a predetermined setting for heating and zero for cooling.

After the waffer had cooled, the strips were wired together with annealed copper wires, carefully removed from the furnace; and encapsulated in metallographic quality expoxy resine. The encapsulated strips were sectioned using a diamond saw and reencapsulated for metallographic polishing. Grinding and polishing was preformed using diamond impregnated disc and slurriers on microcloth. Metallographic inspection of the as-polished specimens was made at 25× and 125× with white, normally reflected light from a Xerron lamp.

2.0 Determination of Cr-Mo Fiber Composition as a Function of P_{O_2}

A simple cold-crucible was fabricated which could be used with Rf heating. The crucible was formed from a 3-cm diameter copper pipe by

brazing six "hair-pin" shaped copper tubes (for cooling water) to the pipe and then sectioning the pipe as shown in Fig. 26. The cold-crucible was fixed into a 2-cm thick, non-conducting fiberglass base which supported a 25 cm diameter × 40 cm high pyrex cylinder. An aluminum plate formed the top of the chamber surrounding the cold-crucible. A water cooled, coaxial Rf feed through was fixed in the base. The Rf feed through was used to support the coil formed around the cold-crucible. The gas inlet was located in the base and the gas outlet and vacuum fitting were located in the top plate. A simple schematic of the Rf cold crucible furnace used in this investigation is given in Fig. 26.

Samples for the cold-crucible experiments were fabricated by hot-pressing the desired powder mixtures at 1600°C for 30 minutes at 3.43 MPa (500 psi). The powders were slurry mixed in H_2O, vacuum filtered, and dried at 140°C overnight. A Rf-heated 3.0-cm I.D. graphite die lined with Mo-foil was used to hot press the powder mixtures into approximately 85% dense pieces 3.0 cm diameter × 4.0 cm height.

CO-CO_2 gas mixtures were used for these experiments. The gas mixtures were prepared and certified by Linde Gas Products Division of the Union Carbide Corporation. The gases in the cold-crucible furnace were maintained at atmospheric pressure by flowing the gas mixture through the furnace at approximately 20 ml/min and allowing the mixture to exit through a mineral oil. The bubbler also prevented leak diffusion of air into the chamber.

A frequency of 2.2 MHz was used to heat the samples in the cold crucible. Frequencies of 0.4, 0.6, 2.2, 3.5 and 6.0 MHz were tested to determine the best conditions for sample melting and heating control.

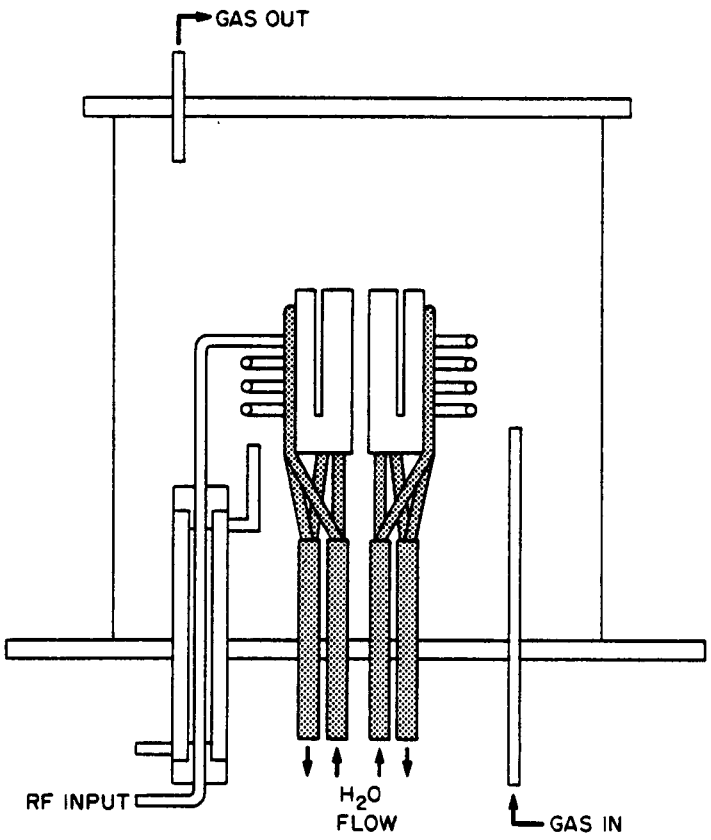


Fig. 26. Cross Section of Cold Crucible Furnace.

Frequencies below 2.2 MHz would not efficiently couple to the cold crucible samples. Above 2.2 MHz, arcing would occur and adequate heating at the sample center was not always accomplished even with the maximum power setting of the generator. Thus, 2.2 MHz proved to be the most practical frequency for cold-crucible heating of the mostly oxide, Cr_2O_3-Mo samples.

The internal zone growth (IZG) technique was also used to investigate the effects of P_{O_2} on the composition of the metallic phase in the Cr_2O_3-Mo composites. However, a description of this technique will not be given in this part of the discussion of experimental technique, but will be described in detail in the next part dealing with directional solidification studies.

The composition of the metallic phase was determined from x-ray analysis. After the sample was removed from the cold-crucible and sectioned with a diamond impregnated saw, small pieces of the composite would be ground on a BN plate and analyzed by the Debye-Scherrer technique to determine the Mo-Cr also lattice parameter. The lattice parameter is directly correlatable to the composition of the Mo-Cr solid solution.

3.0 Directional Solidification Studies by IZG

3.1 Optimization of IZG for Cr_2O_3-Mo Composite Growth

Radio frequency, sample diameter and sample bulk electrical conductivity are the major independent variables which influence the success of the IZG technique [21,22,72]. Since it was expected that the sample bulk electrical conductivity would be the most difficult parameter to reproduce from sample to sample [70], sample preparation was standardized to promote reproducibility.

A simple hot press was constructed which would accommodate a graphite die 12-cm in diameter by 20-cm in length. A schematic of the hot press hot zone is given in Fig. 27. The graphite die would be Rf heated to 1600°C as determined by a alumina sheath protected Pt-Pt(Rd) thermocouple inserted into a well in the die wall. a pressure of 3.45 MPa (500 psi) was applied for 30 minutes at 1600°C. The die was lined with Mo foil to prevent reduction of the chromia by the hot graphite. Under these conditions, a sample density of approximately 85% theoretical density was routinely obtained.

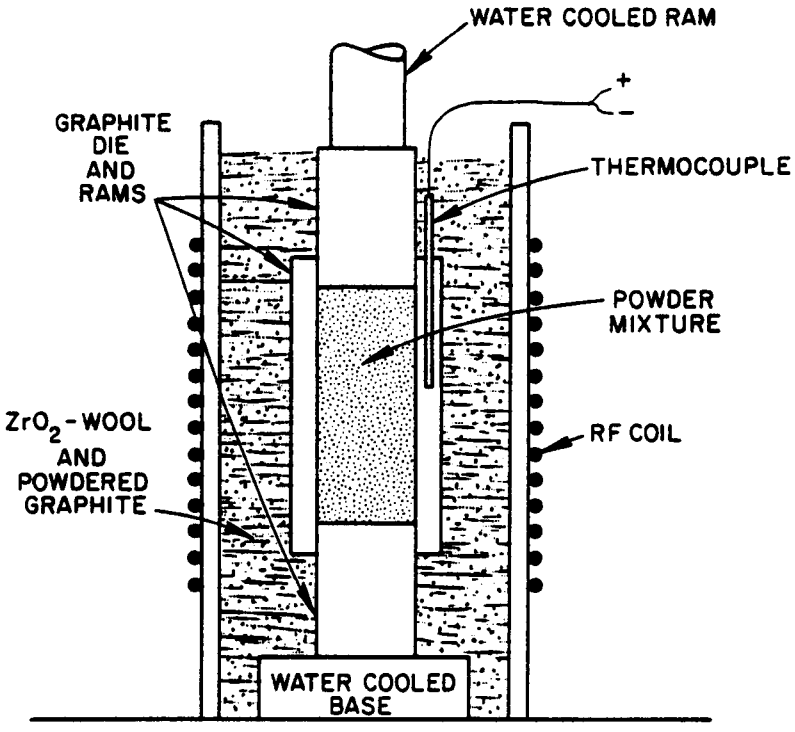


Fig. 27. Rf-heated Hot Press for Large Diameter IZG and Cold Crucible Samples.

Powder mixtures were made by aqueous slurry mixing of 80 μm (−325 mesh) powders of approximately 99.9% purity for 1 h. The slurry would be vacuum filtered and dried at 140°C overnight in air.

Sample diameters of 1.5, 2.0, 2.5, 3.0, 3.5, and 5.0-cm could be fabricated by the standard hot pressing technique. Also, two Rf-generators were available which provided a selection of frequencies from 0.4 to 0.6 and 2.2 to 9.0 MHz. Thus, it was possible to vary the radio frequency, the sample diameter, and the bulk electrical conductivity (by varying metal content) over wide ranges.

A schematic of the IZG furnace for samples of diameter from 1.5 and 2.0 is given in Fig. 28. A simpler arrangement was used for samples of

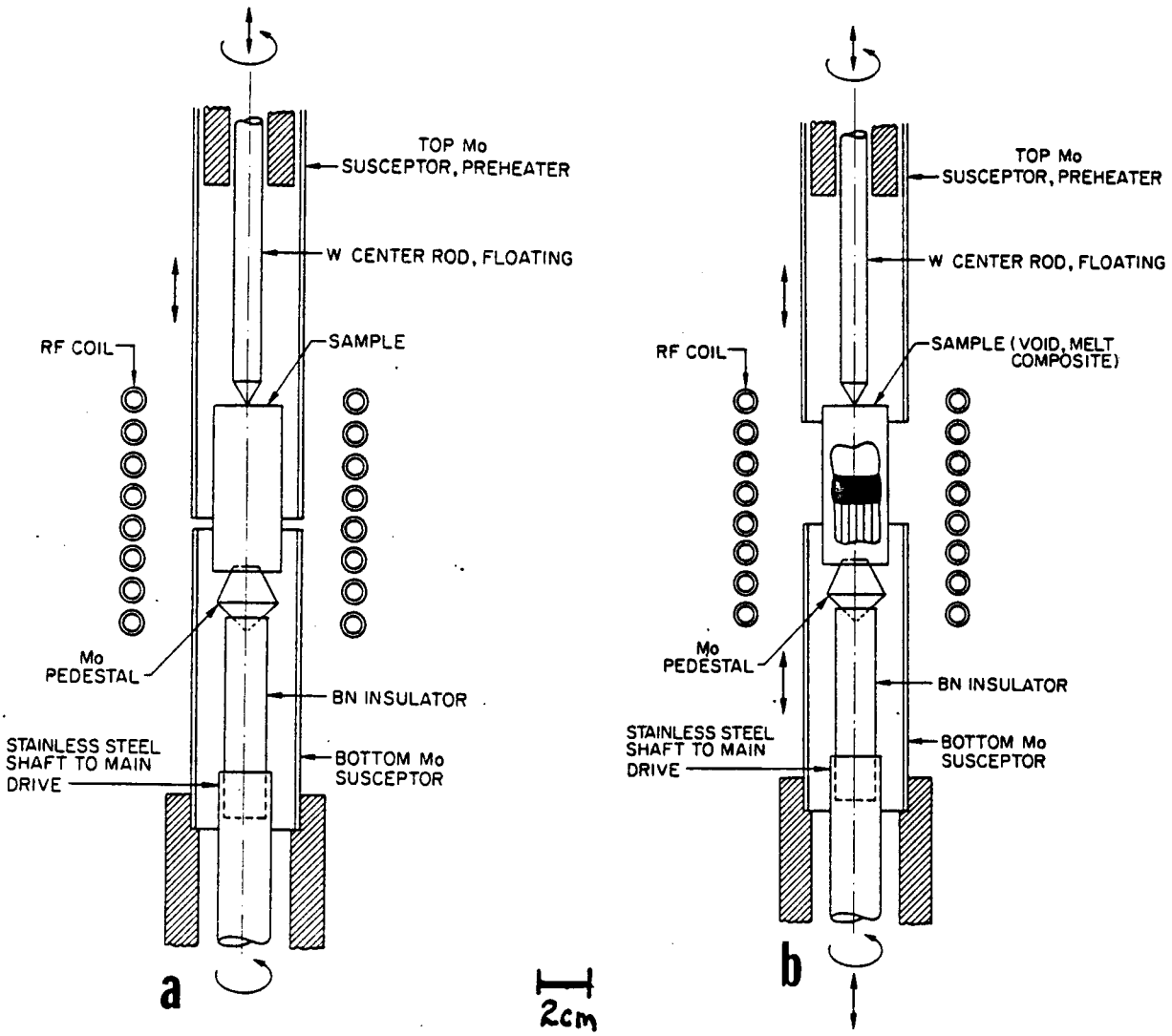


Fig. 28. Susceptor/Rf coil/sample geometry: (a) Preheat Position, (b) Position for Melt Zone Movement.

2.5, 3.0, 3.5 and 5.0-cm diameters as shown in Fig. 29. Other than the size of the Rf coil, the basic difference between the two furnace arrangements is the presence of a top and bottom Mo-preheater susceptor. The Mo-preheater susceptor was used to preheat the 1.5 and 2.0 cm diameter samples to temperatures that would give a bulk electrical conductivity sufficient for efficient Rf heating. The susceptors could be heated to 1700°C before arcing would become a problem.

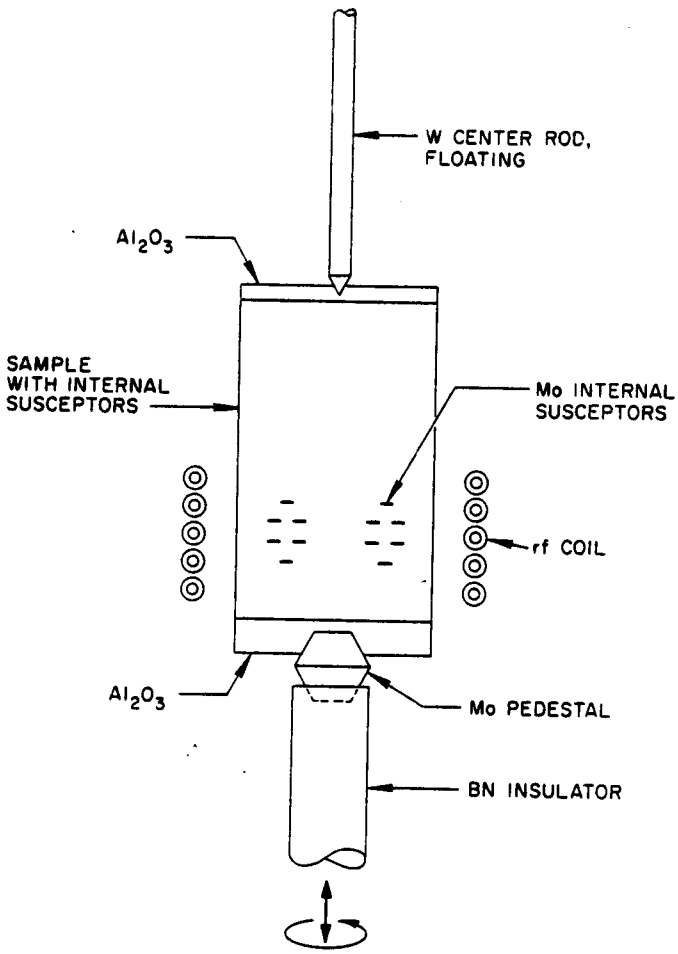


Fig. 29. Cross Section of 5-cm Diameter IZG Sample Showing Internal Susceptor Configuration.

Internal susceptors were used for samples 2.5 cm and larger. The internal susceptors were made by adding over-lapping Mo chips (2 mm × 0.1 mm) to the lower half of the samples. The susceptors were arranged in circles of radius of about 67% the radius of the sample. Usually, no more than a 1% change in total composition would be created by the internal Mo susceptors.

The internal susceptors would be heated by the Rf field until the bulk of the sample in the region of the susceptors reached a temperature sufficiently high for Rf coupling. Even though the localized internal heating caused the samples to crack on the surface, the cracking was apparently not deep into the sample and seemed to be of little or no consequence.

The Rf coil, moveable Mo-preheater susceptors (when needed), and sample support were enclosed in a pyrex cylinder 25-cm diameter × 40-cm high. The cylinder was closed on the top by an aluminum plate which housed a sample-centering rod, gas outlet valve, and vacuum valve. The cylinder was supported by an aluminum plate which held the watercooled Rf coaxial feed through and gas inlet tube. The sample support rod seal-and-bearing housing was attached to below the bottom support. The top and bottom preheater susceptors could be moved by simple rack and pinion mechanisms attached to the top centering support and sample support rod seal-and-bearing housing, respectively.

The Rf coil current was controlled manually by adjusting the power rheostat on the Rf generator. Temperature measurements were made using both a manually operated optical pyrometer and an automatic recording optical pyrometer. Both Rf plate current and Rf grid current were monitored carefully and recorded. The ratio of the Rf grid current to the Rf plate current were found to give a good indication of the coupling efficiency of the work coil to the sample. Both the emf from the automatic optical pryometer and the emf from the Rf grid current meter were recorded on a two-pen chart recorder. The chart recorder indicated only

relative values of sample surface temperature and Rf grid current. However, the trend in temperature and grid current were invaluable in the control of the IZG technique.

A typical IZG experiment was begun by very slowly preheating the hot-pressed sample. The preheat period would last for about four hours while the sample was heated to a temperature where direct Rf coupling to the sample could be accomplished. For a 2-cm diameter sample the required preheat temperature would be 1700°C at a 2.2 MHz frequency. For a 5 cm diameter sample the required preheat temperature would be about 1300°C at a 0.6 MHz frequency. When the sample was sufficiently preheated the Mo-preheater susceptors would be removed for direct Rf coupling. When internal susceptors were used, the direct Rf coupling to the bulk sample was gradual as the sample approached the temperature where internal susceptors would not be necessary for coupling.

Optimum conditions for Rf coupling and zone movement would occur when the coupling efficiency of the solid, unmelted sample heated near the eutectic temperature was just slightly higher than the coupling efficiency of the melt. The coupling efficiency of the solidified composite would consistently be less than the coupling efficiencies of the melt or heated solid above the melt. The optimum conditions for zone movement were determined by trial and error.

The growth rate was controlled by the downward velocity of the sample support rod. The sample was rotated at approximately 20 RPM so that the automatic optical pryometer (set to monitor the hottest area) could scan the circumference of sample. Also it is suspected that the rotation would aid in establishing a symmetric melt zone as is the case in other crystal growth techniques.

At the end of the composite growth sequence, the sample was slowly cooled by gradually reducing the power rheostat setting. The sample would be removed from the IZG furnace, sectioned with a diamond saw, and examined using the standard metallographic technique already described.

Using the technique for IZG just described, samples of constant density and composition were fabricated in 1.5, 2.0, 2.5, 3.0, 3.5, and 5.0-cm diameters. IZG of the various sample sizes was attempted at frequencies of 0.4, 0.6, 2.2, 3.5. Optimum conditions would be those that allowed (1) controllable melting, (2) controllable zone movement, (3) no melt-through of the sample wall, (4) a complete melting of the interior of the sample and (5) a solid-liquid interface slightly convex into the liquid so as to encourage growth of large columnar grains in the center of the sample.

3.2 Extremum Growth, Eutectic Morphology and Growth of Off-Eutectic Compositions

After optimum or nearly optimum conditions for IZG were established for a particular sample size, controlled growth experiments were preformed. One to three different growth rates would usually be attempted per sample. Most compositions were richer in Mo than the literature value of the Cr_2O_3-Mo eutectic composition.

Morphology and rod spacing was studied by metallographic examination. Using an oil emersion lens and reflected white light, micrographs of 1000× could be produced with sufficient resolution to make rod spacing measurements.

4.0 Synthesis of Predicted $LaCrO_3$-Mo, W, Cr and $YCrO_3$-Mo, W, Cr Systems

Equal molar ratios of La_2O_3 and Cr_2O_3, and Y_2O_3 and Cr_2O_3 were mixed with approximately 15% Mo, W, and Cr to produce samples of $LaCrO_3$-Mo, $LaCrO_3$-W, $LaCrO_3$-Cr, $YCrO_3$-Mo, $YCrO_3$-W, and $YCrO_3$-Cr. The samples were hot-pressed into 85% dense pieces 2.0 cm in diameter × 3.0 cm in length. Using the cold-crucible, skull melting technique at 2.2 MHz with a CO-10 vol % CO_2 gas mixture, the samples were heated to form an approximately 1-cm diameter melt-zone.

The samples were sectioned and examined by optical microscopy following standard metallographic preparation. Also, chips from the melt zone were crushed and analyzed by the Debye-Scherrer technique to determine the crystal structure of the oxide matrix.

IV. RESULTS

1.0 Verification of Range of Stability for Cr_2O_3-Cr and $(Cr,Al)_2O_3$-Cr

Waffers of Cr_2O_3-20% Cr and Cr_2O_3-45% Al_2O_3-10% Cr were melted under the conditions given in Table III, column three. The log H_2/H_2O established with the gas mixtures is given in column four of Table III. The H_2/H_2O was determined using a Thermox Oxygen Analyzer as described in Appendix C. The results of each trial are given in the fifth column.

A composite or eutectic-like structure was not observed in any Cr_2O_3-20% Cr trials. This result confirms the predictions based on Fig. 7; i.e., in a temperature gradient the Cr in the sample will be either oxidized or the oxide will be reduced — both components cannot coexist at a fixed gas mixture in a temperature gradient.

Because the addition of Al_2O_3 adds one degree of freedom to the melt-solid/solid equilibrium, Fig. 8 indicates that over a small temperature range both phases of the $(Al,Cr)_2O_3$-Cr melt will be stable for a small range of fixed gas mixtures. This was verified in trials 7, 8, and 9 given in Table III where a zone of eutectic structure was observed to have frozen from the melt.

Figures 30 and 31 show examples of the results of both the Cr_2O_3-Cr and the $(Cr,Al)_2O_3$-Cr sets of experiments. In Figs. 30 and 31 the white is either the W-strip or the Cr-phase, the lighter gray is the oxide waffer, and the darker gray is the epoxy mounting material. The loss of material in the center of the sample indicates that the oxide was reduced and the very volatile oxide of CrO and even more volatile Cr were formed

Table III. Significant Strip Heater Results

Trial Number	Composition in Mole %	Gas Mixture	Log H_2/H_2O	Results
1	Cr_2O_3-20% Cr	Dry N_2 + H_2	2.55	V
2	Cr_2O_3-20% Cr	Dry N_2 + H_2	2.55	V
3	Cr_2O_3-20% Cr	Moist N_2 + H_2	1.37	V + O
4	Cr_2O_3-20% Cr	Moist N_2 + H_2	1.30	V + O
5	Cr_2O_3-20% Cr	Moist Ar + H_2	0.90	V + O
6	Cr_2O_3-20% Cr	Moist N_2 + H_2	0.46	O
7	Cr_2O_3-45%Al_2O_3-10% Cr	Dry N_2 + H_2	1.85	V + E + O
8	Cr_2O_3-45%Al_2O_3-10% Cr	Dry N_2 + H_2	1.88	V + E + O
9	Cr_2O_3-45%Al_2O_3-10% Cr	Dry N_2 + H_2	1.87	V + E + O

V-Melt vaporized implying oxide reduced.
O-Melt formed all oxide phase implying Cr was oxidized.
E-Eutectic structure was formed from melt.

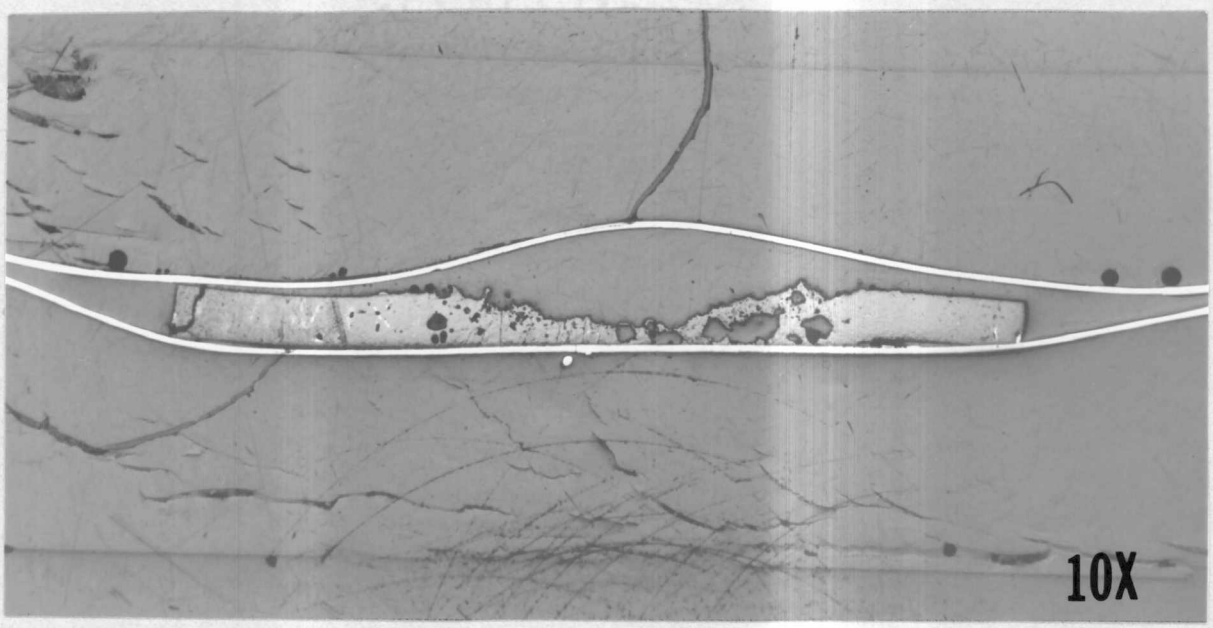


Fig. 30. Strip-Heater Melted Waffer of Cr + Cr_2O_3 Mixture.

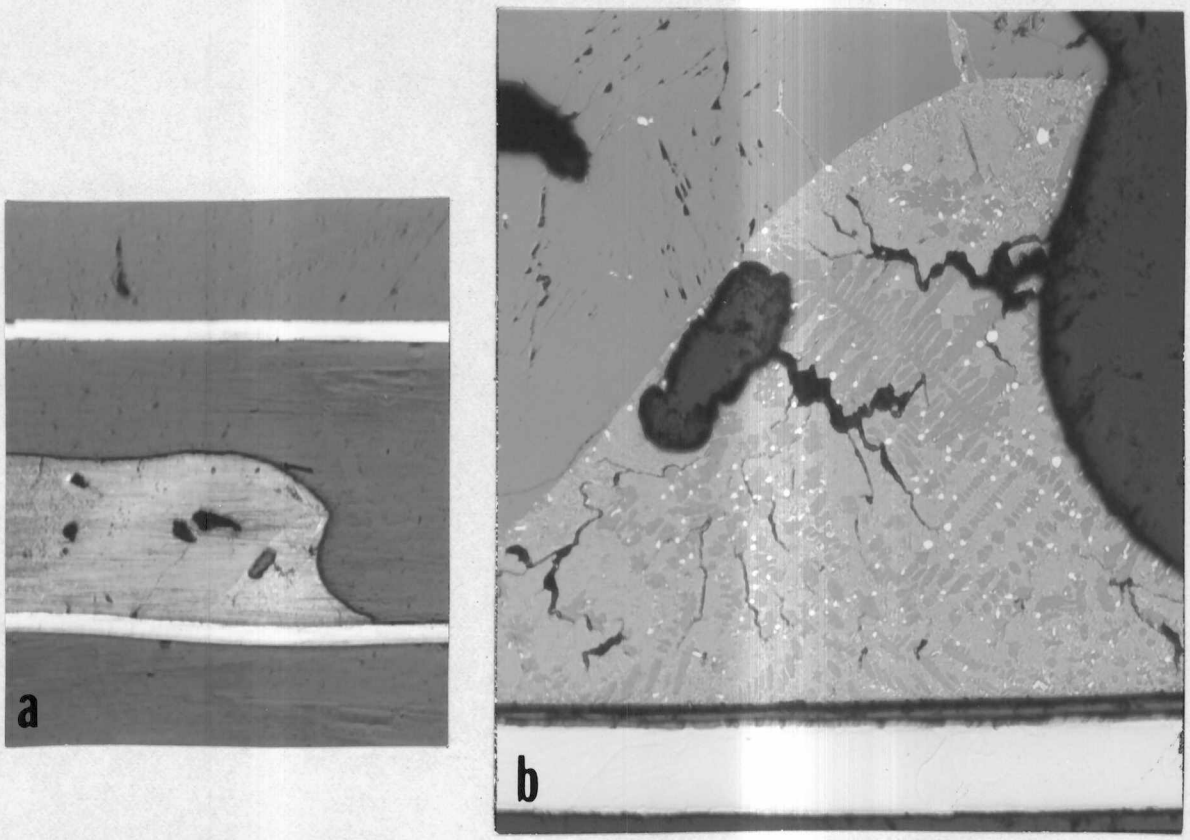


Fig. 31. Strip-Heater Melted Waffer of Cr + $(Cr,Al)_2O_3$ (a) 25×, (b) 125×.

and transported away from the hot zone of the strip heater. Also there is an absence of the Cr-phase in the melted region adjacent to the very porous region, yet no vapor transport seems to have occurred. In this case, it is believed that the Cr has been oxidized to Cr_2O_3.

When Al_2O_3 was present in the melt, a zone of eutectic structure was observed between the totally oxide zero and the zone which suffered severe vapor transport. A good example is given in Fig. 31.

2.0 Cr-Mo Fiber Composition as a Function of P_{O_2}

Mixtures of Cr_2O_3-Mo and Cr_2O_3-Cr-Mo were melted by both IZG and Skull Melting techniques. Gas mixtures of CO-9% CO_2, CO-6.25% CO_2, and CO-1% CO_2 were used to establish three different atmospheres for the melt

environment. All melts produce a rod-type oxide-metal eutectic-like structure. There were no obvious microstructural differences between samples.

Table IV gives findings of the x-ray analysis and variations of Cr content in the metal phase which are compared to that predicted for each gas mixture in Fig. 32. The agreement between calculations and experiment is at least indicative of the P_{O_2}-fiber composition relationship predicted by the regular solution model.

During these experiments it was found that samples of Cr_2O_3-25 mole % Mo with the Mo in the form of chips yielded very reproducible result for % Cr in the Mo fiber except in the case of the skill melting of these samples in a CO-1% CO_2 mixture. The skull melting technique using the cold crucible prevents surface melting thus making equilibration of P_{O_2} inside and outside the sample a much slower process. Since the Cr which appears in the Mo fibers must be won from the Cr_2O_3, oxygen and suboxides of Cr_2O_3 (which are all volatile at 1900°C) could fill the void over the melt resulting in an effectively higher P_{O_2} than intended. The equilibration of CO-6.25% CO_2 and 9% CO_2 gas mixtures with the gas in the void apparently occurred very rapidly because less Cr_2O_3 needed to be reduced than with CO-1% CO_2 mixtures.

To test this explanation of irreproducible fiber composition with CO-1% CO_2 mixtures, samples were prepared with Cr powder additions. Three compositions were attempted as given in Table IV. One composition had excess Cr, one had the calculated Cr content, and one had less Cr than calculations predicted would appear in the Mo-Cr fibers. The results are interesting enough to describe in detail.

Table IV. Observed Metal Fiber Composition as a Function of Gas Mixture and Melting Technique

Gas Composition (Vol %)	Starting Composition (mole %)	Melting Technique	Mo-a_o (A)	Cr in Mo Fiber (mole %)
CO-9%CO_2	Cr_2O_3-25% Mo	IZG	3.1450 ± 0.0006	3.0
		IZG	3.1449 ± 0.0003	3.0
		Skull	3.1445 ± 0.0005	3.0
		Skull	3.1451 ± 0.0003	3.0
CO-6.25%CO_2	Cr_2O_3-25% Mo	IZG	3.13703 ± 0.001	7.5
		Skull	3.13780 ± 0.0005	6.5
CO-1%CO_2	Cr_2O_3-25% Mo	Skull	3.1427 ± 0.003	5.0
	Cr_2O_3-1% Cr-20% Mo	IZG	3.1254 ± 0.007	13.4
	Cr_2O_3-5% Cr-20% Mo	IZG	3.1214 ± 0.0026	15.0
	Cr_2O_3-8% Cr-20% Mo	IZG	3.1241 ± 0.0053	14.0

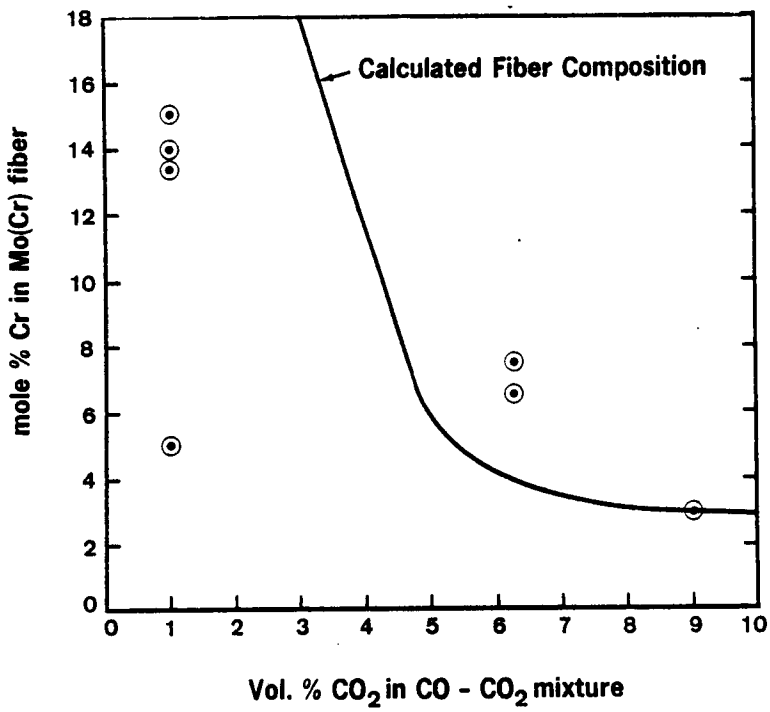


Fig. 32. $CO-CO_2$ Gas Mixture vs Chromium Content of Molybdenum Fibers in $Mo(Cr)-Cr_2O_3$ Composites.

Samples with excess Cr melted at a lower temperature and Rf-power than expected. The melt could be maintained for a few minutes but then would freeze causing loss of Rf-heating efficiency and overloading of the Rf-generator due to load mismatching. It seems likely that a Cr_2O_3-Mo-Cr melt was formed with excess Cr; as Cr was oxidized to Cr_2O_3 as the melt composition moved along the monovariant trough. The melting temperature increased and the melt solidified. The Rf-power was insufficient to continue heating the sample since most of the Mo-chips were dissolved by the melt.

Samples with Cr content near the calculated composition produced a well formed melt zone which could be maintained for as long as desired. There was no smoking or spluttering due to gaseous discharge during melting.

Samples with less Cr than calculated were completely uncontrollable. Practically all the melt that was formed was forced out of the sample through surface cracks. In fact, much of the melt was "shot" through openings in the cold crucible. All indications are that an extreme gas pressure existed within the sample due to Cr being won from Cr_2O_3. Since melting of Cr_2O_3-Mo samples in CO-1% CO_2 were not nearly so violent, it must be suggested that the Mo powder present in the Cr_2O_3-Cr-Mo samples (with less than calculated Cr) was a major contribution to the catastrophic gas evolution. Apparently, the finely divided particles of Mo immediately reacted with sufficient amounts of Cr_2O_3 releasing sizeable quantities of gaseous suboxides of Cr_2O_3 and maybe even oxygen to cause extreme internal pressures.

3.0 Optimization of IZG for Cr_2O_3-Mo Composite Growth

The starting place for the series of experiments which resulted in the controlled IZG of 5-cm diameter Cr_2O_3-Mo samples at 600 KHz was with the same sample size and frequency that resulted in the successful growth of the UO_2-W composite; i.e., 1.5-cm or 2.0-cm diameter at 3.0–7.0 MHz. Each attempt to Rf-couple, melt, and stabilize a melt zone resulted in either uncontrollable heating and melting or uncontrollable cooling to below 1000°C as soon as the preheater Mo susceptors were removed. The lack of success was attributed to poor IZG technique until Hartzell and Sekerka calculated that runaway heating and uncontrollable melting was caused by the nonlinear coupling of Rf-heating and heat transfer in 2.0-cm diameter oxide samples at radio frequencies on the order of 3 MHz. Hartzell and Sekerka's calculation is given in Fig. 33.

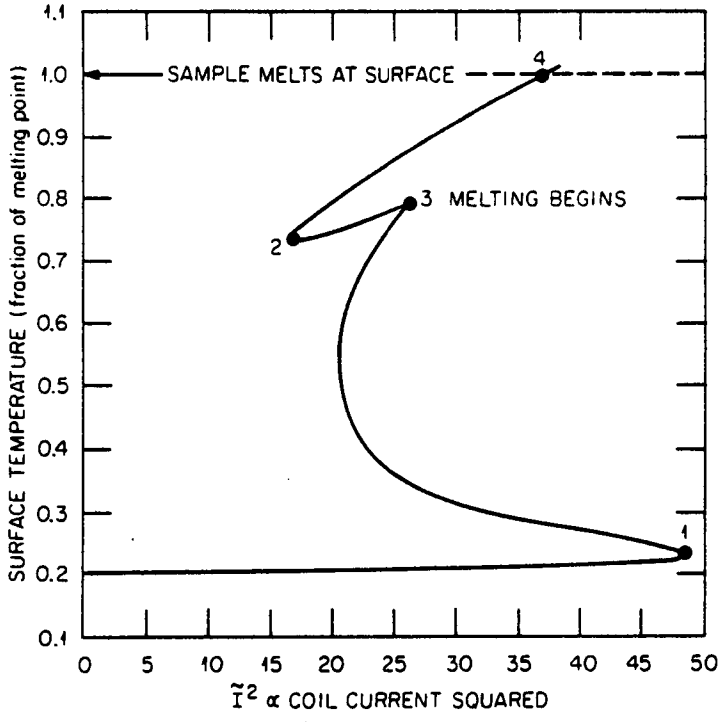


Fig. 33. Hartzell and Sekerka's Calculations for Rf-Heated Mo-Cr_2O_3 Compact (2 cm Diameter, 3 MHz frequency).

Characteristics of the instability depicted in Fig. 33 have all been routinely observed in 2.0-cm diameter samples.

Point 1 in Fig. 33 indicates that a large amount of power would be required to generate heat in the sample. The break in the curve at Point 3 is due to a internal change in electrical conductivity due to melting. Point 2 to Point 3 indicates that initial melting will be uncontrollable and that the melt zone will be unstable and just as likely to freeze in and lose temperature (almost to room temperature). At Point 4 the melt zone penetrates the surface and would be lost. Hartzell and Sekerka's calculation indicates that if a sample could survice the instability, controlled growth could be obtained. The curve between points 2 and 4 would correspond to those conditions which would maintain a stable; internal melt zone. However, the surface temperature could become extreme.

After obtaining an understanding of the runaway heating characteristics of the 1.5 and 2.0-cm diameter samples at frequencies around 3 MHz, several samples were successfully brought through the instability and a zone pass was made at one to three different growth rates. As it was predicted, the sample surface temperatures were usually in excess of 1800°C and occasionally melt loss did occur.

In order to lessen the instability, larger samples were fabricated. Samples with 2.5 and 3.0-cm diameters were attempted at 3.0 MHz. The instability was not as pronounced as with the smaller diameters, but surface melting and melt zone spillage remained a difficulty. The frequency was lowered to 2.2 MHz to reduce surface melting, but little or no improvement was observed. When a frequency of 0.6 MHz was used, the instability became so pronounced that melt was spunned out by the sample with such a force that the furnace chamber walls were damaged (see Fig. 34).

To lessen the instability at the lower frequency, samples of 3.5 and 5.0-cm diameter were made. The 3.5-cm diameter sample was not much more manageable than the 3.0-cm diameter samples. On the other hand, the 5.0-cm diameter sample was so well behaved that the certainty of internal melting was not obtained until the sample was removed from the furnace and sectioned.

Since a 5.0-cm diameter sample was the maximum size that could be made without reconstructing the hot-press furnace, larger samples were not attempted. Thus, for the existing equipment, the optimum conditions for IZG of Cr_2O_3-Mo were a 5.0-cm diameter sample at 0.6 MHz frequency. Cross sections of two samples are given in Fig. 35.

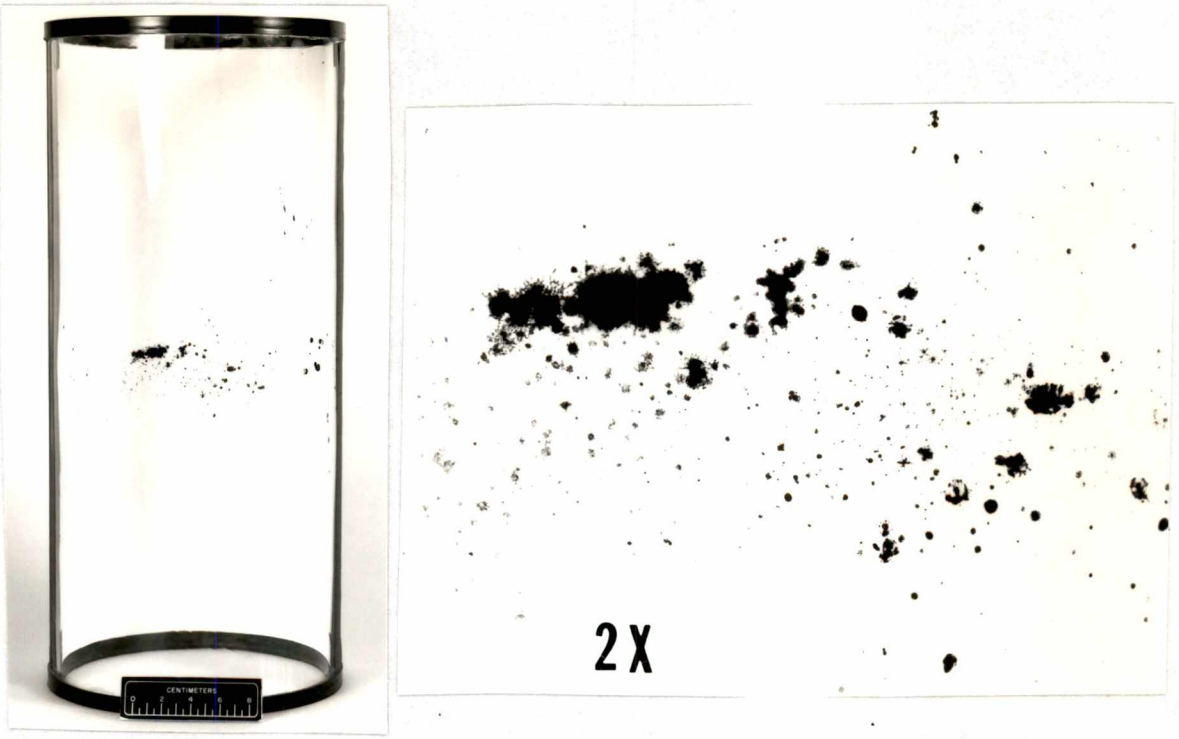


Fig. 34. Melt Splats on Chamber Walls Due to Uncontrollable Melting in Rf-Heating Instability.

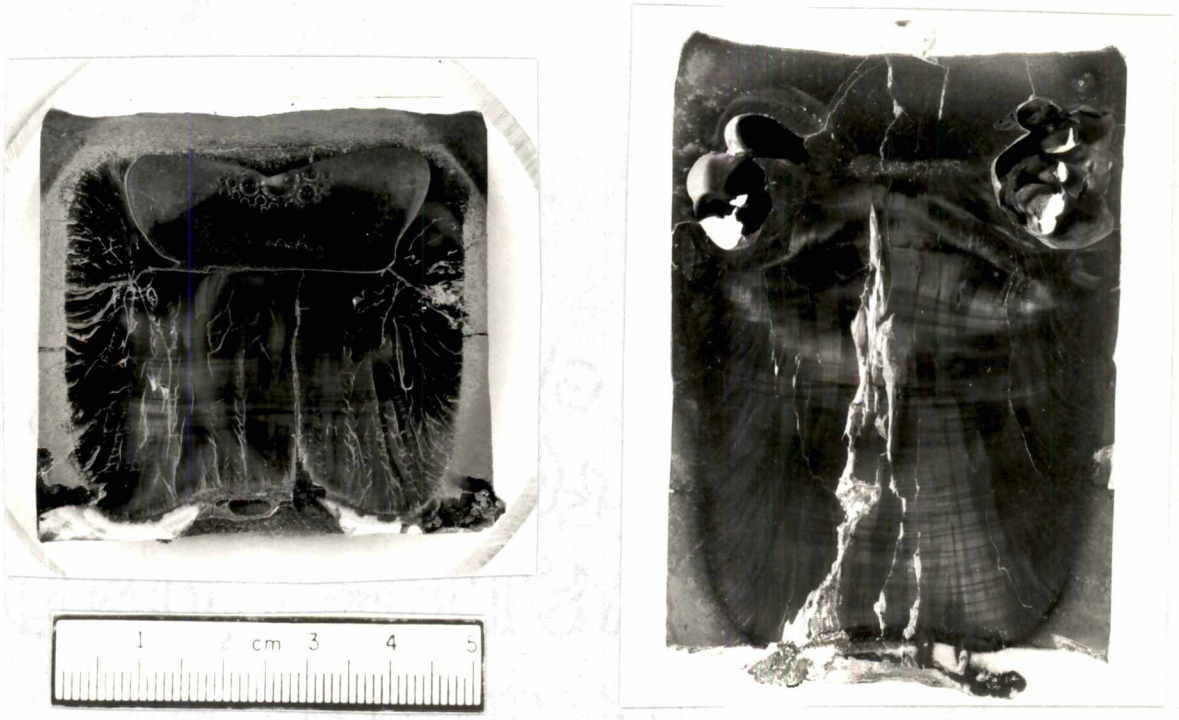


Fig. 35. Cross Sections of Large Diameter Samples of Mo + Cr_2O_3 Composite Grown by IZG.

4.0 Investigation of the Growth of Off-Eutectic Composition, Eutectic Morphologies, and Extremum Growth of Cr_2O_3-Mo Composites

Samples of composition from 10 mole % Mo to 40 mole % Mo have been successfully grown at growth rates of 0.5 to 5.0 cm/h. Neither a dendritic nor cellular structure was ever observed in the center section of the samples where growth was most uniform. Occasionally a metal-phase dentrite would be located near the edge of the melt zone, but uniform growth of a dendritic structure was never observed.

Figure 36 gives the typical microstructure that was consistently observed in the Cr_2O_3-Mo composites grown by both the skull melting and IZG techniques. The minor phase is the Mo(Cr) fiber. The only exception to the regular array of metal rods in the oxide matrix was occasionally

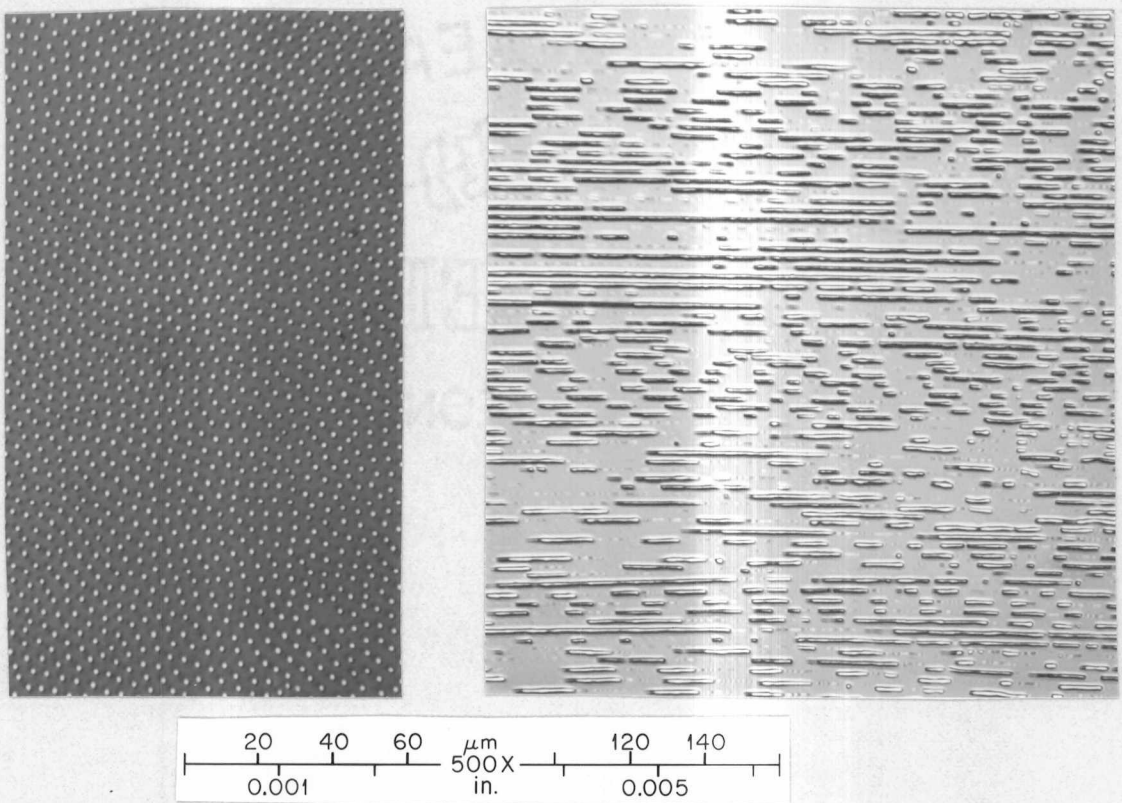


Fig. 36. Typical Rod Structure of Cr_2O_3-Mo(Cr) Composite Produced by IZG: (a) Transverse (b) Longitudinal.

observed at a growth rate of 5.0 cm/h. In some grains the rods would align in what would appear to be rows or sheets when observed in the transverse section. An example of such a microstructure is given in Fig. 37. An explanation for this unusual array configuration has not been proposed though it must surely be a crystallographic related phenomenon.

Rod spacing measurement were made at three growth rates for the Cr_2O_3-40 mole % Mo composition. In samples grown at 5.0 cm/h both the regular and row-type arrays were observed; measurements were only made on the regular array structure. A plot of the rod spacings versus growth rate to the −1/2 power indicates that the composite was grown under extremum growth condition; i.e., $\lambda^2 R$ = constant. Figure 38 gives the relationship of rod-spacing to growth rate for Cr_2O_3-40 mole % Mo composite [40].

5.0 Synthesis of $LaCrO_3$-Mo, W, Cr and $YCrO_3$-Mo, W, Cr Composites

Melts were easily formed of all six compositions. The chromite-Mo and chromite-W mixtures melted at approximately 1950°C and the chromite-Cr mixtures melted near 1750°C. Micrographs of each structure are given in Fig. 39. All structures are definitely eutectic-like. Microprobe and x-ray analysis identified each oxide matrix to be the chromite compound desired and the metal phases were shown to be either Mo, W or Cr. Thus, it appears that all six binary eutectics exist as predicted [66].

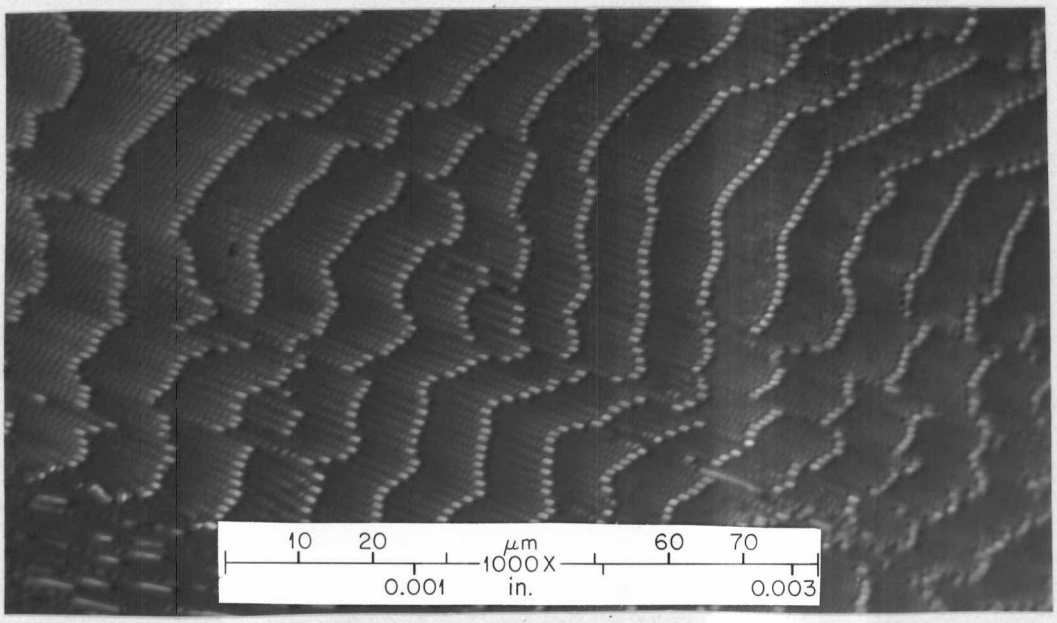


Fig. 37. Microstructure of Rods in Row or Sheet Array (Transverse Section).

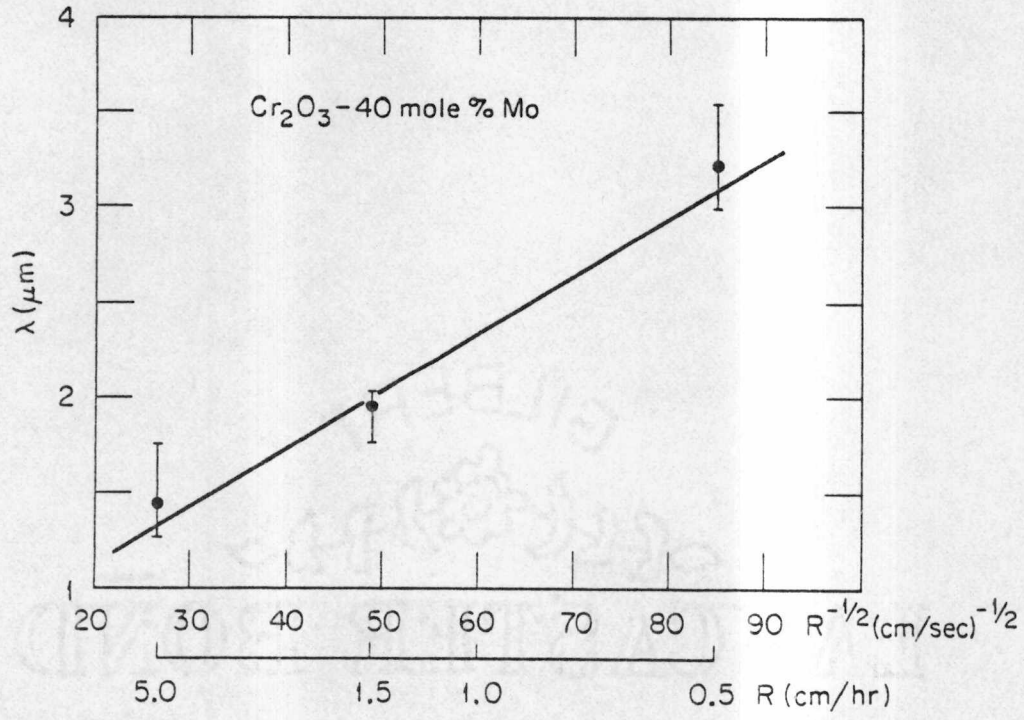


Fig. 38. $\lambda^2 R$ Relationship for Cr_2O_3-40 Mole % Mo Eutectic Composites.

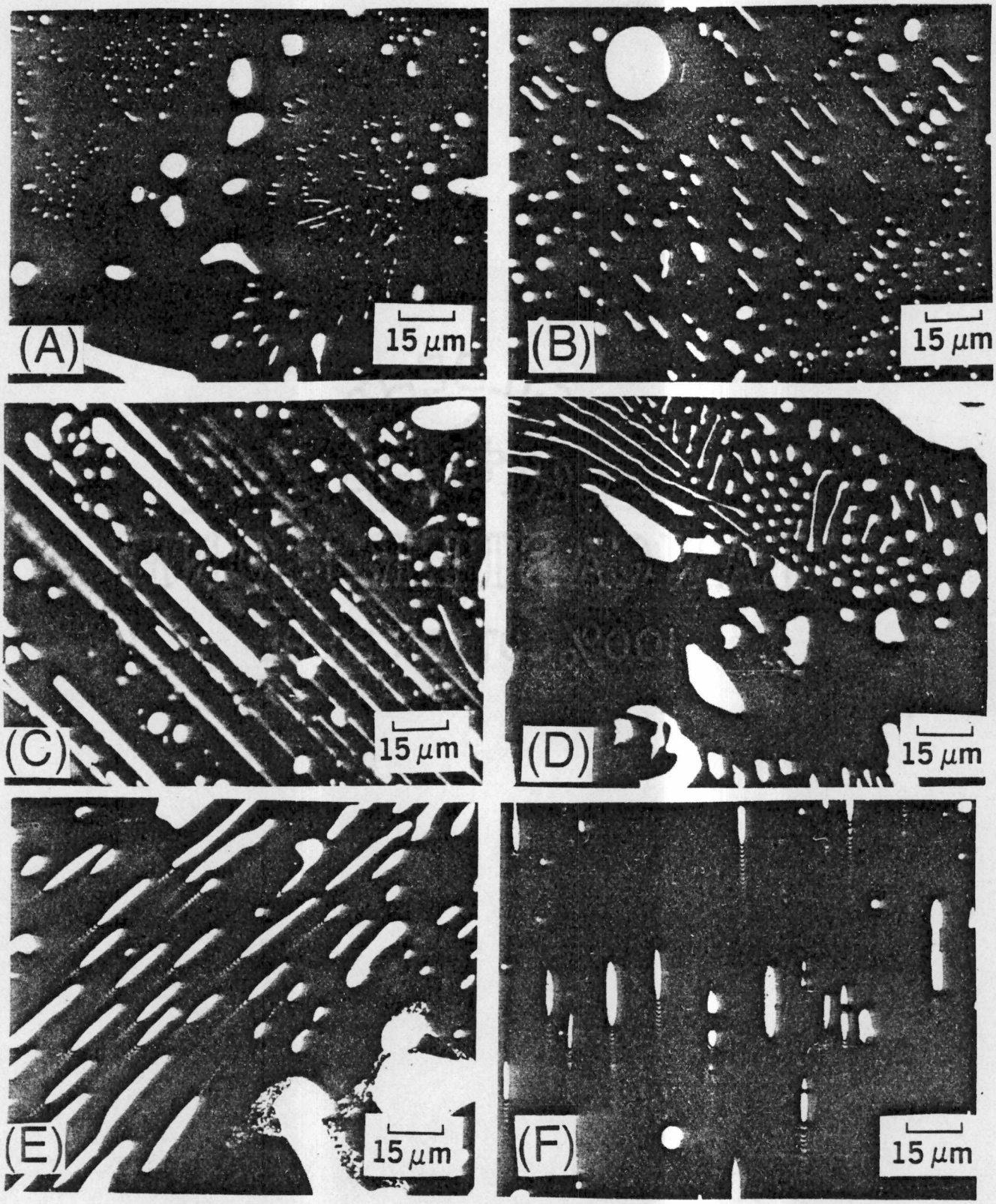


Fig. 39. Representative Microstructures of Chromite-Metal Melt Zones: (a) $LaCrO_3$-W, (b) $LaCrO_3$-Mo, (c) $LaCrO_3$-Cr, (d) $YCrO_3$-W, (e) $YCrO_3$-Mo, (f) $YCrO_3$-Cr.

V. CONCLUSIONS

Synthesis of oxide-metal eutectic composites has been investigated with respect to certain aspects of melt chemistry and basic directional solidification phenomenon. The internal zone growth (IZG) technique has been utilized for directional solidification studies with emphasis on experimentally verifying certain key predictions made in Hartzell and Sekerka's numerical analysis of the IZG process. The following conclusions have been reached on the basis of this study:

1. Oxide-metal eutectics of the type M_xO_y-M (the oxide phase is an oxide of the metal phase, e.g., Cr_2O_3-Cr) cannot be directionally solidified in a buffered atmosphere of fixed oxygen concentration or a fixed gas mixture used to set the oxygen activity of the system. The composite structure cannot be grown because the components cannot coexist in the melt over a temperature range of more than a few degrees.

2. Oxide-metal eutectics of the type M_xO_y-M′ (where M′ ≠ M, e.g., Cr_2O_3-Mo), $(M,M')_xO_y$-M (where M′ ≠ M, e.g., $(Cr,Al)_2O_3$-Cr), or more complex systems such as $M_x M'_y O_z$-M′′ (where M ≠ M′ and M ≠ M′′, e.g., $LaCrO_3$-Mo) can be directionally solidified in a buffered system of fixed oxygen concentration or fixed gas mixture if:

   (1) The atmosphere of the furnace provides oxygen partial pressures which are reducing to all higher oxide states of the oxide phase but not reducing to the oxide phase.

   (2) The atmosphere of the furnace provides oxygen partial pressures which are reducing to all oxides of the metal phase.

Standard free energy of formation of the oxides being considered can be used to calculate maximum and minimum oxygen pressures. These pressures define a range of oxygen partial pressures within which the oxide and metal phases will be stable in the liquid and the solidified eutectic composite.

3. When a range of oxygen partial pressures is suitable for the stability of both the oxide and metal component, the liquid solution in equilibrium with the two solid phases must have at least one degree of freedom. This was found to be the case for the Cr_2O_3-Mo system when x-ray analysis clearly indicated the metallic phase to be a Mo-Cr alloy. The ternary regular solution model proved adequate to calculate the chromium activity coefficient which in turn was used to calculate equilibrium oxygen pressures for the oxide melt which would yield a desired monovariant Cr_2O_3-Mo(Cr) pseudo binary eutectic composite.

4. Selection of gas mixtures for the furnace atmosphere which minimizes melt losses due to oxidation volatilization has been calculated for the Cr_2O_3-Mo eutectic system. Qualitative experimental results closely agrees with the calculated minimum.

5. Eutectics of $LaCrO_3$-Mo, W, Cr and $YCrO_3$-Mo, W, Cr were synthesized after being predicted by the regular solution model.

6. Adequate conditions for controllable Rf-coupling, melting and zone movement were found to be 600 KHz for a 5-cm diameter sample size for both Cr_2O_3-Mo and $(Cr,Al)_2O_3$-Mo. Under these conditions compositions varying in metal content from 10 to 20 mole % Mo could be synthesized.

7. The Rf-heating instability predicted by Hartzell and Sekerka's analysis of the IZG technique [21,22] is readily observed in 5-cm and

smaller samples of Cr_2O_3-35 mole % Mo (or less) at 600 KHz and 3.5-cm and smaller samples of Cr_2O_3-40 mole % Mo (or less) at 2 MHz (90% theoretical density, <8 μm particle sizes, well mixed).

8. The Rf-heating instability and uncontrollable surface melting is lessened by increased sample diameter and the use of lower frequencies as predicted by Hartzell and Sekerka's f_{max}/f_{min} rules.

9. An extremely high thermal gradient exist in the oxide liquid at the solid-liquid interface allowing eutectic composite growth at high growth rates for alloy compositions well off the eutectic or monovariant trough compositions.

10. The typical Cr_2O_3-Mo and $(Cr,Al)_2O_3$-Mo eutectic morphology was found to be a very regular hexagonal array of Mo rods (fibers) aligned in the direction of growth of the oxide matrix. At a growth rate of 5 cm/h it was not unusual to observe some grains with Mo-rods arranged in rows (as seen in viewing a section in the plane of growth) or as sheets of rods (as seen viewing a section oblique to the plane of growth).

11. The $\lambda^2 R$ = constant extremum growth condition was observed in Cr_2O_3-Mo eutectic composite growth indicating that normal eutectic growth occurs during directional solidification.

12. A Soret-modified eutectic constitution supercooling criterion has been rederived using a more general Soret flux contribution term. It was found that the G/R ratio is not dependent on the magnitude of the thermal gradient at the freezing interface as earlier predicted. Thus, the Soret-diffusion contribution should not be a noticeable factor in predicting the onset of dendritic growth by the simple constitutional

supercooling criteria (CSC) even though the value of G is at least an order of magnitude greater than the best obtainable gradients in metal matrix eutectic composite systems.

VI. DISCUSSION

Two of the most fundamental aspects of oxide-metal eutectic composite synthesis, melt chemistry and growth by directional solidification, have been developed to a degree of better understanding in this research project. Perhaps the most valuable contribution to the science of eutectic growth from this work is the realization that oxide-metal eutectic systems of the type M_xO_y-M′ (where $M \neq M'$) are thermodynamically pseudo-binary eutectics. Because three components comprise the liquid that freezes to give the binary, eutectic-like, oxide-metal composite, the reaction has one degree of freedom. The importance of the partial pressure of oxygen in the composite growth environment is brought into focus — the oxygen pressure basically controls the composition of the composite.

Prior to this work it had yet to be demonstrated that oxide-metal eutectic growth obeyed what are presently taken as laws of steady state eutectic growth. However, the reproducible normal eutectic morphology was already a clear indication that steady state growth must occur. Thus, it seems that the most significant contribution from this investigation to the area of directional solidification is the further development of the use and understanding of the internal zone growth (IZG) technique. Methods of sample preparation and simplifications in furnace design have been described which should provide the basic starting point for the growth of IZG of any oxide-metal system. Also, Hartzell and Sekerka's rules for the selection of radio frequency when given certain sample chracteristics and their description of a Rf heating instability

have been shown to be qualitatively accurate. It is hopeful that this work will convince those who intend to produce oxide-metal eutectics by IZG that valuable insight can be obtained (perhaps is even necessary) from an understanding of Hartzell and Sekerka's model of IZG.

The flexibility and freedoms of engineering oxide-metal eutectic composite materials that have been discovered in this investigation are summarized. It has been shown that a relatively simple thermodynamic model, the regular solution model, can be used to predict the conditions necessary for the growth of a binary metallic phase of a given composition. The predictable behavior of more complex oxides formed from simple oxides which form simple oxide-metal eutectics has been demonstrated. Rules for the selection of furnace gases have been developed that will ensure the stability of the desired phases in the composite along with a minimum of material loss due to oxidation volatilization of the melt. Lastly, oxide-metal composites with compositions well off the pseudo-eutectic monovariant trough composition can be grown at moderately high growth rates.

Finally, many of the techniques and thermodynamic calculations used in this work can be applied to other nonmetal-metal combinations which have similar characteristics; i.e., very refractory, subject to gas-metal reactions, and have relatively low thermal and electrical conductivities. Such systems would be combinations of refractory metals with metal sulfides and metal oxysulfides. Also combinations of metal nitrides, metal borides, or metal carbides with metal oxides, metal sulfides, and metal oxysulfides would be candidates for a similar but more complex treatment (more complex due to the necessity of specifying a combination of gas-metal reactions). It is hoped that this work has not only expanded the

understanding of oxide-metal eutectic composite growth but has also helped to set the course for the development of other refractory nonmetal-metal composite materials that could be produced by directional solidification.

LIST OF REFERENCES

LIST OF REFERENCES

1. A. T. Chapman, G. W. Clark, and D. E. Hendrix, J. Amer. Ceram. Soc., 55 (1970) p. 60.

2. M. Hansen, Constitution of Binary Alloys, McGraw-Hill, New York, 1958.

3. H. Bibring, J. P. Trottier, M. Rabinovitch, and G. Seibel: Mem. Sci. Rev. Met., 1971, vol. 67, p. 23

4. E. R. Thompson and F. D. Lemkey: Met. Trans., 1970, vol. 1, p. 2799.

5. J. L. Walter and H. E. Cline: Met. Trans., 1970, vol. 1, p. 1221.

6. P. E. Hart, Proceedings of the Conf. on In Situ Composites, Vol. III, Nat. Ac. Sc., Publ. NMAB-308-3, 1973, pp. 119-27.

7. A. T. Chapman, et al., Melt-Grown Oxide-Metal Composites, Reports 1-5, ARPA Order No. 1637, School of Ceramic Engineering, Georgia Institute of Technology, 1972.

8. N. Claussen, "Hot-Pressed Eutectics of Oxides and Metal Fibers," J. Am. Ceram. Soc., 56(8) 442 (1973).

9. E. M. Levin, C. R. Robbins, and H. F. McMurdie, Phase Diagrams for Ceramists, The American Ceramic Society, Columbus, Ohio, 1964, p. 121.

10. R. P. Nelson and J. J. Rasnussen, J. Am. Ceram. Soc. 53, 527 (1970).

11. T. A. Johnson and J. F. Benzel, "Unidirectional Solidification of Stabilized HfO_2-W," J. Am. Ceram. Soc., 56(4) 234 (1973).

12. Chi-Chin Jen and J. F. Benzel, "Unidirectional Solidification of the UO_2-Mo, UO_2-Nb, and UO_2-Ta Systems," J. Am. Ceram. Soc., 57(5) 232-33 (1974).

13. N. Claussen, G. Petzow, and J. Jahn, High-Melting Metal-Ceramic Eutectics, ORNL Translation 2873, Max-Planck Institut fur Metallforschung, Stuttgart, 1974.

14. J. Briggs and P. E. Hart, "Refractory Oxide-Metal Eutectics, J. Am. Ceram. Soc., 59(11-12) 530-31 (1976).

15. M. D. Watson, Stabilized ZrO_2-W Composites Produced by Unidirectional Solidification, M. S. Thesis, School of Ceramic

Engineering, Georgia Institute of Technology, December 1973.

16. J. A. Graves, Unidirectional Solidification of Y_2O_3 (CeO_2)-Mo and Y_2O_3 (CeO_2)-W Composites, M. S. Thesis, School of Ceramic Engineering, Georgia Institute of Technology, December 1973.

17. G. W. Clark and J. Wilson, unpublished work.

18. J. Briggs, F. R. Mollard, and B. Lux, Conf. on In Situ Composites-II, p. 115; Xerox Individualized Publishing, Lexington, Mass., 1976.

19. C. O. Hulse, Ibid., p. 99.

20. K. Roser and N. Claussen, Ibid., p. 127.

21. R. A. Hartzell, Modeling of Internal Centrifugal Zone Growth, Ph.D. Dissertation, Department of Metallurgy and Materials Science, Carnegie-Mellon University, September 1977.

22. R. F. Sekerka and R. A. Hartzell, Kinetics, Morphology, and Thermodynamics of the Solid-Liquid Transition of Non-Metals, Progress Report COO-2407-6, USDOE Contract No. Ey-S-02-2407, November 1977.

23. A. S. Yue: J. Phys. Chem. Solids Suppl., 1967, Vol. B28, pp. 197–200.

24. A. S. Yue and J. T. Yue: J. Cryst. Growth, 1972, Vol. B/14, pp. 797-803.

25. J. D. Verhoeven, J. C. Warner, and E. D. Gibson: Met. Trans., 1972, Vol. 3, pp. 1437–41.

26. G. V. Samsonov, ed., The Oxide Handbook, IFI/Plenum, New York, 1973.

27. L. S. Darken and R. W. Gurry, Physical Chemistry of Metals, McGraw-Hill, New York, 1953.

28. H. Schick, Thermodynamics of Certain Refractory Compounds, Vol. 2, Academic Press, New York and London (1966).

29. E. A. Gulbransen and K. F. Andrew, J. Electrochem. Coc. Vol. 107, 1960, p. 619.

30. E. A. Gulbransen, Corrosion-NACE, Vol. 26, No. 1, 1970, p. 19.

31. H. C. Graham and H. H. Davis, J. Amer. Ceram. Soc., Vol. 54, No. 2, 1971, p. 19.

32. H. C. Graham and H. H. Davis, J. Amer. Ceram. Soc., Vol. 54, No. 2, 1971, p. 89.

33. C. A. Stearns, F. J. Kohl and G. C. Fryburg: Oxidative Vaporization Kinetics of Chromium (III) Oxide in Oxygen from 1270 to 1570 K, Report No. TN-D-7628, NASA Lewis Research Center, May 1974.

34. Constitution of Binary Alloys, pp. 537-539.

35. Phase Diagrams for Ceramists, p. 121 (Al_2O_3-Cr_2O_3).

36. A. G. Knapton, J. Inst. Metals, 87 (1958-59) pp. 62-64.

37. J. M. Dickinson and L. S. Richardson, ASM Trans. 51 (1959) pp. 1055-1071.

38. D. R. Gaskell, Introduction to Metallurgical Thermodynamics, 1973 McGraw-Hill, N.Y. pp. 337-342, 364.

39. F. D. Richardson, Physical Chemistry of Melts in Metallurgy, Vol. 1, 1974, Academic Press, N.Y. pp. 141–156.

40. J. D. Holder and G. W. Clark, Conf. on In Situ Composites-II, p. 107; Xerox Individualized Publishing, Lexington, Mass., 1976.

41. F. L. Brady, J. Inst. Metals., 28 (1922) p. 369.

42. A. Kofler, Z. Metall., 40 (1950) p. 221.

43. E. Scheil, Z. Metall., 45 (1954) p. 298.

44. F. R. Mollard and M. C. Flemings, Trans. TMS-AIME, 239 (1967) p. 1526.

45. K. A. Jackson and J. D. Hunt, Trans. TMS-AIME, 236 (1967) p. 1129.

46. W. A. Tiller, K. A. Jackson, J. W. Rutter, and B. Chalmers: Acta Met., 1953, vol. 1, p. 428.

47. J. D. Holder and B. F. Oliver, Met. Trans., 5 (1974) p. 2423.

48. M. D. Rinaldi, R. M. Sharp, and M. C. Flemings, Met. Trans., 3 (1972) p. 3139.

49. W. T. King and B. F. Oliver, Conf. on In Situ Composites-III, p. 17; Guinn Custom Publishing, Lexington, Mass., 1979.

50. W. W. Mullins and R. F. Sekerka, J. Appl. Phys., 1964, vol. 35, p. 444.

51. H. E. Cline, Trans. TMS-AIME, 1968, vol. 242, p. 1613.

52. J. D. Hunt and K. A. Jackson, Trans. TMS-AIME, 1967, vol. 236, p. 1129.

53. C. Zener, AIME Trans., 167 (1946) p. 550.

54. F. R. Mollard and M. C. Flemings, Trans. TMS-AIME, 239 (1967) p. 1534.

55. G. A. Chadwick, J. Inst. Metals., 92 (1963) p. 18.

56. Ha-Quac Bao and F.C.O. Durand, J. Cryst. Growth, 15 (1972) p. 291.

57. A. T. Chapman and G. W. Clark, J. Amer. Ceram. Soc., 48 (1965) p. 494.

58. V. I. Aleksandrov, V. V. Osiko, A. M. Prokhorov, and V. M. Tatarintsev, Vestnik Akad. Nauk SSSR, 12 (1973) p. 29.

59. J. F. Wenckus et al., Study, Design an Fabricate a Cold Crucible System, AF CRL-TR-75-0213, Arthur D. Little, Inc., March 1975.

60. C. Ludwig: S. B. Akad. Wiss. Wien, 1859, Vol. 20, pp. 539–45.

61. C. Soret: C. R. Acad. Sci. Paris, 1880, Vol. 91, pp. 289–98.

62. S. R. DeGroot: L'Effet Soret, North Holland Co., Amsterdam, 1945.

63. H.J.V. Tyrrell, Diffusion and Heat Flow in Liquids, Butterworth, London, 1961.

64. F. R. Winter and H. G. Drickamer: J. Phys. Chem., 1955, Vol. 59, pp. 1229–30.

65. M. Hansen: Constitution of Binary Alloys, 2nd ed., p. 1107, McGraw-Hill Book Co., New York, 1958.

66. J. D. Holder, R. A. Hartzell, and G. W. Clark: J. Am. Ceram. Soc., 1980, Vol. 63, No. 5–6, pp. 344–345.

67. J. W. Rutter and B. Chalmers, Can. J. Phys., 1953, Vol. 31.

68. M. Hillert, "Fundamental Aspects of Aligned Growth," Conf. on In Situ Composites-III, 1979, Gunn Publishing, pp. 1-15.

69. C. E. Wicks, ed., Thermodynamic Properties of 65 Elements — Their Oxides, Halides, Carbides, and Nitrides, U.S. Bureau of Mines Bulletin 605, 1963.

70. R. A. Hartzell and R. F. Sekerka, private communication on the electrical conductivity and RF heating of 2 cm diameter $Cl2O_3$-Mo composites.

71. J. D. Holder, G. W. Clark, and B. F. Oliver: Conf. On In Situ Composites, Vol. III, pp. 351–56, Guinn Publishing, Lexington, Mass., 1979.

72. J. D. Holder and G. W. Clark: Conf. On In Situ Composites, Vol. III, pp. 78 - 81, Guinn Publishing, Lexington, Mass., 1979.

APPENDICES

APPENDIX A

CALCULATION OF THERMOCHEMICAL DIAGRAMS

Kellogg-type equilibrium thermochemical diagrams have been constructed for the chromium-molecular oxygen system and the molybdenum-molecular oxygen system at 1500 K, 1800 K, and 2200 K (2223 K is the approximate Cr_2O_3-Mo eutectic temperature). The range of oxygen pressures considered extend from oxygen pressures for the $\frac{4}{3}$ Cr + O_2 = $\frac{2}{3}$ Cr_2O_3 equilibrium to the oxygen pressures for the Mo + O_2 = MoO_2 equilibrium. Equilibrium coefficients were determined from a plot of lower temperature log kp's versus T^{-1} for each vapor species. Extrapolated values of the kp's at 1500 K, 1800 K, and 2200 K are given in Table A-I. The equilibrium thermochemical diagrams constructed from the k_p values are given in Figs. A-1, A-2, and A-3.

Table A-I. Calculated Log K_p for Vapor Species in Equilibrium with Cr_2O_3 and Mo at 1500 K, 1800 K and 2200 K

Specie	Calculated From Log K_p			Calculated From Log K_p =
	1500 K	1800 K	2200 K	
Cr(g)	-6.23	-3.8	-1.8	Log P_{Cr}-log a_{Cr}
CrO(g)	-1.803	0.1	0.6	Log P_{CrO}-1/2 log P_{O_2}-log a_{Cr}
CrO_2(g)	3.98	3.18	2.6	Log P_{CrO_2}-log P_{O_2} a_{Cr}
CrO_3(g)	7.91	6.0	4.3	Log P_{CrO_3}-3/2 log P_{O_2}-log a_{Cr}
$(CrO_3)_3$(g)	29.08	20.0	11.6	Log $P(CrO_3)_3$-9/2 log P_{O_2}-3 log a_{Cr}
Cr_2O_3(s)	26.01	19.2	13.3	Log $A_{Cr_2O_3}$-2 log a_{Cr}-3/2 log P_{O_2}
MoO(g)	-8.0	-5.92	-4.0	Log P_{MoO}-1/2 log P_{O_2}
MoO_2(g)	1.6	1.45	1.4	Log P_{MoO_2}-log P_{O_2}
MoO_3(g)	8.9	6.75	5.1	Log P_{MoO_3}-3/2 log P_{O_2}
$(MoO_3)_3$(g)	14.2	10.37	7.3	1/3 log $P(MoO_3)$-3/2 log P_{O_2}

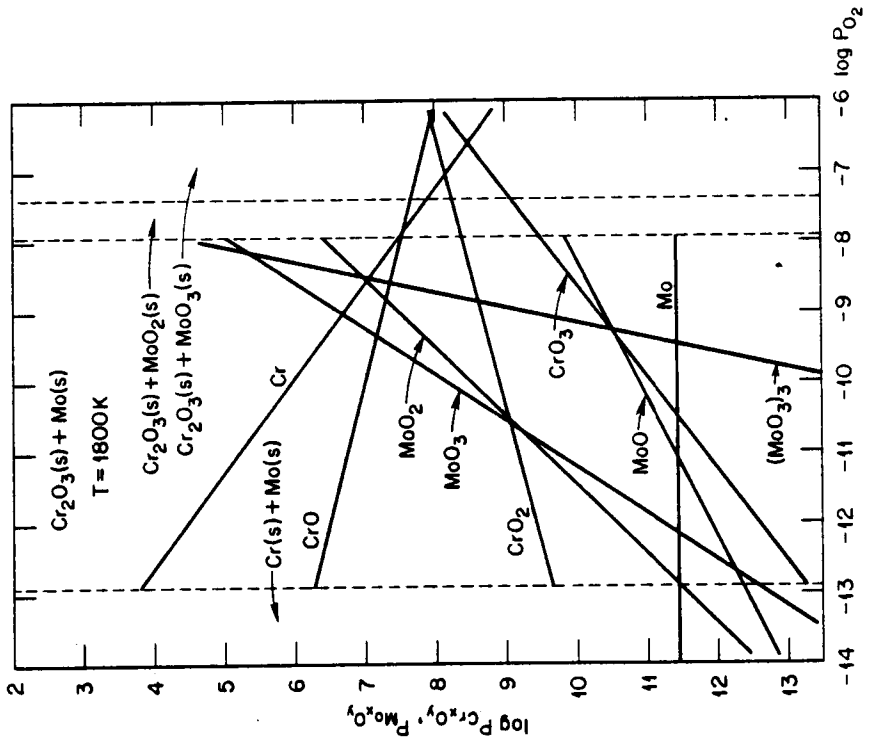


Fig. A-2. 1800 K Kellogg Diagram for Cr_2O_3-Mo.

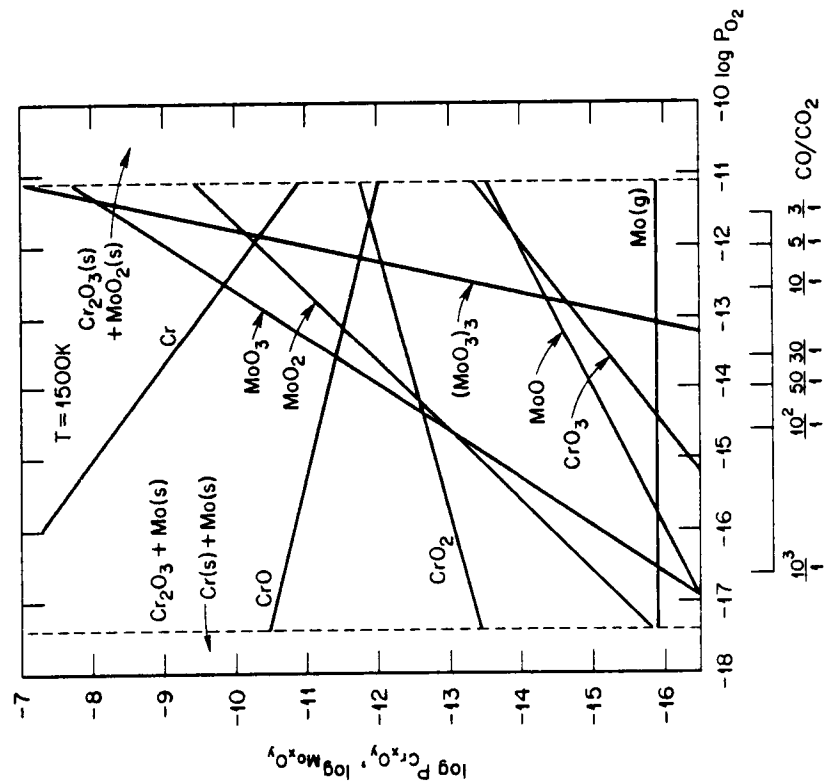


Fig. A-1. 1500 K Kellogg Diagram for Cr_2O_3-Mo.

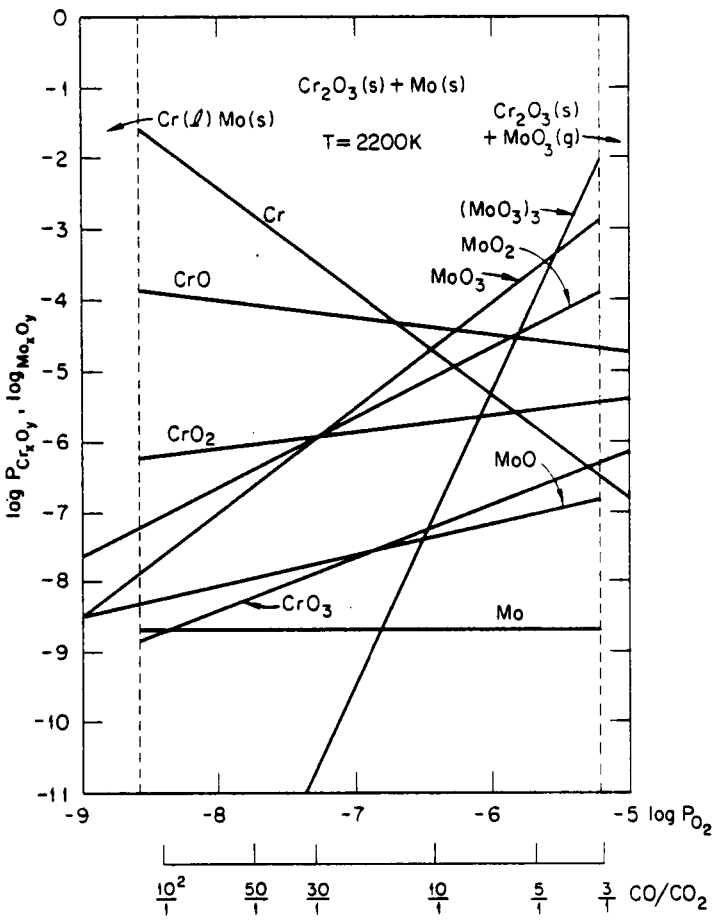


Fig. A-3. 2200 K Kellogg Diagram for Cr_2O_3-Mo.

APPENDIX B

CALCULATION OF REGION OF STABILITY

Calculations have been made for what will be called the "region of stability" for the components in the Cr_2O_3-Mo, Cr_2O_3-Cr, $Cr_2O_3(Al_2O_3)$-Cr systems. The region of stability is defined as the area on a partial oxygen pressure versus temperature plot which lie between the curves for the oxidation of the proposed metallic phase and the reduction of the proposed oxide phase. Stability in this sense means that the metallic phase, if separated from the system, would not be prone to oxidize and the oxide phase, similarly, would not be prone to be reduced. The possibility of the oxide phase undergoing further oxidation is also considered in defining the "region of stability."

Calculations are straightforward if values of ΔG_f° (Gibbs free energy of formation) are available as they are for the cases being considered.

1. For the reaction $Cr(s) - 3/2O_2(g)$ $CrO_3(s)$ from 298 to 460 K:

$$\Delta G_f^\circ = -138.6 - 0.311(10)^{-3}\, T\ln t - 0.646(10)^{-6}T^2$$
$$-0.646(10)^2T^{-1} + 63.69(10)^{-3}\, T + 0.113 \text{ Kcal/gm-mole } CrO_3(s), [26],$$

and for $Cr(s) + 3/2O_2(g) = CrO_3(\ell)$

from 460-1000 K:

$$\Delta G_f^\circ = -138.6 - 9.232(10)^{-3}T\ln t + 1.351(10)^{-6}T^2$$
$$-1.650(10)^2T^{-1} + 0.112\ T + 2.981 \text{ Kcal/gm-mole } CrO_3(\ell), [26].$$

2. For the reaction $Cr(s) + O_2(g) = CrO_2(s)$ from 298 to 1660 K, [26]:

$$\Delta Gf^\circ = 141.115 - 2.51(10)^{-3}T\ln t - 0.203(10)^{-6}T^2$$
$$+ 0.347(10)^2T^{-1} + 60.392(10)^{-3}T - 1.093 \text{ Kcal/gm-mole } CrO_2(s).$$

3. For the reaction $2Cr(s) + 3/2O(g) = Cr_2O_3(s)$ from 298 to 2166 K

$\Delta G_f^\circ = -271.3 + 61.82(10)^{-3}T$ Kcal/gm-mole $Cr_2O_3(s)$, [26] and for

$2Cr(\ell) + 3/2O_2(g) = Cr_2O_3(s)$ from 2166 to 2773 K.

$\Delta G_f^\circ = -287.9 + 70.00(10)^{-3}T$ Kcal/gm-mole $Cr_2O_3(s)$, [26].

4. Tabulated values of ΔG_f° for the reactions

$Mo + O_2 = MoO_2$ and

$Mo + 3/2O_2 = MoO_3$ [26] were used for calculations to construct Fig. 1. Values of ΔG_f° appearing in Fig. 1 have been adjusted to Kcal per gm mole O_2 and a nomagraph has been constructed for P_{O_2} and CO/CO_2 following the technique of Darken and Gurry [27]. Values of P_{O_2} versus T which were used to construct Fig. 5, were obtained using the nomagraph in Fig. 1. Figure 7 gives the partial oxygen pressures for the $4/3Cr(s) + O_2 = 2/3Cr_2O_3(s)$ equilibrium for temperatures up to 1660°C, the Cr_2O_3-Cr eutectic temperature. At temperatures beyond 1660°C, the activities of Cr_2O_3 and Cr at 1810°C have been estimated by assuming ideal mixing behavior (see Fig. B-1). For the eutectic composition, $a_{Cr} = 0.81$ and $a_{Cr_2O_3} = 0.96$. From the relationship given in 3

$$\Delta G_f^\circ = -RT\ell n \frac{a_{Cr_2O_3}}{(a_{Cr})^2 (P_{O_2})^{3/2}},$$

$P_{O_2} = 10^{-9.86}$ atm. For compositions of 0.75 mole fraction Cr_2O_3, corresponding to the Cr liquidus, and 0.83, for the Cr_2O_3 liquidus, oxygen pressures of $10^{-9.83}$ and $10^{-9.93}$, respectively, are calculated. Lines constructed through these points through the point at 1660°C should approximate the boundaries of the region of stability that exist due to solution formation at temperatures above the eutectic temperature.

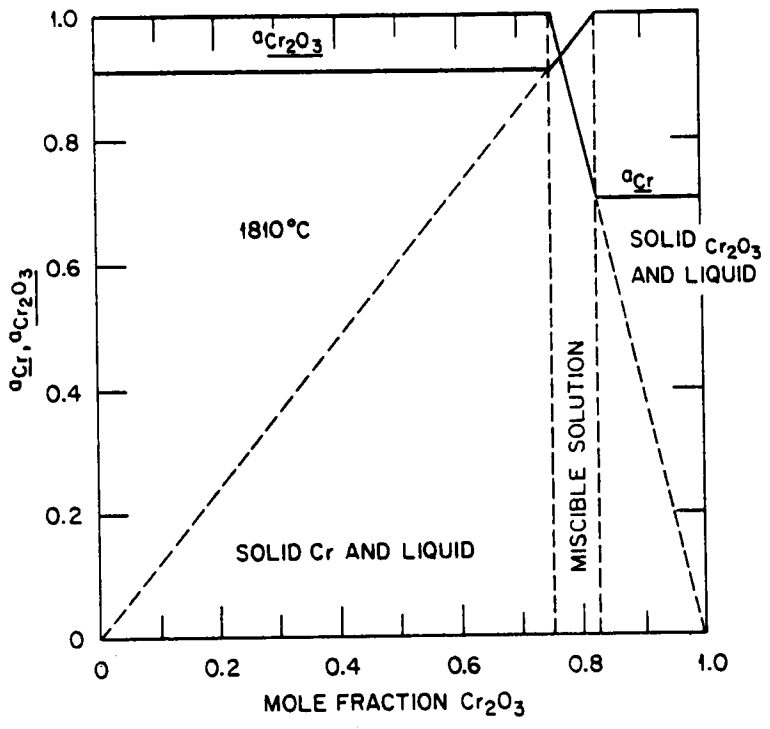


Fig. B-1. Approximation of Cr and Cr_2O_3 Activities at 1810°C.

In the construction of Fig. 8, ideal mixing of Al_2O_3 and Cr_2O_3 is assumed on the basis of the Al_2O_3-Cr_2O_3 equilibrium phase diagram. Thus, the region of stability boundary for the reduction of the Cr_2O_3 in the Cr_2O_3-Al_2O_3 solid solution is calculated using $a_{Cr_2O_3} = 0.5$ and $a_{Cr} = 1$. The boundary for the oxidation of Cr is calculated, as before, taking a $a_{Cr_2O_3} = 1$ and $a_{Cr} = 1$.

APPENDIX C

THERMOX CALIBRATION

A Thermo Lab Instruments, Inc., Thermox Oxygen Analyzer was used to measure the oxygen fugacity of hydrogen-water gas mixtures in the strip heater and composite growth experiments where pre-mixed and certified gases were not used. A Thermox Analyzer is a small, portable, self-contained Y_2O_3 stabilized ZrO_2 electrochemical cell through which a steady stream of the gas is to be tested is passed to obtain an emf which corresponds to a unique oxygen fugacity. The Nerst equation gives the relationship between the emf and the oxygen fugacity:

$$\text{emf} = AT \log \frac{\text{reference } f_{O2}}{\text{sample } f_{O2}} \qquad \text{(C-1)}$$

where

A = constant,

T = cell temperature, 1018 K,

reference f_{O2} = concentration of O_2 in ambient air, and

sample f_{O2} = concentration of O_2 in sample.

The readout system on the Thermox Analyzer available for this work was limited to a maximum of 10 mv cell emf which corresponded to a minimum of 0.1 ppm oxygen concentration (2×10^{-8} atm O_2). In order to read oxygen fugacities in the required experimental range of 10^{-19} down to 10^{-29} MPa ($10^{-18} - 10^{-28}$ atm) a high accuracy Hewlett-Packard DC Differential Voltmeter, Model 3420B, was connected to the electrochemical cell. The cell was then calibrated for this range of oxygen fugacities using H_2,

Ar-4% H_2 and N_2-11% H_2 gases in the as-received dry condition or bubbled through ice water. A fractory calibrated Panametrics Model 2000 Hygrometer was used to measure the water content of the gas being analyzed. Table C-I gives the compositions of the calibration gases and the resulting emf.

Table C-I. Calibration Data for Thermox Oxygen Analyzer

Mixture	Measured H_2O (ppm)	Calculated Log H_2/H_2O	Measured Emf, volts
Dry N_2-11% H_2	4	2.55	1.1725
H_2 bubbled through ice water	4700	2.21	1.1430
N_2-11% H_2 bubbled through ice water	4700	1.369	1.0683
A-3.7% H_2 bubbled through ice water	4700	0.896	1.0241

From the reaction $2H_2 + O_2 = 2H_2O$ and Eq. (C-1), it is seen that a linear relationship should exist between the emf of the cell and the logarithm of the H_2-H_2O ratio:

since $K_p = \frac{f_{H2O}}{f_{O_2} \; f_{H_2}}$, Eq. (C-1) can be

rewritten

$$\text{emf} = AT \log \frac{\text{reference } f_{O_2}}{\text{sample } \frac{f_{H_2O}}{K_p f_{H_2}^2}}$$

$$= AT \log 2K_p \left(\text{reference } f_{(O_2)}\left(\text{sample } \frac{f_{H_2}}{f_{H_2O}}\right)\right)$$

$$= AT \log 2K_p \left(\text{reference } f_{O_2}\right) + AT \log \left(\text{sample } \frac{f_{H_2}}{f_{H_2O}}\right)$$

$$\text{emf} = A' + B' \log \left(\text{sample } \frac{f_{H_2}}{f_{H_2O}}\right)$$

where A' and B' are constants at constant T and constant reference f_{O_2}.

This relationship helps to confirm the accuracy of the results of the Thermox Analyzer calibration by plotting emf versus log f_{H_2O} as given in Fig. C-1. Since all experiments are conducted at approximately 0.1 MPa total pressure, partial pressures are equal to fugacities. For reasons of consistency between measured and metered gas compositions, the terms of partial pressures will be used.

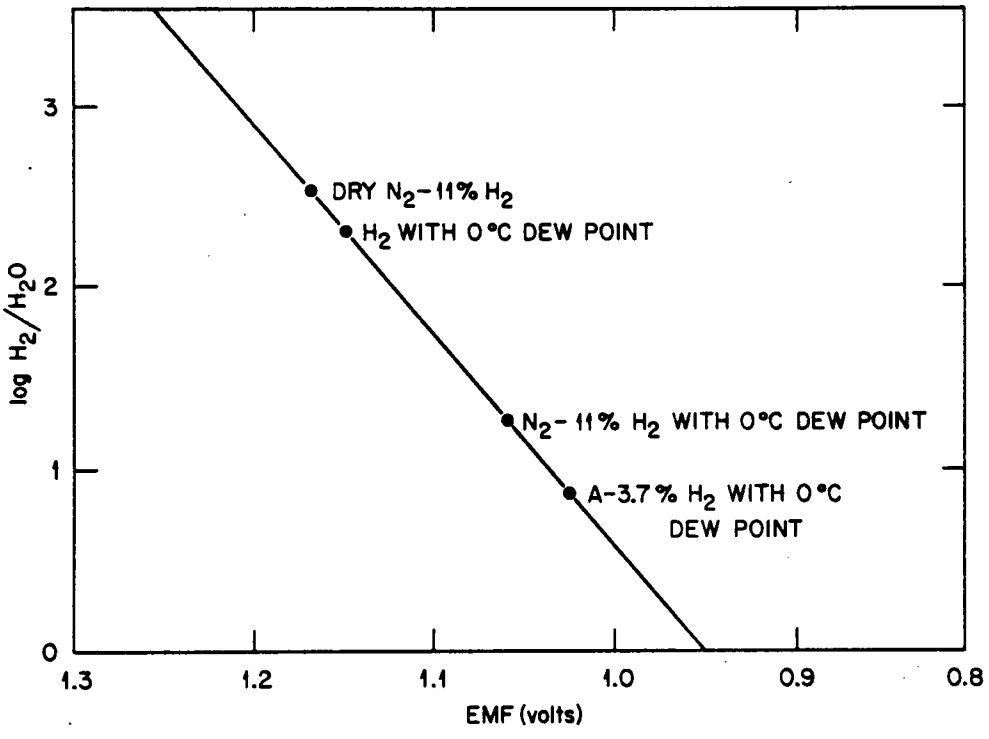


Fig. C-1. Calibration Curve for Thermox Oxygen Analyzer.

APPENDIX D

CALCULATION OF EQUILIBRIUM OXYGEN PRESSURE FOR MONOVARIANT Cr_2O_3-Mo(Cr) ALLOYS

It is predicted that a monovariant trough exist between the Cr_2O_3-Mo eutectic and the Cr_2O_3-Cr eutectic. If this is a correct prediction, then there will be a unique oxygen pressure for each monovariant composition at the temperature for each respective monovariant reaction (i.e. liquid Cr_2O_3 + Mo(Cr) + liquid'). These oxygen pressures can be calculated using the free energy of formation for the reaction:

$$\frac{4}{3}\,\underline{Cr} + O_2 = \frac{2}{3}\,\underline{Cr_2O_3}\ , \qquad \text{(D-1)}$$

The underlining indicating that the specie is in solution. The value of the free energy is usually obtained as follows:

e.g. at some T, $\frac{4}{3}\,Cr(\ell) + O_2(g) = \frac{2}{3}\,Cr_2O_3(s)$ $\quad \Delta G°(1)$

$\frac{4}{3}\,\underline{Cr} = \frac{4}{3}\,Cr(\ell)$ $\quad \Delta G°(2)$

$\frac{2}{3}\,Cr_2O_3(s) = \frac{2}{3}\,\underline{Cr_2O_3}$ $\quad \Delta G°(3)$

$\frac{4}{3}\,\underline{Cr} + O_2 = \frac{2}{3}\,\underline{Cr_2O_3}$ $\quad \Delta G°(4)$

where the solution contains Mo, Cr_2O_3 and Cr. Using $\Delta G°(4)$ for the reaction given by Eq. (D-1),

$$\Delta G°(4) = RT\ \frac{(a_{\underline{Cr_2O_3}})^{2/3}}{P_{O_2}(a_{\underline{Cr}})^{4/3}}\ , \qquad \text{(D-2)}$$

the P_{O_2} can be calculated if $a_{\underline{Cr_2O_3}}$ and $a_{\underline{Cr}}$ can be determined.

The activity of $\underline{Cr_2O_3}$ will be estimated assuming Raoultian behavior. Thus, if the standard state of Cr_2O_3 is taken as pure solid Cr_2O_3, then at the monovariant temperature

$$a_{\underline{Cr_2O_3}} \simeq a_{Cr_2O_3(s)} \simeq X_{Cr_2O_3(s)} ,$$

where $X_{Cr_2O_3}$ is mole fraction of Cr_2O_3 in the composite.

The activity of $\underline{Cr}$ is not expected to be ideal when it is dilute. It should, however, approach ideality when it is the predominant component of the metal phase of the composite. To obtain values of $a_{\underline{Cr}}$ in a melt that freezes to give a Mo-rich metal phase, the regular solution model can be used to obtain values of $\gamma\underline{Cr}$, the activity coefficient of Cr dissolved in the oxide melt.

From the regular solution model:

$$\Delta H^M = X_A X_B a'_{AB} + X_A X_C a'_{AC} + X_B X_C a'_{BC} .$$

Since $RT\ell n\gamma_A = \left(\frac{\partial \Delta \underline{H^M}}{\partial n_A}\right)_{n_B, n_C, P, T}$,

$$RT\ell n\gamma_A = d'_{AB} X_B (X_B + X_C) + a'_{AC} X_C (X_B + X_C) - X_B X_C a'_{BC} .$$

So for $\underline{Cr}$:

$$\gamma\underline{Cr} = \exp \frac{1}{RT} [a'_{Cr,Mo}(X_{Mo} + X_{Cr_2O_3}) + a'_{Cr,Cr_2O_3} X_{Cr_2O_3}(X_{Mo} + X_{Cr_2O_3})$$

$$- X_{Cr_2O_3} X_{Mo} a'_{Cr_2O_3,Mo}] \qquad (D\text{-}3)$$

When X_{Cr} can be specified (along with $X_{Cr_2O_3}$ and T) and by using Eq. (D-2), the equilibrium P_{O_2} can be calculated for that particular alloy. Table D-I

Table D-I. Calculated Values for Mo-Cr Fiber Composition vs $CO-CO_2$ Mixture

Fiber Composition (mole % Cr)	$X_{Cr_2O_3}$	X_{Cr}	X_{Ms}	T,K(°C)	γ_{Cr}	P_{O_2}, MPa	$\%CO_2$ in CO_2 at T
3	0.75	0.0075	0.2425	2220.8 (1947.8)	3.5777	$10^{-7.35}$	8.95
5	0.75	0.0175	0.2325	2217.9 (1944.9)	3.5836	10-7.86	5.25
10	0.75	0.0250	0.2250	2215.8 (1942.8)	3.5880	$10^{-8.07}$	4.20
20	0.75	0.0500	0.2000	2208.5 (1947.8)	3.5777	$10^{-7.35}$	8.95

gives the results of calculations for the equilibrium P_{O_2} for Cr_2O_3-25 mole % Mo(Cr) melt which would result in Mo-35, 10 and 20 mole % Cr fibers. A step by step example calculation follows:

EXAMPLE CALCULATION

For $X_{Cr_2O_3} = 0.75$, and a Mo — 20% Cr fiber which gives

$$X_{Cr} = 0.05$$

$$X_{Mo} = 0.20$$

$$T = 2208.5 \text{ K}$$

where the temperature is approximated by assuming a monovariant trough with a constant slope ($T = 1950 - 290X_{Cr} + 273$ in K).

From Eq. (D-3), with $a'_{Cr_2O_3,Cr} \simeq 10$ Kcal, $a'_{Cr_2O_3,Mo} \leq 10$ Kcal and $a'_{Cr,Mo} = 0$,

$$\gamma_{Cr} = \exp \frac{1}{(1.987)(2208.5)} [10^4(0.75)(0.95) - 10^4(0.75)(0.20)]$$

$$\gamma_{Cr} = 3.6032$$

Since values for $\Delta G°(2)$ and $\Delta G°(3)$ are not known, $\Delta G°(4)$ will be assumed to be approximately equal to $\Delta G°(1)$. From Fig. 16, assuming $\Delta G°(1) = \Delta G°_f$ for $\frac{2}{3} Cr_2O_3 = \frac{4}{3} Cr + O_2$ at 2208.5 K, or $\Delta G°(1) = -85$ Kcal per mole O_2. Using Eq. (D-2).

$$P_{O_2} = \frac{(X_{Cr_2O_3})^{2/3}}{(\gamma_{Cr}X_{Cr})413} e^{\frac{WG°_f(4)}{RT}}$$

$$= 3.14(10)^{-8} \text{ ATM}$$

$$P_{O_2} = 10^{-7.50} \text{ ATM or } 10^{-8.50} \text{ MPa}$$

A CO-CO_2 mixture of CO — 2.75% CO_2 will give this partial pressure oxygen at 2208.5 K.

VITA

John Davis Holder received his B.S. in Metallurgical Engineering in 1972 and M.S. in Metallurgical Engineering in 1973 from The University of Tennessee. His M.S. topic was The Directional Solidification of Pb-Sn-Cd Alloys. After completing the M.S. program, he was employed by the Aluminum Company of America as a Process Engineer at ALCOA's Smelting Facility in Alcoa, Tennessee. While with ALCOA, he worked in the areas of high purity aluminum smelting and composition control in anode assembly cast iron alloys.

Mr. Holder left ALCOA to join the materials science research staff at the Oak Ridge National Laboratory, Metals and Ceramics Division. While at ORNL he developed the research topic for his Ph.D. dissertation and reentered the graduate studies program at The University of Tennessee. Parts of Mr. Holder's research results have already been published in the Journal of the American Ceramic Society and in the Proceedings of the Conferences on In-Situ Composites-II and -III. He has been priviledged to present his work in an invited review paper at the Verbundwerkstoffe-1980, Konstanz, West Germany; also Mr. Holder has presented seminars on his work at the Virginia Technicalogical University, Blacksburg, Va., Max-Planck-Institut, Stuttgart, W. Germany, Giesserei-Institute, Technische Hachehule, Aachen, W. Germany, and Technische Hogeschool, Eindhover, Holland.